1-1-2015

A Systems Approach to Hemostasis: How the Feedback Between Thrombus Structure and Molecular Transport Regulates the Hemostatic Response

John Douglas Welsh
University of Pennsylvania, jwels@mail.med.upenn.edu

A Systems Approach to Hemostasis: How the Feedback Between Thrombus Structure and Molecular Transport Regulates the Hemostatic Response

Abstract
After vascular injury numerous chemical signals are released to induce platelet activation, coagulation, and post-hemostatic events. This thesis aims to investigate the interplay between thrombus structure and the spatiotemporal distribution and transport of biologically relevant solutes, and how this impacts thrombus formation in vivo. Using intravital microscopy we have previously described a characteristic architecture of thrombi formed in vivo. The architecture consists of a core of highly-activated and tightly packed platelets covered by a loose shell of less activated platelets. Initially, we developed a novel platelet-targeted sensor capable of reporting on thrombin activity, a potent platelet agonist, within thrombi formed ex vivo or in vivo. We found that thrombin activity was high in the core region, but restricted from the shell. We then designed another sensor capable of tracking soluble protein transport within thrombi formed in vivo, and found significant retention of soluble proteins within the platelets that would go on to form the core region. Using computational methods we found that the platelet packing density between the platelets restricted the diffusion of proteins within the core region, and allowed for rapid elution of proteins that made it to the shell. To test this in vivo we used mice with a defect in platelet retraction, but not platelet sensitivity to agonists. The mutant mice showed a much faster rate of solute elution using our transport sensor, and we also observed decreased platelet activation and thrombin activity within the thrombus. Next, we extended this model of thrombi as regulators of protein transport by examining how thrombus architecture altered the leakage of plasma proteins into the surrounding tissue. We found that extravascular solute gradients were sensitive to commonly used anti-platelet agents as well as small changes in platelet packing densities. Finally, we developed a new intravital imaging technique to visualize thrombus architecture formation in the mouse femoral artery and vein to extend our observations into the macrocirculation. Together, this thesis proposes a novel mechanism of thrombus regulation, which is dependent upon molecular transport properties shaped by the local hemodynamics and the intrathrombus microenvironment.

Degree Type
Dissertation

Degree Name
Doctor of Philosophy (PhD)

Graduate Group
Biochemistry & Molecular Biophysics

First Advisor
Lawrence F. Brass

Second Advisor
Scott L. Diamond

Keywords
Blood, Hemostasis, Platelets, Thrombin, Transport

Subject Categories
Biochemistry | Biology | Biophysics

A SYSTEMS APPROACH TO HEMOSTASIS: HOW THE FEEDBACK BETWEEN THROMBUS STRUCTURE AND MOLECULAR TRANSPORT REGULATES THE HEMOSTATIC RESPONSE

John Welsh

A DISSERTATION

in

Biochemistry and Molecular Biophysics

Presented to the Faculties of the University of Pennsylvania

in

Partial Fulfillment of the Requirements for the

Degree of Doctor of Philosophy

2015

Supervisor of Dissertation

_____

Dr. Lawrence F. Brass

Professor of Medicine

Co-Supervisor of Dissertation

_____

Dr. Scott L. Diamond

Arthur E. Humphrey Professor and Chair of Chemical and Biomolecular Engineering

Graduate Group Chairperson

_____

Dr. Kim A. Sharp, Chair Graduate Group in Biochemistry and Molecular Biophysics

Dissertation Committee:

Dr. John Weisel, Professor of Cell and Developmental Biology

Dr. Sriram Krishnaswamy, Professor of Pediatrics

Dr. Charles Abrams, Francis C. Wood Professor of Medicine

Dr. E. James Petersson, Associate Professor of Chemsitry

A SYSTEMS APPROACH TO HEMOSTASIS: HOW THE FEEDBACK BETWEEN THROMBUS STRUCTURE AND MOLECULAR TRANSPORT REGULATES THE HEMOSTATIC RESPONSE

DEDICATION

For my fiancé Emalee Popoff because you have made me completely and totally happy. And for my parents who deserve the credit for any success I have in life, as my original teachers and constant supporters.

ACKNOWLEDGMENT

I would like to acknowledge my advisors Dr. Lawrence Brass, Dr. Scott Diamond, and Dr. Timothy Stalker. Along with Dr. Maurizio Tomaiuolo, Dr. Thomas Colace, and Dr. Ryan Muthard this has been a very special collaborative team that I am so proud to have been a part of. I would also like to acknowledge my sister Sara Kulp and her husband Dr. Daniel Kulp who have provided emotional, professional, and emotional support throughout my academic career. Finally, I would like to acknowledge my friends who were always able to brighten my days with laughter: Nicole Owens, Joe O'Brien, Sarah Fenton, Jamie Knox, Francesca Tuazon, and Cory Rice.

ABSTRACT

A SYSTEMS APPROACH TO HEMOSTASIS: HOW THE FEEDBACK BETWEEN THROMBUS STRUCTURE AND MOLECULAR TRANSPORT REGULATES THE HEMOSTATIC RESPONSE

John Douglas Welsh

Dr. Lawrence Brass

Dr. Scott Diamond

After vascular injury numerous chemical signals are released to induce platelet activation, coagulation, and post-hemostatic events. This thesis aims to investigate the interplay between thrombus structure and the spatiotemporal distribution and transport of biologically relevant solutes, and how this impacts thrombus formation in vivo. Using intravital microscopy we have previously described a characteristic architecture of thrombi formed in vivo. The architecture consists of a core of highly-activated and tightly packed platelets covered by a loose shell of less activated platelets. Initially, we developed a novel platelet-targeted sensor capable of reporting on thrombin activity, a potent platelet agonist, within thrombi formed ex vivo or in vivo. We found that thrombin activity was high in the core region, but restricted from the shell. We then designed another sensor capable of tracking soluble protein transport within thrombi formed in vivo, and found significant retention of soluble proteins within the platelets that would go on to form the core region. Using computational methods we found that the platelet packing density between the platelets restricted the diffusion of proteins within the core region, and allowed for rapid elution of proteins that made it to the shell. To test this in vivo we used mice with a defect in platelet retraction, but not platelet sensitivity to

agonists. The mutant mice showed a much faster rate of solute elution using our transport sensor, and we also observed decreased platelet activation and thrombin activity within the thrombus. Next, we extended this model of thrombi as regulators of protein transport by examining how thrombus architecture altered the leakage of plasma proteins into the surrounding tissue. We found that extravascular solute gradients were sensitive to commonly used anti-platelet agents as well as small changes in platelet packing densities. Finally, we developed a new intravital imaging technique to visualize thrombus architecture formation in the mouse femoral artery and vein to extend our observations into the macrocirculation. Together, this thesis proposes a novel mechanism of thrombus regulation, which is dependent upon molecular transport properties shaped by the local hemodynamics and the intrathrombus microenvironment.

TABLE OF CONTENTS

LIST OF TABLES

LIST OF ILLUSTRATIONS

CHAPTER 1: The biochemistry and biophysics of thrombus formation

1.1 Thrombus formation and architectural differentiation

In response to vascular damage, circulating platelets become activated and aggregate at the site of injury. Reinforced by fibrin, the platelet mass forms a hemostatic plug capable of preventing blood loss and restoring local hemodynamics. Disruption of this process can result in either continued blood loss from the injury site, or excessive thrombus formation that occludes the vessel and causes ischemic injury to the surrounding tissue.

Circulating platelets remain quiescent and free from adhesion and aggregation due to endothelial signaling, and a lack of activating signals. However, upon vessel damage platelet activation is initiated by a variety of agonists. Extensive studies [1-6] have produced a general model of how agonists induce thrombus formation. Vessel wall damage exposes subendothelial matrix proteins, such as collagen, inducing platelet adhesion and subsequent activation. Von Willebrand Factor (vWF), released from damaged endothelial cells or circulating in the plasma, binds to both collagen and platelets facilitating further platelet accumulation and activation. In response to sufficient activation platelet δ-granules are secreted releasing small molecule agonists, namely ADP and thromboxane A2 (TxA2), which further drive local platelet activation. Concurrently, thrombin generation is initiated on the surface of the damaged endothelial cells and platelet membranes exposing phosphotidylserine (PS). Thrombin production drives both potent platelet activation and fibrin deposition, which helps to increase

thrombus stability. These various activating signals are then integrated by the adherent platelets, resulting in a mass of activated platelets and fibrin covering the injury site.

Numerous studies have found that platelet activation, granule release, platelet packing density, and fibrin distribution are heterogeneous within thrombi formed both *in vivo* and *ex vivo* [7-12]. Our recent studies, using *in vivo* models of hemostatic thrombus formation, in the mouse microvasculature, have revealed that this heterogeneity can be classified into a hierarchical architecture. This architecture consists of a core of highly-activated platelets covered by a shell of less-activated platelets. The core is differentiated from the shell by surface P-selectin expression, indicating sufficient activation to induce α-granule exocytosis. Also the platelets within the core region have an increased packing density and stability compared to the shell [12]. Finally, the core region is also enriched with fibrin deposition compared to the shell, due to increased local thrombin activity. This architecture consistently forms in response to mechanical or laser induced penetrating injuries in the mouse microcirculation, and is reproduced in microfluidic models of thrombus formation using human blood [13]. Despite the consistency of the observation of the core/shell architecture, it is unclear what role it has in regulating hemostasis or thrombosis.

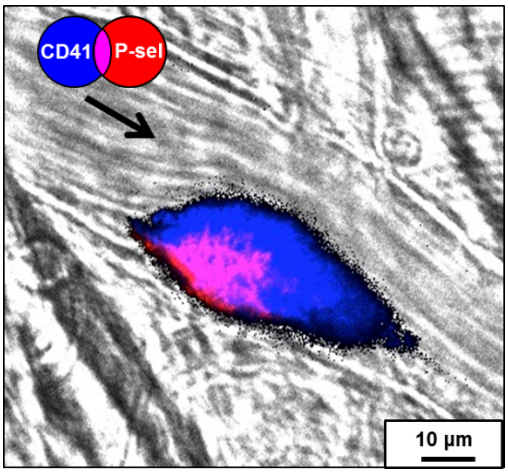

Figure 1- 1 Architecture of a hemostatic thrombus formed in a mouse cremaster arteriole after laser injury.

A representative image of a thrombus formed 10 minutes after laser injury of a mouse cremaster arteriole (bright field). Platelets are labeled with anti-CD41 antibody (blue), and surface P-selectin is visualized with anti-CD62P antibody (red). Thus the core of P-selectin positive platelets is pink, and the shell is the P-selectin negative blue region.

1.2 Pathological thrombus architecture in humans.

While the core-shell architecture observed in the mouse is reproduced with human blood in microfluidic devices, the architecture of thrombi formed under pathological conditions in humans is difficult to ascertain. Microvascular thrombi are difficult to study in human patients as they are not typically removed from the patient, and are too small for structural analysis. The mechanism behind microvascular thrombosis is also quite different from analysis of hemostatic thrombi formed in vivo. Microvascular thrombosis is often induced by systemic defects such as - sepsis, disseminated intravascular coagulation, heparin induced thrombocytopenia – which present several key differences compared to discrete vascular injuries. These disorders lead to circulating agonists such as lipopolysaccharide (LPS), thrombin, and high molecular weight vWF driving systemic

platelet activation [14-18]. Also local inflammation and circulating thrombin drive extensive endothelial cell activation leading to multiple sites of platelet adhesion and nucleation points for thrombus formation [14-16,19-21]. This is in stark contrast to hemostatic thrombus formation in which a discrete injury induces local agonist production and thrombin generation, and at least during initial thrombus formation, appears to be largely independent of inflammatory pathways or cells.

Venous macrovascular thrombi, resulting from deep vein thrombosis (DVT), are able to be isolated and the structure analyzed. DVT results in formation of red clots consisting of a mix of platelets, inflammatory cells, red cells, fibrin, and DNA (NETs). This structure is quite different from the white clots formed ex vivo with human blood and in vivo with mice using hemostatic models, which consist mainly of platelets with fibrin deposited at the injury site and within the core region [12,13,22]. These differences in thrombus structure are likely due to the different mechanisms of thrombus initiation and local hemodynamics. DVT is initiated by activated inflammatory cells and endothelial cells in the presences of very low blood flow, leading to the release of vWF from endothelium, and initiation of thrombin production on the surface of inflammatory cells and NETs released from neutrophils. Together, these events activate platelets, drive fibrin deposition [23-25], which along with NETs and inflammatory cells are all capable of trapping red cells under low flow conditions [23,26,27].

Similarly, studies of the composition of coronary thrombi showed that they had a much more heterogeneous structure than observed ex vivo or in vivo. Thrombi removed from patients after coronary plaque rupture consisted mostly of fibrin with almost equal parts of red cells and platelets, and a large component of cholesterol crystals [28]. Also

observed in coronary thrombosis is the formation of the Lines of Zahn, which are formed by overlaying regions of platelets/fibrin and red cells forming distinct regions [29]. Also of note is the difference in fibrin deposition, which is in close proximity to the injury site in the mouse model, but is deposited throughout the thrombi formed in human coronary arteries [28,30].

However, it is possible that initial pathological thrombus growth in both DVT and arterial plaque rupture is similar to events we observe during hemostatic thrombus formation in mice and human blood ex vivo. It has been noted that at the site of plaque rupture a platelet head is commonly formed, suggesting that initial thrombus formation is a platelet driven response as we see in the mouse [30]. Similarly, the initiation of DVT thrombus formation is dependent upon circulating platelet accumulation [23-25]. This suggests that in both of these pathologies canonical thrombus formation is platelet dependent, and may mirror platelet recruitment events observed in laboratory models. The disparities in thrombus structure, such as increased fibrin deposition and red cell incorporation, is correlated with increased times of ischemia after plaque rupture or low flow conditions during DVT, suggesting that these thrombus growth events are dependent upon low flow conditions [28,31]. Therefore the events we observe in vivo and ex vivo, under flow conditions, may mirror the initial thrombus formation during pathological thrombus formation, but in the healthy mouse vasculature thrombus formation fails to occlude the vessel preventing increased local thrombin activity driving fibrin deposition and red cell entrapment.

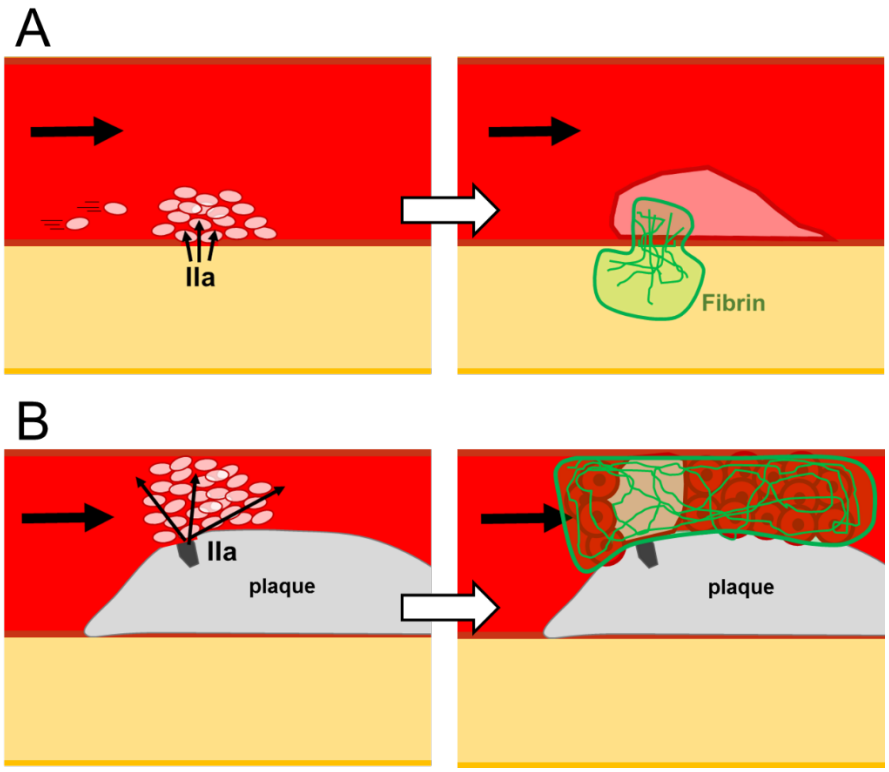

Figure 1- 2 Model of hemostatic and pathological thrombus formation

(A) A model of hemostatic thrombus formation. Rapid platelet accumulation is followed by local thrombin activity that drives further platelet activation and fibrin deposition at the injury site. Continued flow delivers anti-thrombotic compounds and elutes thrombin from the thrombus. (B) A model of pathological thrombus formation. Initial platelet deposition leads to vessel occlusion allowing for continued thrombin activity driving extensive fibrin deposition and red cell entrapment.

1.3 The spatiotemporal distribution of agonists drives thrombus architecture.

The differentiation of the thrombus architecture into the core and shell regions is driven by differences in the distributions of the various platelet agonists during thrombus formation. In our previous studies of thrombus architecture in the mouse microcirculation

we found that inhibition of thrombin activity prevented the formation of the core region, while blockade of ADP $P2Y_{12}$ receptors with cangrelor or TxA2 formation with aspirin led to shell depletion without any effect on the core. Therefore we concluded that, in the mouse microcirculation, core formation is thrombin driven, and that ADP and TXA2 recruit the shell [12]. However, whether or not this specific pattern of agonist driven architecture formation is consistent in other injury models or vasculatures is unknown.

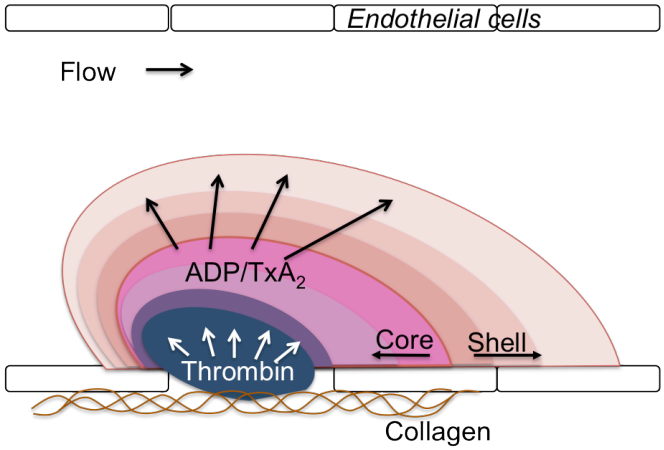

Figure 1- 3 Model of agonist distributions and resulting thrombus architecture in the mouse microvasculature injury model.

After laser induced injury to the mouse microvasculature endothelium thrombin soluble agonists are released/formed at the injury site. Thrombin activity is localized to the core region and drives α-granule release and fibrin deposition. ADP and TXA2 released from activated platelets extend beyond the core and recruit circulating platelets which make up the shell region.

Agonist distributions are shaped by the kinetics and location of agonist release or generation, as well as the transport properties of the agonist. For example, collagen exposed at the injury site is in the vessel wall and immobile, thus adherent platelets rapidly cover the exposed collagen limiting the effects of collagen/GPVI signaling. Conversely, ADP is released from sufficiently activated platelets at various times and

locations during thrombus formation, and is highly diffusible within the intrathrombus environment [1]. Thrombin generation is dependent upon the accumulation of multiple coagulation factors on procoagulant surfaces formed after injury. Formation of the membrane-bound prothrombinase complex leads to prothrombin cleavage into thrombin. Once released from the prothrombinase complex, thrombin is free to diffuse within the thrombus. However, thrombin is less diffusible than small molecule agonists, and is capable of being sequestered by multiple binding partners including: fibrin, thrombomodulin on endothelial cells, GPIb, PAR-1 and -4 on platelets, and antithrombin III in plasma [1,32]. These various factors all contribute the distribution of agonists, and thus platelet activation and fibrin deposition, within the forming thrombus.

Agonist production is also dependent upon the mechanism and extent of injury, and the vascular bed which is being injured [33-35]. Generally, all injuries create thrombi that are sensitive to $\alpha_{IIb}\beta_3$ and $P2Y_{12}$ antagonists, but the contribution of thrombin and collagen signaling are dependent upon injury type and severity [36,37]. In the cremaster arterioles inhibition of thrombin activity reduces thrombus size by 80-90% and abolishes P-selectin(+) core formation [12]. However, it has also been reported that in the mesentery arterioles thrombin activity is dependent upon injury severity [36,38,39], with more mild penetrating injuries being dependent upon thrombin and collagen induced signaling, and severe injuries shifting to more thrombin signaling dependency [36]. In the venous macrocirculation, Getz et al., showed that low tissue factor mice had no hemostatic defect in response to laser induced vessel rupture [40], suggesting a limited role for thrombin. Similar to thrombin, the importance of GPVI signaling during thrombus formation is dependent upon the mechanism and extent of injury. In models of injury in which there is extensive endothelial cell denudation, exposing subendothelial collagen,

GPVI signaling is crucial in driving thrombus formation [39,41-43]. In general, increasing the severity of penetrating injuries increases the importance of thrombin signaling and lessens the impact of GPVI defects [36-39]. Endothelial denudation by mechanical pinching of the abdominal aorta shows thrombus dependence on GPVI signaling [44], however, a similar injury technique used in the carotid artery demonstrated thrombus formation was independent of GPVI signaling [37], suggesting that variations in vessel biology also impact agonist exposure/production. Similarly, even within the same tissue arteries and veins also have different mechanisms underlying thrombus formation [33,34]. Therefore local agonist concentrations impact thrombus development, but their relative contribution appears dependent upon the biology of the injured vessel, the extent and mechanism of injury, and the transport properties of the agonists at the site of injury.

Differences in thrombus formation in the macro- and microcirculation are of specific interest because clinically relevant thrombosis often occurs in the macrovasculature, but current intravital imaging techniques are limited to the microvasculature. Therefore, the architecture and dynamics of thrombus formation in these larger vessels are largely unknown. The macro- and microcirculation differ in hemodynamics [45-47] and vessel wall structure [48], and biology [49,50]. Therefore, agonist production and retention may be vastly different between the vasculatures, which raises interesting questions about how thrombus formation and architecture may vary between the macro- and microcirculation.

1.4 The intrathrombus microenvironment impacts solute transport and thrombus formation

As described above, agonist distribution is a critical factor responsible for the observed differences in the extent of platelet activation, and the distribution of soluble agonists is highly dependent on the physical architecture of the platelet mass as it evolves. The microenvironment within the platelet mass consists of aggregated platelets and fibrin densely packed together, the structure of which we have only recently been able to be interrogate in real time and under physiological conditions. In this regard, the use of microfluidic devices has allowed for accurate measurement of the permeability of human platelet aggregates formed under flow conditions. Using such an approach, a mature platelet mass was found to have a permeability approaching that of an intact endothelial cell layer (2×10^{-14} cm^2) [51]. This permeability was increased by 3-fold when platelet retraction was inhibited and 2-fold when fibrin formation was blocked, highlighting the importance of these events in regulating this property of a platelet plug [51]. Detailed measurements of thrombus permeability in vivo are difficult, so investigators have instead used computational modeling based in images of thrombus structure obtained in vivo. One study examining a platelet plug with the core and shell architecture described above determined that the core region has greatly reduced permeability (100-fold) and greatly increased tortuosity in the paths between platelets compared to the shell [52]. Taken together, the *in vitro*, *in silico* and *in vivo* findings demonstrate that the microenvironment of a hemostatic plug is a dense mesh of platelets and proteins with winding and narrow gaps, which restrict solute movement, particularly in the core region.

Computational models of platelet plugs formed *in situ, in vitro* or *in vivo* all show that low permeability will greatly reduce plasma flow within the intraplug microenvironment compared to the lumen [52-55]. The reduction of flow also means a reduction in the rate of solute transport within the platelet plug [52,53,55,56]. Importantly, under low flow conditions

within the platelet plug microenvironment the diffusibility of a solute becomes a dominant factor in its transport properties [51,52,55]. Solute diffusibility is determined in part by size, decreasing as size increases. Solute movement is increasingly hindered within the growing platelet core as gap sizes decrease and path tortuosity increases [52,55,56]. Large solutes can even be excluded from the densely packed core region [12]. As a result, the platelet plug microenvironment becomes a molecular sieve capable of restricting movement of solutes dependent upon their size [52,53,55,56]. In aggregate, computational and *in vivo* studies show that the platelet mass microenvironment alters plasma velocity and solute diffusion to regulate solute transport within the platelet mass.

The formation of this molecular sieve is also important in regulating the transport of bioactive molecules into the extravascular tissue plane. The extravascular tissue provides a source of tissue factor to initiate coagulation, and local immune cells capable of contributing to post-hemostatic inflammation and tissue homeostasis [19,21,57]. Therefore, thrombus formation regulates the delivery of plasma borne molecules into the tissue, and platelet granule release at the site of injury facilitates the delivery of platelet-borne molecules into the tissue. Also the extravascular tissue provides a sink for thrombin produced on the tissue factor surfaces in the vessel wall and extravascular tissue. Thrombin in the extravascular tissue is also restricted from diffusion into the thrombus and further into the lumen. Therefore, tight platelet packing in the core region not only facilitates thrombin retention driving stable thrombus formation, it also reduces excessive thrombin transport from the extravascular space into the lumen driving continued thrombus growth. In various pathological thrombotic disorders that lack vessel rupture, such as DVT and plaque rupture, this sink is unavailable and may contribute to occlusive thrombus formation (Figure 1-3).

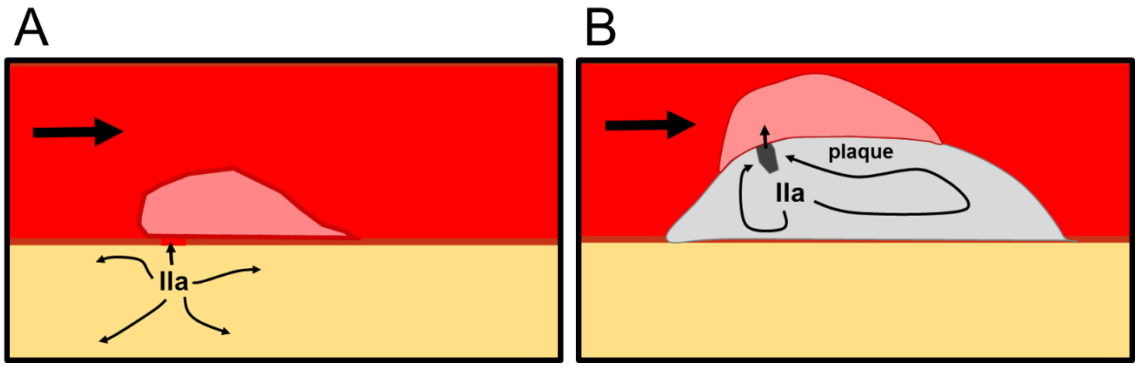

Figure 1- 4 Model of extravascular transport of thrombin during hemostasis and thrombosis.

(A) A schematic of thrombin transport after vessel rupture and hemostasis. Thrombin produced in the extravascular tissue is free to diffuse within the tissue or back into the restrictive thrombus. (B) A schematic of thrombin transport within a ruptured plaque. Thrombin within the plaque is limited in its ability to diffuse away and may be shunted back through the thrombus driving futher platelet activation and accumulation.

Transport has long been recognized as important for platelet mass formation as a mechanism for delivery of coagulation factors to the injury site, as well as elution of platelet agonists from within the platelet mass [58-60]. Coagulation is affected by solute transport as limited delivery of coagulation factors restrains thrombin generation, while limited transport of thrombin out of the platelet mass increases its effective concentration. Microfluidic assays have demonstrated that platelets create a physical barrier that covers up tissue factor surfaces and exclude plasma-borne coagulation factors altering the rate of fibrin deposition [59]. These findings suggest that the intrathrombus microenvironment impacts agonist retention shaping thrombus architecture.

1.5 The state of the field

To summarize the information presented above: thrombi formed *ex vivo* and *in vivo* form a highly conserved architecture consisting of a core and shell region that vary in both biological and physical properties, thrombus architecture is regulated by variations in agonist gradients formed within the intrathrombus environment, and the physical nature of the intrathormbus environment is capable of altering solute transport properties and resulting biochemical processes.

These observations raise interesting questions about: how platelet activation and retraction shape the physical nature of the intrathrombus environment, the extent to which the intrathrombus environment shapes agonist transport and gradient formation, and how these two processes feedback to one another to drive core and shell formation. Extending these questions is how intrathrombus environment structure impacts solute extravasation, shaping solute gradients within the tissue surrounding sites of vascular damage, and how these processes are different in different vascular beds that vary in biological and physical composition.

The following chapters show work using novel biosensors and intravital imaging techniques to address those questions and advance the understanding of how molecular physics shape the biology of thrombus formation. Chapter two describes a novel biosensor capable of measuring thrombin activity within thrombi formed ex vivo and in vivo. Using this sensor we demonstrated that thrombin activity is dependent upon local transport conditions in a microfluidic device, and is restricted to the core region in vivo. To determine if local transport properties are different within the core and shell regions in

vivo we developed a soluble protein transport sensor in chapter three. This sensor demonstrated that within the platelets that go on to form the core region soluble proteins are retained significantly longer than the platelets that make up the shell region. Chapter 4 describes computational studies done in order to test how various structural changes within the thrombus can impact local protein transport, and demonstrates that differences in platelet packing within the core and shell region likely drive the observed differences in protein transport. In chapter five we test this hypothesis using mice with a defect in platelet retraction causing increased protein transport rates in the core region. This alteration of protein transport correlated with decreased thrombin function within the thrombus leading to decreased core size and fibrin deposition.

We extended our model of thrombus structure regulating solute distributions in chapter 6 measuring how thrombus development alters delivery of plasma proteins into the surrounding tissue plane. Finally, in chapter 7 we developed a novel technique to observe thrombus formation in the mouse femoral artery and vein to compare to our observations in the mouse microcirculation. In aggregate, this thesis aims to determine how the interplay between thrombus structure and the spatiotemporal distribution and transport of biologically relevant solutes impacts thrombus formation in various biologically relevant conditions.

CHAPTER 2: Platelet-targeting sensor reveals thrombin gradients within blood clots forming in microfluidic assays and in mouse

This research was originally published in the *Journal of Thrombosis and Haemostasis*. Welsh JD, Colace TV, Muthard RW, Stalker TJ, Brass LF, Diamond SL. *J Thromb Haemost*. 2012;10(11):2344-2358.

2.1 Introduction

During coagulation, membrane associated prothrombinase (Xa/Va) cleaves prothrombin to release active thrombin, a soluble protease that can cleave protease activated receptors (PAR1 and PAR4 on human platelets) as well as activate fibrinogen to fibrin monomer. As a soluble species, thrombin is subject to diffusive transport as well as convective transport via intrathrombic permeation (if pressure gradients exist [54,61]) or via blood flow once thrombin leaves the clot [62,63]. Additionally, thrombin can bind platelet GPIb to localize its activity on the platelet surface [64,65] or thrombin can be inhibited by antithrombin or sequestered into polymerizing fibrin. The generation and subsequent transport of activated Factor X (Xa) and thrombin from tissue factor (TF)-rich sites of Xa and activated Factor IX (IXa) formation have an important controlling effect on the rate and extent of thrombus growth through platelet activation and fibrin stabilization [59,66]. Formation of the intrinsic tenase (Factors IXa/VIIIa), as well as feedback pathways such as thrombin-mediated production of Factor XIa also may impact the spatiotemporal concentration profiles of thrombin within a clot [67]. Thrombin activation of platelets induces the release of ADP, thromboxane, as well as pro-inflammatory cytokines and

surface display of P-selectin, thus promoting white blood cell recruitment and inflammation [16].

Various techniques currently exist to monitor thrombin in closed systems. These techniques measure endogenous end-products like thrombin-antithrombin (TAT) or exogenously added reporter substrates [68-71]. Under physiological flow conditions, thrombin detection becomes extremely difficult due to the convective removal of coagulation products or fluorogenic sensing molecules. Fibrin deposition can be monitored under flow as an important surrogate of thrombin activity. However, fibrin deposition is also subject to convective effects via fibrin monomer dilution and flow-modulation of fibrin assembly [60,72]. Also, thrombin can affect platelet deposition at concentrations below that needed to generate fibrin [62,66].

Despite its central role, thrombin activity has never been visualized in vivo. We developed a thrombin sensitive antibody (ThS-Ab) that binds platelet CD41 (α_{IIb}) to ensure its incorporation throughout the growing thrombi. The sensor consisted of a thrombin sensitive peptide (ThS-P) that was linked to an anti-CD41 antibody and was rapidly cleaved by thrombin to provide a fluorescent signal. In this study, we characterized this thrombin sensor to provide novel information about thrombin localization on activated platelets and within clots.

2.2 Materials and Methods

2.2.1 Materials

Thrombin-sensitive peptide (ThS-P) *azidoacetyl alanine-K(5FAM)GALVPRGSAGK(CPQ2*) was custom synthesized (2143 MW, >95% purity; CPC scientific, Sunnyale, CA) and dissolved in DMSO (20 mM ThS-P). The cleavage site VPR|G was chosen based on the strong preference by thrombin for proline in the P2 position [60] and the prior use of boc-Val-Pro-Arg-MCA [16]. The following reagents were stored according to manufacturers' instructions: dibenzylcyclooctyne-NHS ester (DBCO) (Click Chemistry Tools, Scottsdale, Az), mouse monoclonal anti-human CD41 PM6/248 (azide free; AbD Serotec, Raleigh, NC), PE-mouse monoclonal anti-human CD61, Cy-5 Annexin V (BD Pharmigen, San Diego, CA), Cy5-anti human fibrin (Gift from Dr. M. Poncz, Children's Hospital of Pennsylvania), anti-collagen type 1 antibody and PE-mouse monoclonal anti-human CD42b (Ak2; Abcam, Cambridge, MA), anti-mouse CD41 F(ab)2 fragments (clone MWReg30, BD Bioscience), anti-mouse fibrin (clone 59D8, gift from Dr. H Weiler, Blood Center of Wisconsin), thrombin, Gly-Pro-Arg-Pro (GPRP), corn trypsin inhibitor (CTI; Haematologic Technologies, Essex Junction, VT), sodium citrate (Sigma-Aldrich, St. Louis, MO), HEPES ((N-(2-hydroxyethyl)piperazine-*N'*-2-ethanesulfonic acid; Fisher Scientific, Pittsburg, PA), recombinant tissue factor (Sekisui, Stamford, CT), phosphatidylcholine (PC), phosphatidylserine (PS), and biotinylated phosphoethanolamine (bPE, Avanti Polar Lipids, Alabaster, Al), Streptavidin and Triton X-100 (Sigma-Aldrich, St. Louis, MO), and BioGel P-6 gel (Bio-Rad, Hercules, CA). In accordance with University of Pennsylvania Internal Review Board, human blood was collected from healthy donors via venipuncture and anticoagulated with CTI (50 μg/mL)

or sodium citrate (1:9 by volume) and then recalcified with $CaCl_2$ (15 mM final concentration).

2.2.2 Thrombin sensitive antibody (ThS-Ab) synthesis

The thrombin sensitive antibody was used for microfluidic and in vivo studies, but all kinetic data was obtained from the peptide alone. Therefore, the exact concentration of thrombin sensitive peptide per antibody molecule is unknown limiting the interpretation of the resulting signal. A volume of 10 μL of anti-human CD41 (1 mg/mL, azide free) was mixed with 5 μL of DBCO-NHS ester (357 μM, 0.7% DMSO by vol. in HEPES Buffered Saline (HBS), pH 7.4) and brought to a final volume of 40 μL with HBS. The DBCO-NHS ester labeling reaction was incubated at room temperature for 30 min. DBCO-NHS ester labeling of the anti-human CD41 was then quenched by the addition of 2.5 μL of TRIS-HCl (1 M, pH 8.0). After quenching, 4.5 μL of ThS-P (2 mM, 10% DMSO by volume in HBS) was added to a final reaction volume of 47 μL. The ThS-P labeling reaction was incubated in the dark at room temperature for 4 hr. ThS-Ab was isolated by gel filtration on P6-Gel maintained in HBS, resulting in 110 μL of purified ThS-Ab (0.05 mg/mL, as measured by absorption at 280 and Bradford assays) in HBS (Figure 2-1). ThS-P and ThS-Ab fluorescence was measured in a FluoroSkan Ascent (485 nm excitation/538 nm emission). ThS-Ab fluorescence on platelets was measured by flow cytometry (Accuri C6) based on a forward scatter/side scatter gate or by positive signal for PE-anti-CD42b.

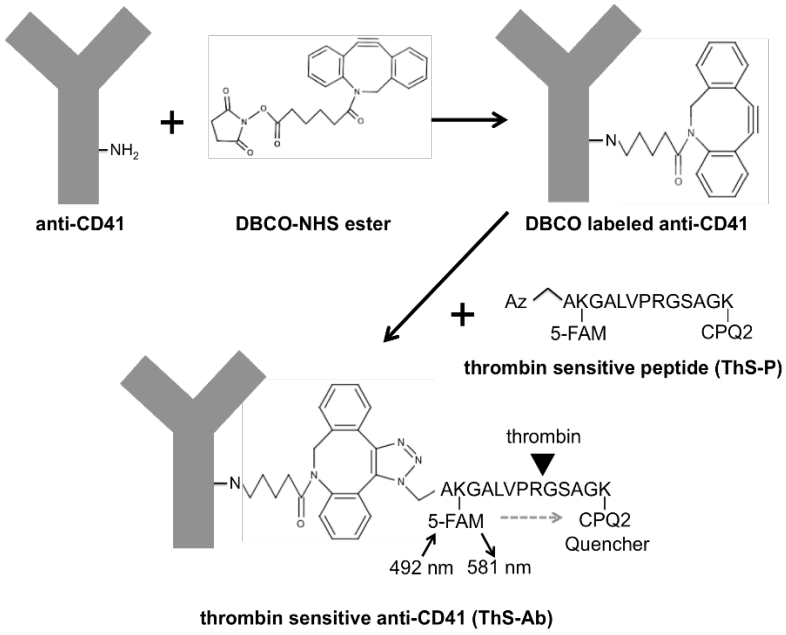

Figure 2- 1 Click chemistry for cross linking a thrombin-sensitive N-terminal azidopeptide (ThS-P) to anti-CD41.

Dibenzylcyclooctyne-NHS ester (DBCO) was used to label free amine groups on anti-human CD41. The ThS-P contains a 5-FAM labeled Lys_2 and a CPQ2 (quencher) Lys_{13}. The Lys_2 and Lys_{13} are separated by a thrombin cleavage site at Arg_8. The azide group specifically attacks the triple bond in DBCO linking the ThS-P to the anti-human CD41. Thrombin-mediated cleavage of the peptide releases the CPQ2 quencher, resulting in a fluorogenic signal at 581 nm.

2.2.3 Microfluidic device for clotting on collagen/tissue factor surfaces

Polydimethylsiloxane (PDMS) microfluidic channels (250-μm wide x 60 μm-high) were generated as previously described [66,73]. Tissue factor liposomes (PS/PC/bPE) were generated for linking to collagen via streptavidin-conjugated anti-collagen antibody [66,73,74]. A PDMS device was used to pattern fibrillar collagen (Chronolog) in a 250 μm-wide stripe followed by binding of the biotinylated lipidated TF. A second PDMS device

created flow channels to run perpendicular across the collagen/TF surface. Whole blood with ThS-Ab (5 μg/mL) and Cy5-anti-fibrin (0.5 μg/mL) was perfused at a shear rate of 100 s^{-1} over the coated surface using a syringe pump (Harvard Apparatus PHD 2000, Holliston, MA). Fluorescent microscopy (IX81, Olympus America Inc., Center Valley, PA) was used to image clot formation in real time.

2.2.4 Microfluidic device for generation of transthrombus pressure gradient

An additional PDMS microfluidic device was used for creating a transthrombus pressure gradient across a thrombus as it forms on a porous collagen/TF liposome surface (Figure S2-7). Pressure was measured upstream, downstream, and at the exit of the collagen scaffold using pressure transducers (Honeywell Sensing & Control, Golden Valley, MN). Initial wall shear rate (521 s^{-1}) and constant pressure were maintained using an upstream syringe pump (Harvard Apparatus PHD Ultra, Holliston, MA) containing CTI-treated whole blood along with a downstream syringe pump containing a Ca^{2+} buffer (5 mM). Each syringe pump was controlled by LabVIEW (National Instruments, Austin, TX) to achieve a specified blood flow rate and pressure at the site of the collagen plug. Thrombotic events were visualized on a side view of the collagen scaffold which contained 50 μm diameter posts and a 250 μm-long blood contact region [75,76]. Prior to loading the collagen scaffold onto the posts, the PDMS device was placed on a Sigmacote (Sigma-Aldrich, St. Louis, MO) treated glass slide and coated with 10% BSA for 30 min. Human type I collagen (Advanced BioMatrix, San Diego, CA) was polymerized at 2.4 mg/mL in a ratio of 8:1:1 mixture of collagen, 0.09M NaOH, 10X PBS. Biotinylated goat polyclonal anticollagen (4 μg/mL) and streptavidin (10 μg/mL) were

added subsequently in 5 minute intervals at a 1:10 ratio with polymerized collagen. TF liposomes were then added in a 1:20 ratio with collagen for 10 min. Collagen/TF solution was pulled through the upstream and downstream pressure ports into the collagen scaffold region on the device using a 1 mL syringe. Immediately following collagen/TF localization, channels were rinsed with Ca^{2+} buffer (5 mM). Imaging protocols were identical to the previously mentioned device and real time pressure data was collected through LabVIEW (Figure S1B).

2.2.5 Mouse intravital microscopy

Mouse studies were approved by the IACUC of the University of Pennsylvania. Intravital microscopy was performed as previously described [76]. Mice were anesthetized with sodium pentobarbital (90 mg/kg), and maintained at 5 mg/kg through a jugular vein cannula. The cremaster muscle was exposed and kept under constant drip of buffer (135 mM NaCl, 4.7 mM KCl, 2.7 mM $CaCl_2$, 18 mM $NaHCO_3$, pH 7.4) The mThS-Ab (4.5 μg) and anti-mouse fibrin (5 μg) were infused into the mouse. Injuries, in selected arterioles, were made with a pulsed nitrogen dye laser at 440 nm. Confocal fluorescent and brightfield images were taken every 30 sec for 10 min after injury using an Olympus BX-61WI fluorescence microscope (Olympus) coupled to a CSU-X1 spinning disk confocal head (Yokogawa) and CoolSnap HQ CCD camera (Photometrics).

2.3 Results

2.3.1 Characterization of thrombin cleavage of ThS-P and ThS-Ab

The Michaelis-Menten parameters for thrombin cleavage of ThS-P at 50 nM thrombin at 37C were K_m = 40.3 μM and k_{cat} = 1.5 s^{-1} (Figure 2-2A). ThS-P signal in response to thrombin generated by whole blood activation was tested by addition of 0, 2.5, or 25 pM TF to citrated whole blood diluted 1:10 with HBS with 15 mM $CaCl_2$ (Figure 2-2B). Without TF, the contact pathway was insufficient at this dilution of blood to generate ample thrombin during a 1600 sec incubation (Figure 2-2B, triangles). Upon the addition of increasing amounts of lipidated TF, the extrinsic tenase pathway was sufficient to trigger thrombin generation after a short initiation phase. The dose response and rates of thrombin cleavage of ThS-Ab were quite similar to those observed with ThS-P, indicating that the synthesis reaction did not significantly alter the kinetics of ThS-P cleavage by thrombin (Figure 2-2C). To determine the specificity of thrombin cleavage of ThS-P, hirudin (1.75 μM), a thrombin specific inhibitor, was added to whole blood (treated with CTI and diluted 1:5 with Hepes buffer pH 7.4) in the presence of TF (25 pM) leading to complete ablation of ThS-P signal (Figure S2-8), demonstrating that the sensor was highly specific for detection of thrombin activity. The maximal ThS-Ab signal was ~50-fold less than that of the maximal ThS-P signal due to the concentration of the ThS-Ab stock solution (50 μg/mL) deployed in order to avoid over-diluting the blood.

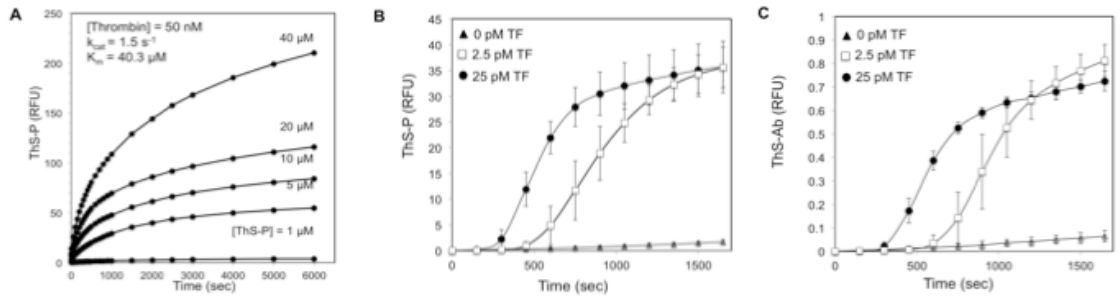

Figure 2- 2 Kinetics of ThS-P cleavage by thrombin was determined by titrating ThS-P concentration in the presence of 50 nM thrombin.

Thrombin cleavage resulted in a 35-fold increase in ThS-P fluorescence (K_m = 40.3 µM and k_{cat} = 1.5 s^{-1}) **(A)**. To determine if the synthesis of ThS-Ab affected the rate of cleavage by thrombin both ThS-Ab (0.05 mg/mL) **(B)** and ThS-P (5 µM) **(C)** were added to citrated whole blood (re-calcified) with added tissue factor (TF 2.5 pM or 25 pM). Both ThS-P and ThS-Ab had similar rates of cleavage as well as a dose response to increasing amounts of TF.

2.3.2 Platelet surface localization of ThS-Ab and signal in response to thrombin

To detect thrombin activity on the platelet surface, flow cytometry was performed on whole blood labeled with ThS-Ab in the presence or absence of added TF (25 pM) (Figure 3). Citrated whole blood was incubated for 5 min with ThS-Ab (10 µg/mL) and then diluted 1:10 with the addition of 5 mM GPRP peptide to prevent fibrin polymerization and 15 mM $CaCl_2$. Without the addition of TF, very little change in ThS-Ab signal was observed after 15 min (Figure 2-3A). With 25 pM TF, thrombin was generated as indicated by a 20-fold increase in signal by 14 min. To confirm the ThS-Ab signal was platelet specific, only cells positive for CD42b were positive for ThS-Ab signal in response to thrombin generation (Figure S2-8).

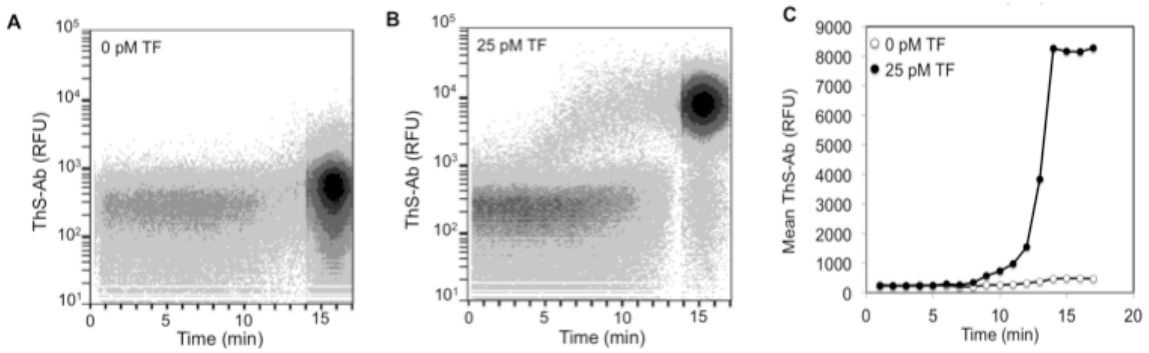

Figure 2- 3 Real time flow cytometry of whole blood labeled with ThS-Ab to detect platelet localized thrombin activity following TF addition.

Whole blood was incubated with ThS-Ab (1:50 volume) either in the absence (A) or presence of 25 pM TF (B). The mean fluorescence of the gated events demonstrated that TF caused a large increase in the platelet-specific thrombin signal (C).

2.3.3 Thrombin sensing in a microfluidic model of thrombosis

Thrombin localization within a growing thrombus under hemodynamic conditions was observed by perfusion of ThS-Ab labeled whole blood (CTI-treated) over a patterned collagen surface with antibody-linked lipidated TF at a shear rate of 100 s^{-1}. The collagen patterning of a stripe resulted in a discrete 250 μm wide x 250 μm long square of collagen when the fluidic channel was overlaid perpendicular to the stripe. The upstream end of this discrete collagen region can be seen in Fig. 2-4 and Fig. S3. At 0, 0.1, or 1 molecule-TF/μm^2 (as determined based on ref. 19), the simultaneous platelet deposition, fibrin deposition, and ThS-Ab signal were monitored in real time (Figure 2-4A-C). Whole blood with the thrombin inhibitor PPACK (100 μM) was perfused over the 1 molecule-TF/μm^2 surface. In comparing Fig. 2-4C and 2-4D where blood was perfused over TF-labeled collagen with and without PPACK, PPACK caused a >50 %

decrease in platelet deposition and blocked detectable fibrin signal. However, even 100 μM PPACK was unable to fully block generation of the ThS-Ab signal (Figure 2-4D). This indicated that thrombin produced as a result of the TF surface was able to cleave the platelet bound ThS-Ab before cleaving fibrinogen or encountering PPACK. Thus, ThS-Ab was a more sensitive metric of local thrombin production than antibody-based detection of fibrin polymerization.

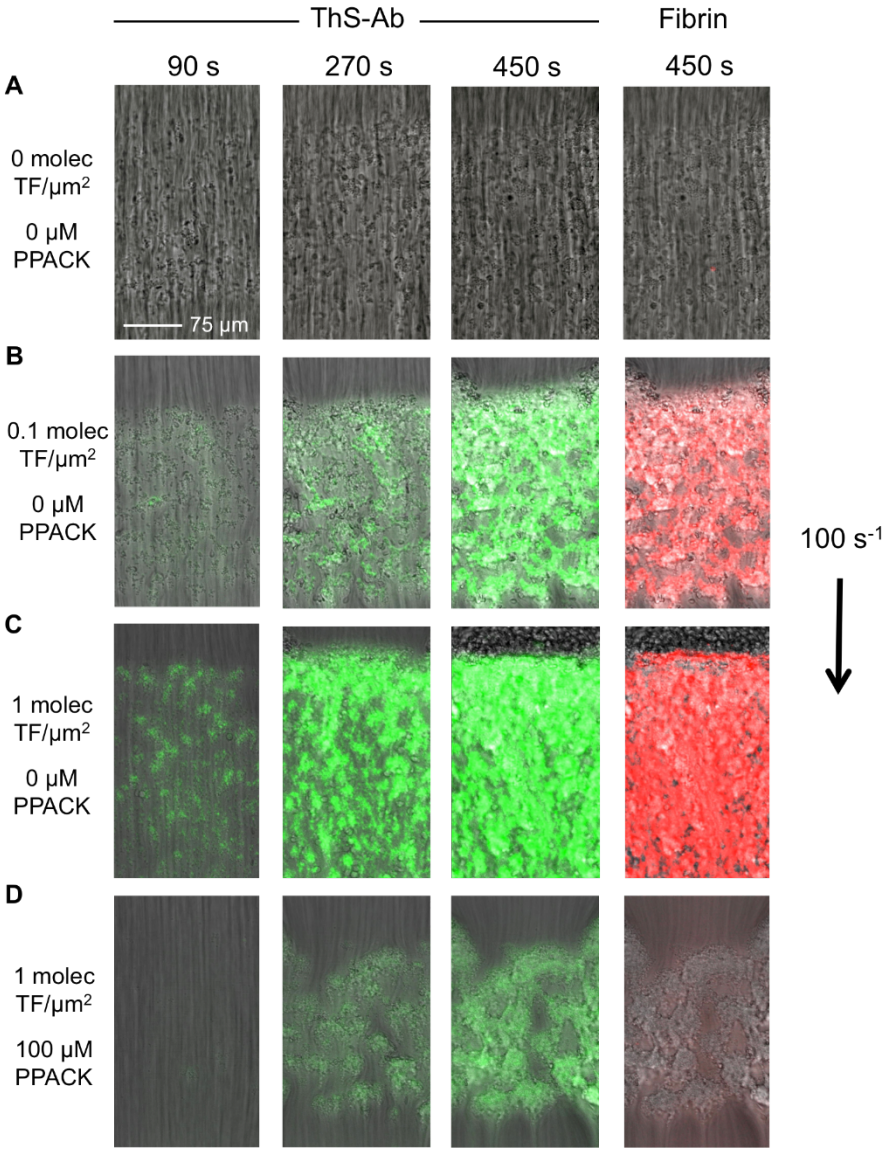

Figure 2- 4 Detection of thrombin in a blood clot forming under flow conditions.

A microfluidic model of coagulation was generated by flowing whole blood (100 s^{-1}) over collagen with linked lipidated TF. ThS-Ab (green) and fibrin (red) were observed over time while flowing over collagen (A), collagen and TF (0.1 molec/μm^2) (B), collagen and TF (1 molec/μm^2) alone (C), and collagen and TF (1 molec/μm^2) in the presence of 100 μM PPACK (D).

At 0.1 molecule-TF/μm^2, the amount of thrombin generation decreased by ~65% (as indicated by fluorescence intensity) compared to 1 molecule-TF/μm^2. Unique localized zones of thrombin generation were detectable at early times during thrombus formation (especially near the side walls of the device) that coexisted with other zones in the image field that lacked ThS-Ab fluorescence (Figure S2-9). During early time points of blood perfusion over 0.1 molecule-TF/μm^2, slightly more platelet deposition was seen at the front of the collagen/TF surface while the ThS-Ab and anti-fibrin signal was located down stream of the platelet mass (as previously observed [66]). This indicated that the observed signal was in fact due to increased levels of thrombin activity and not increased platelets with bound ThS-Ab. The shear rates on the periphery side walls of the flow chamber were lower than in the center with consequent reduced rates of dilution of thrombin from the surface into the flow stream, thus allowing for increased accumulation of thrombin and fibrin along the periphery of the chamber [77]. Without added TF, no thrombin or fibrin was formed after 450 sec. After 10 to 13 minutes of flow over collagen (no TF), ThS-Ab fluorescence and fibrin formation were finally detected (not shown), most likely due to formation of XIIa despite the presence of CTI [16].

2.3.4 Microfluidic model of transthrombus pressure gradient-driven permeation during hemostasis

As a thrombus builds up at a site of vascular rupture or wounding, a pressure drop (ΔP) exists across the clot because the intraluminal pressure (up to arterial levels of 60 to 120 mm-Hg) exceeds the interstitial pressure (~10-12 mm-Hg) [78,79]. The pressure-driven permeation of plasma or serum across the porous clot structure and into the porous interstitial matrix at the point of injury represents a convective transport mechanism. To drive transthrombus permeation, a microfluidic device was developed that allowed a thrombus to form on a supported porous collagen plug at a controlled shear rate of blood perfusion (Figure 2-5A). Since atmospheric pressure was maintained on the opposite (non-blood contacting) side of the collagen plug, a controlled pressure drop independent of the wall shear rate was maintained across the collagen and thrombus (Figure 2-5A and Figure S2-7), thus mimicking a bleed into the interstitial space. The pressure drop was set to ΔP = 3200 Pa (32 mm-Hg) or ΔP = 0 Pa (by blocking the outlet) to control the permeating flow across the thrombus (Figure S2-7). Blood labeled with ThS-Ab, fluorescent anti-CD61, and fluorescent anti-fibrin was perfused at 521 s^{-1} over the collagen/TF plug. At ΔP = 3200 Pa, the increased permeation of thrombin across the thrombus resulted in ThS-Ab signal being only present in thin areas within the thrombus nearest the collagen/TF surface (Figure 2-5B). At ΔP = 3200 Pa, ample fibrin was formed within the collagen due to permeation of thrombin and fibrinogen into the collagen (Fig. 2-5D). Without a pressure drop (ΔP = 0), the thrombin transport within the thrombus was largely due to diffusion since no permeation across the collagen was possible. This resulted in a 5-fold increase in ThS-Ab signal generated within the

thrombus, compared to the case of ΔP = 3200 Pa (Figure 2-5B-C). Fibrin signal was measured at the surface of the collagen/TF matrix as well as 10 μm into the thrombus to observe the rate of deposition (Figure S2-11). At the surface of the collagen/TF matrix, the rate of fibrin deposition was unchanged by the change in ΔP and altered thrombin localization pattern (Figure S2-11A). However, at 10 μm into the thrombus, the rate of fibrin deposition was decreased ~45% when ΔP = 3200 Pa and thrombin levels were decreased within the thrombus (Figure S2-11B).

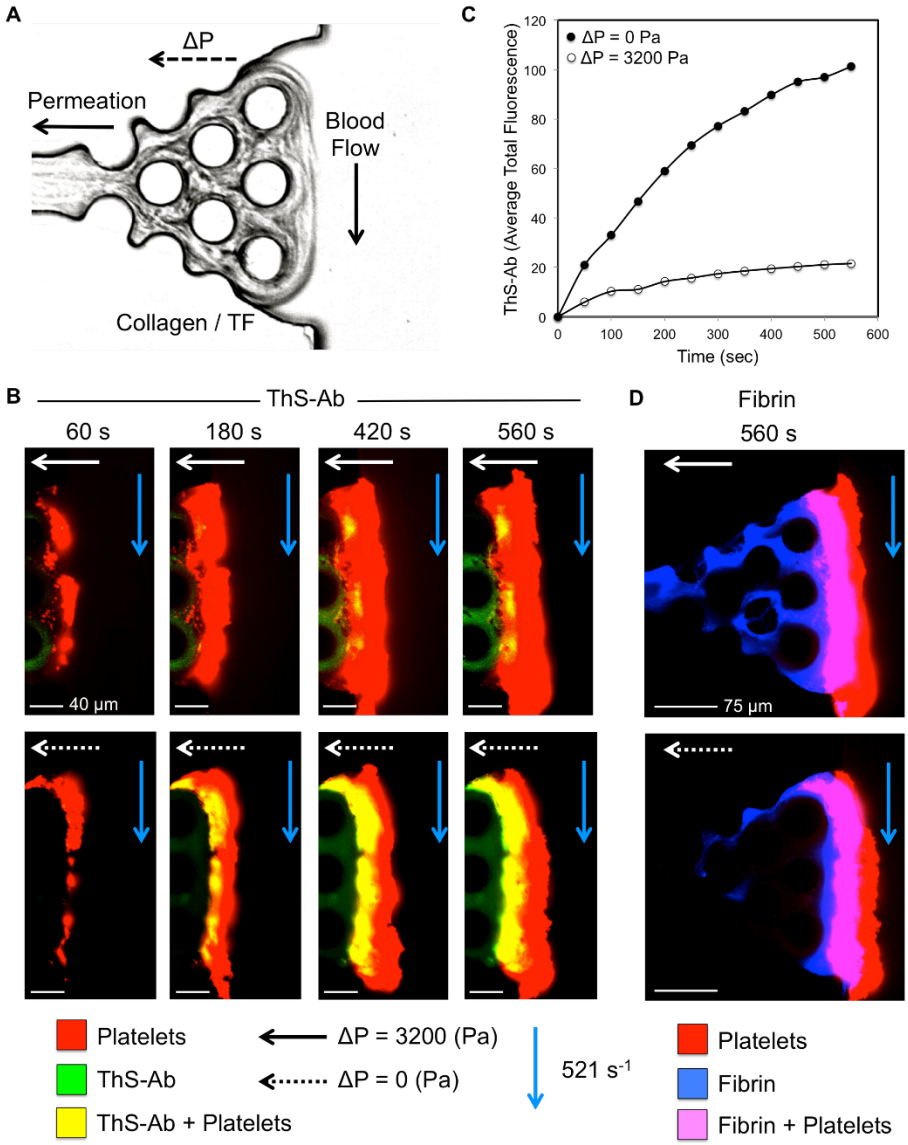

Figure 2- 5 A microfluidic model of transthrombus pressure gradient modulation.

A thrombogenic surface of collagen and TF was used in a microfluidic device to provide a side view of thrombus formed under flow conditions while a transthrombus pressure gradient drives permeation across the clot (A). Blood was perfused at 521 s^{-1} and ThS-AB (green), anti-fibrin (blue) and anti-CD61 (red) were observed over time during thrombus formation. The pressure drop across the surface was altered to change the transport pattern of thrombin (ΔP = 3200 Pa or 0 Pa) (B). The pressure drop caused a decrease in thrombin presence in the clot (C). To quantify the rate of fibrin deposition the fluorescence signal of anti-fibrin was monitored at different distances from the coagulation surface (0 and 10 μm) for the different pressure drop states (D).

2.3.5 In vivo monitoring of thrombin within a thrombus

Laser induced injury created stable thrombi in mouse cremaster arterioles [76]. Mice were perfused with anti-fibrin and ThS-Ab anti-mouse CD41 (mThS-Ab) prior to injury. Images were taken of the bright field thrombus formation as well as fibrin deposition and mThS-Ab every 30 sec for 10 min. Similar to microfluidic model thrombosis, the mouse thrombi showed a core of mThS-Ab signal that co-localized with fibrin deposition (Figure 2-6 and Supplemental Movie M1). Thrombus growth was stabilized where high mThS-Ab signal was present, as low mThS-Ab regions appeared to be more prone to shearing forces of the blood flow and disassociated from the thrombus over time. The stable thrombus core nearest the injury site had the highest mThS-Ab signal and was anchored by a layer of fibrin deposition at the vessel wall at the site of injury. During early thrombosis the thrombus mass was large with a core of high mThS-Ab signal and a more diffuse signal occurred in the outer zones of the thrombus. After 5 min, the

remaining clot was stable and had high mThS-Ab signal and high fibrin deposition (Figure 2-6). To specifically inhibit thrombin function, 15 μg of hirudin was infused prior to injury and inhibited >90% of ThS-Ab signal 2 minutes post-injury (Figure S2-12). Similar to the in vitro findings with hirudin, ThS-Ab is a specific detector of thrombin activity, even in an *in vivo* thrombotic setting.

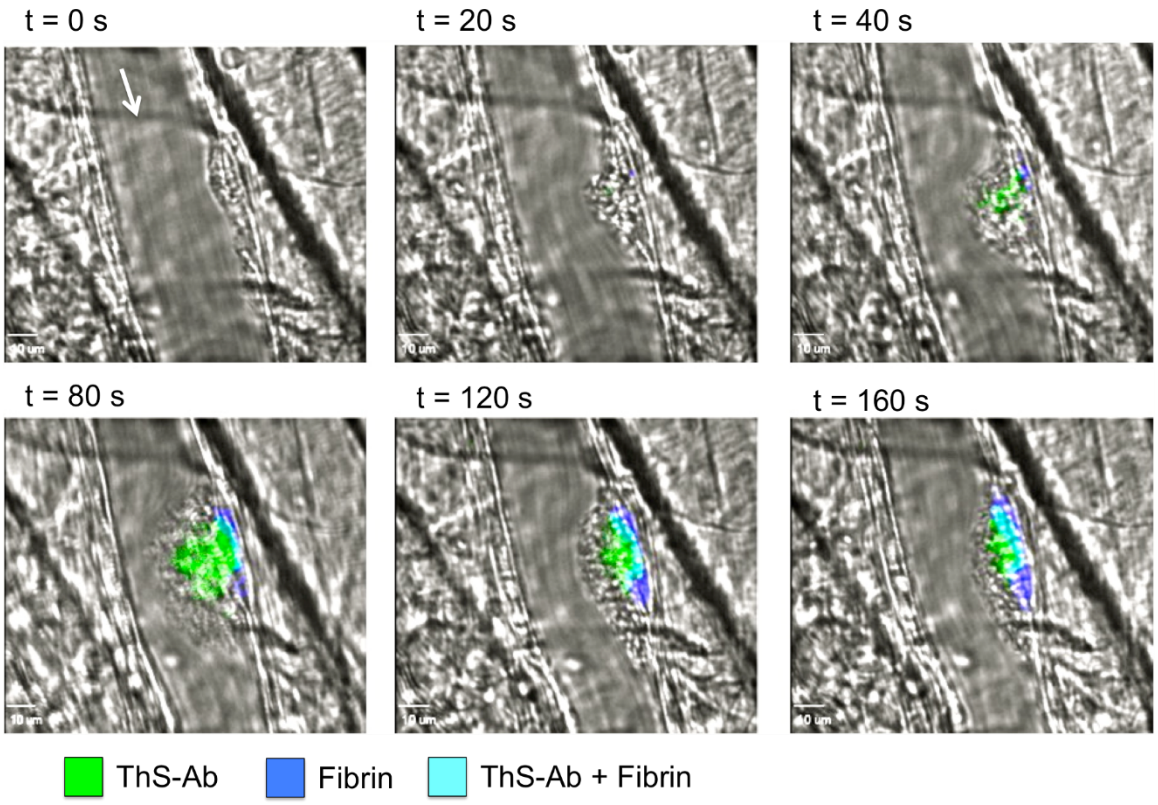

Figure 2- 6 A mouse laser injury model was used to observe mThS-Ab signal in vivo.

A mouse laser injury model was used to observe mThS-Ab signal *in vivo*. The site of injury was observed using confocal fluorescent microscopy. Blood flow is denoted by an arrow at t = 0. ThS-Ab signal (green) is first observed at 40 seconds post-injury that co-localizes with fibrin (blue). As the clot grows ThS-Ab signal spreads away from the vessel wall as fibrin stays close to the vessel wall. After 2 minutes post-injury the clot

begins shrinking and the core remains the area of high fibrin and high ThS-Ab signal and a shell of platelets that are thrombin-negative.

2.4 Discussion

The localization of thrombin is dictated by the site of generation and the movement of thrombin which is controlled by diffusion, binding, and convection. Detection of thrombin activity via fluorogenic substrates is less suited under flow conditions due to convective removal of the soluble reporter. We report, for the first time, detection of intrathrombus thrombin activity under flow conditions using ThS-Ab in microfluidic assays and in mouse.

In order for ThS-Ab to serve as a stable marker for platelet surface-thrombin activity, it must localize to the surface of platelets and provide a robust signal upon thrombin generation. By flow cytometry, platelets displayed a ~20-fold increase of ThS-Ab signal after 10 minutes of incubation with TF (Figure 2-3). Platelets became positive for ThS-Ab signal, as determined by co-staining with platelet-specific anti-CD42b and ThS-Ab signal (Figure S2-9). ThS-P cleavage has a $k_{cat}/K_m = 0.375$ while fibrinogen has a $k_{cat}/K_m = 11.3$ [78]. Despite the difference in kinetics, both *in vitro* and *in vivo* thrombosis models showed fibrin deposition and ThS-Ab signal as spatially and temporally co-localized (Figure S2-10 and Figure 2-6).

To visualize the activity of thrombin within a hemostatic thrombus, a microfluidic device was used to trigger thrombosis on a pro-coagulant surface (collagen and TF) which provided a side view observation. To further enhance the physiological relevance of this

microfluidic system, a pressure drop was established across the pro-coagulant surface to study the effect of transthrombus permeation (Figure 2-5A). We have previously demonstrated that there is plasma loss using fluorescent plasma tracers as well as visible red blood cell escape into the endothelial space following laser injury. The microfluidic device in Fig. 2-5 recreates certain aspects of in vivo vessel injury such as movement of blood or plasma across a porous clot or wall structure due to a pressure-driven permeation or flow. By combination of ThS-Ab with a novel microfluidic device that mimics hemostasis, this is the first study of thrombin levels in clots formed with a transthrombus pressure drop to drive permeation in a direction perpendicular to blood flow and in the direction of the interstitial space. Transthrombus permeation into the interstitial space reduced platelet-associated thrombin activity and enhanced fibrin polymerization into the interstitial region (Figure 2-5B-D). Fibrin is shown occurring in the interstitial space especially when a pressure drop exists across the collagen-TF/thrombus surface (Fig. 2-5D and Figure S2-11). With zero pressure drop, the high level of thrombin formed at the collagen-TF/platelet interface (Fig. 2-5B) resulted in rapid fibrinogen conversion to immobile fibrin, which does not move into the collagen region. When the pressure drop is present, lower levels of thrombin accumulate (possibly because of dilution by permeation into the interstitial space). Fibrinogen and lower levels of fibrin monomer can thus undergo permeation into the collagen region. This allows the fibrin to polymerize within the interstitial region as fibrin monomer is driven by the permeation of plasma through the interstitial space. While fibrin polymers are unable to penetrate into the interstitial space, thrombin is still highly diffusible and can enter into the interstitial space even without pressure drop induced flow. ThS-Ab free in solution is also able to penetrate into the interstitial area by diffusion. Consistent with the *in vitro* observation of Fig. 2-5, interstitial fibrin has routinely been detected in the mouse laser

injury model [12]. While not well studied, the formation of fibrin in the interstitial region outside a blood vessel may be an attribute of in vivo hemostasis due to pressure driven-permeation across a platelet mass.

To verify the ThS-Ab sensor in an *in vivo* context, ThS-P was attached to anti-mouse CD41, infused into mice, and observed following laser injury of the cremaster muscle (Figure 2-6). Platelets quickly formed a plug at the site of injury without thrombin activity (t = 0 sec), and 20 sec after the injury both fibrin and thrombin signal appeared at the site of injury (Figure 2-6). The fibrin signal was localized close to the vessel wall while the thrombin signal was highest close to the vessel wall but thrombin appeared to diffuse out into the thrombus as well. After 80 sec post-injury, there was a large amount of fibrin deposition along the vessel wall that co-localized with the highest concentration of thrombin activity, however lower thrombin activity was also detected away from the vessel wall in the thrombus, but thrombin activity was not detected in the outer most shell of the thrombus. After 80 sec post-injury, the thrombus decreased in size and the area positive for platelet also decreased, as the outer most shell of the thrombus remained thrombin-negative. These results indicate that thrombin initially localizes at high concentrations at the site of injury and was capable of producing fibrin. Decreased thrombin activity and increased convection may also contribute to the lack of fibrin formation further away from the vessel wall. At 160 seconds post-injury, the fibrin plug and areas of high thrombin activity remain stably with an outer shell of thrombin-negative platelets. These results show that thrombin was produced at the site of injury and was most active along the vessel wall leading to a stable fibrin plug. Thrombin was also active further from the vessel wall but to a lesser extent and did not produce stable platelet deposits or fibrin polymers at large distances from the site of injury (Figure 2-6).

To our knowledge, this is the first direct imaging of thrombin activity in a forming thrombus in vivo.

The use of a fluorogenic peptide sequence linked to an antibody by click chemistry represents a simple and general approach for visualizing proteases. The approach may have also utility for the study of other proteases involved in thrombosis, inflammation, or metastasis. We demonstrated that thrombin activity can be detected on the time frame of a real clotting event. The sensor allowed a very sensitive detection of thrombin in situations where fibrin was not necessarily generated. Also local transport processes within the clots were shown to modulate the thrombin signal.

2.5 Supplemental Materials

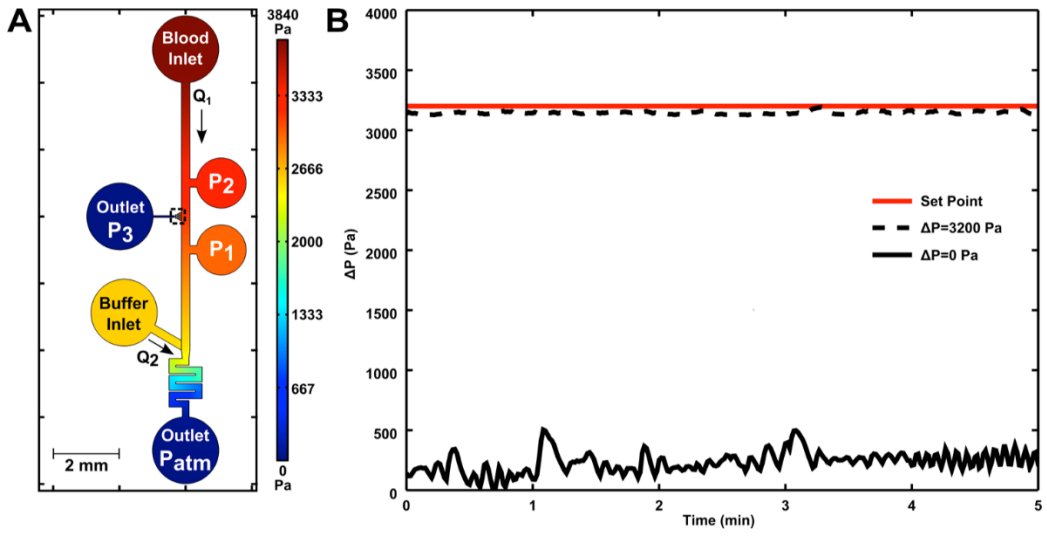

Figure 2- 7 Design of microfluidic device to measure transthormbus pressure drop.

A microfluidic device for perfusion of blood at flow rate Q1 from an inlet across a collagen plug that covers an outlet maintained at P3 = atmospheric pressure. Control of buffer flowrate (Q2) controls the pressure at P2 and P1 as well as the pressure drop maintained across the collagen plug. A COMSOL simulation of the microfluidic device shows pressure control throughout the device (A). Positions P_1, P_2, and P_3 demonstrate the locations of 0-1 psig pressure transducers that were used to measure the pressure drop across the coagulation matrix. Pressure was controlled and measured in real time through LabVIEW. The pressure drop was set at 3200 Pa (dashed line) to mimic physiological arterial pressure drops and reduced near 0 Pa (solid line) by obstructing flow exiting the collagen scaffold (B).

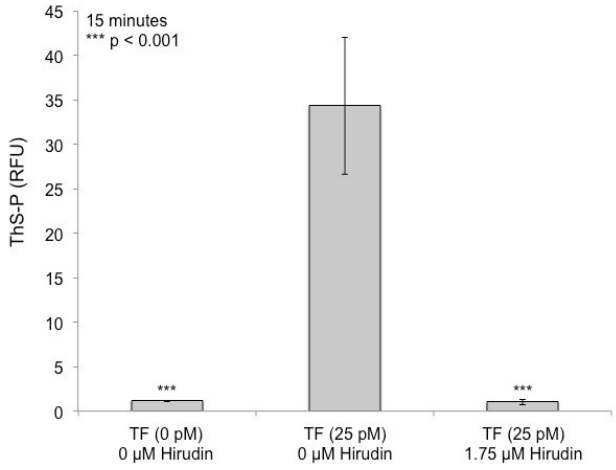

Figure 2- 8 ThS-P is specific from thrombin cleavage.

The cleavage of ThS-P was monitored using a fluorescent plate reader. ThS-P (5 μM) was incubated with whole blood treated with CTI and diluted 1:5 with Hepes buffer. The reactions were then incubated with TF (either 0 pM or 25 pM), and Hirudin (either 0 μM or 1.75 μM) and ThS-P cleavage was monitored over time. Samples without TF failed to produce thrombin while TF (25 pM) was capable of inducing ThS-P cleavage that plateaued at 15 minutes. When Hirudin, a thrombin specific inhibitor, was added even TF at 25 pM was unable to induce ThS-P cleavage.

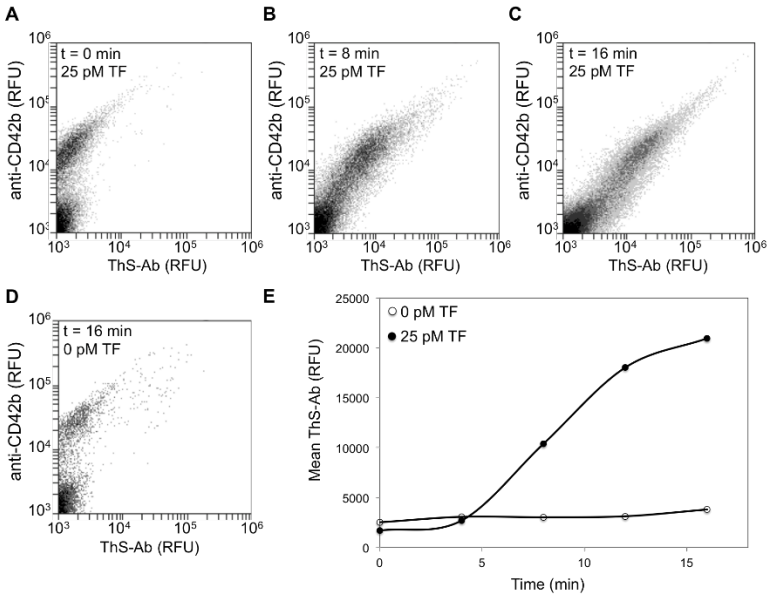

Figure 2- 9 Kinetics of thrombin activity detected with ThS-Ab.

Flow cytometry of clotting whole blood demonstrated that the ThS-Ab signal detected thrombin generation specifically on platelet surfaces. Citrated whole blood was labeled with platelet marker anti-CD42b and ThS-Ab (1:50 volume). The blood was exposed to TF (25 pM) and $CaCl_2$ at t = 0. Samples were taken at 0 min (A), 8 min (B), or 16 min (C). In a replicate well with no TF added, a sample was taken at 16 min (D). The mean fluorescence of the anti-CD42b positive cells were graphed of both TF exposed and unexposed (E).

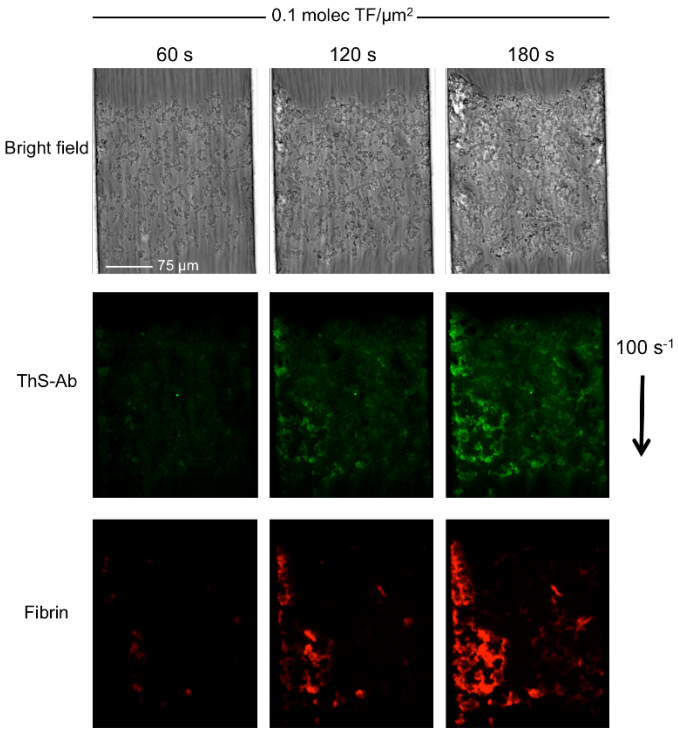

Figure 2- 10 Co-localization of ThS-Ab and fibrin during thrombus formation under flow.

During platelet deposition on collagen/TF surfaces, the platelet deposits displayed heterogeneity in thrombin activity and fibrin deposition. Whole blood was perfused ($100s^{-1}$) over a collagen and TF (0.1 mol/μm^2) surface and fluorescent microscopy was used to observe ThS-Ab and anti-fibrin signal during coagulation. Distinct areas of high thrombin generation were indicated by ThS-Ab (green) and these regions co-localized with areas of high fibrin deposition (red).

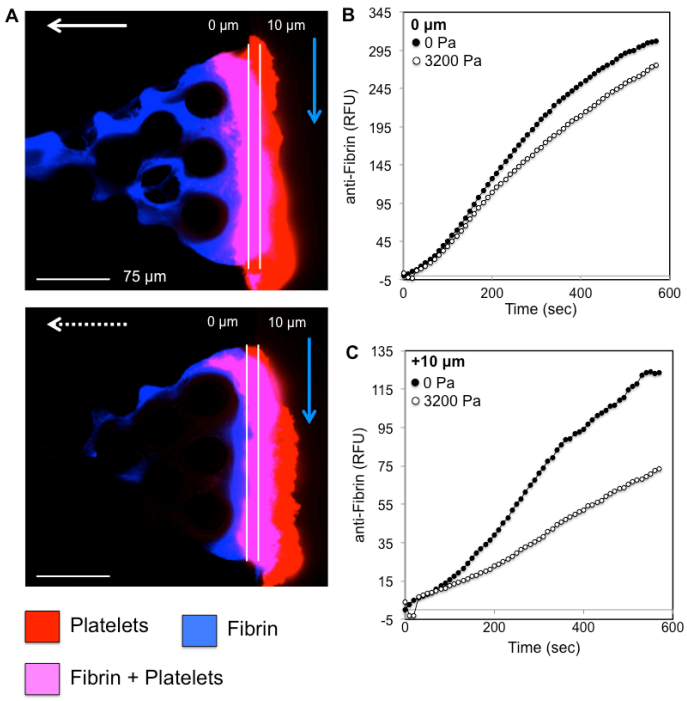

Figure 2- 11 The effect of a transthrombus pressure gradient on fibrin deposition kinetics.

Fibrin deposition at the collagen/thrombus surface (0 μm) or 10 μm depth into the thrombus was measured using anti-fibrin fluorescence. The rate of fibrin deposition at the collagen/thrombus surface was largely unaffected by presence or absence of a pressure drop across the fibrin (A). The rate of deposition fibrin deposition at 10 μm into the thrombus was significantly reduced by the presence of a pressure drop across the thrombus (3200 Pa) (B).

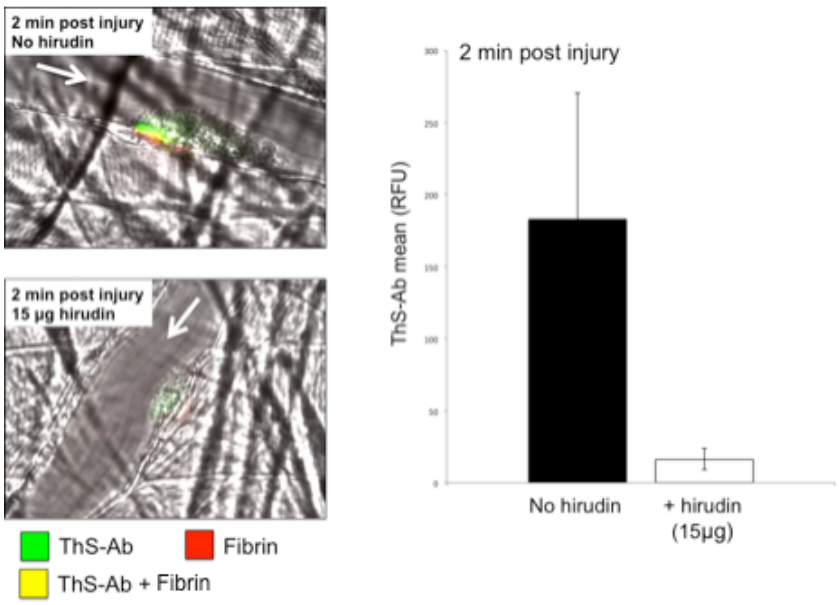

Figure 2- 12 The effect of a direct thrombin inhibitor on ThS-Ab signal in vivo.

Intravital microscopy of mouse laser injury model was used to monitor ThS-Ab and fibrin signal during thrombosis. The mice were injured and then infused with hirudin (15μg) and re-injured to observe the inhibition of hirudin on ThS-Ab signal (green) and fibrin (red). Images show the thrombus formation, ThS-Ab signal, and fibrin signal 2 minutes after injury both with and without hirudin. The graph quantifies the difference in ThS-Ab signal 2 minutes post-injury from several injuries.

CHAPTER 3: A systems approach to hemostasis: 1. The interdependence of thrombus architecture and agonist movements in the gaps between platelets

This research was originally published in *Blood*. Welsh JD, Stalker TJ, Voronov R, Muthard RW, Tomaiuolo M, Diamond SL, Brass LF. *Blood*. 2014;124(11):1808-15.

3.1 Introduction

The hemostatic response balances the need to halt bleeding with the need to avoid inappropriate vascular occlusion. Recent reports of hemostatic thrombi formed *in vivo* have demonstrated that the extent of platelet activation within a growing thrombus is heterogeneous [12,36,80-82] and can result in a characteristic core-and-shell architecture. We have shown that the core region develops adjacent to the injury site and consists of fully-activated, closely-packed platelets that have undergone α-granule exocytosis, which allows them to be recognized by the appearance of the α-granule membrane protein, P-selectin, on their surface [12]. The shell is a less stable region that coats the core and consists of loosely-packed, less activated platelets [12].

Regional differences in the extent of platelet activation can potentially be driven by multiple factors. Here we have adopted a systems biology perspective, looking beyond the events in any one platelet to test the idea that the emerging architecture of the hemostatic response serves as both a driver and a reflection of differences in intrathrombus molecular transport rates and consequent differences in agonist

distribution. Numerous platelet agonists are present during vascular injury, including collagen, thrombin, ADP and TxA_2 [83]. Each of these varies in origin, potency and mobility. Collagen, for example, is immobile, while thrombin distribution is limited by interactions with other proteins, including inhibitors [84,85]. By comparison, ADP and especially TxA_2 are freely diffusible [86].

Our goal in this study was to develop and apply methods to understand the relationship between molecular transport, platelet packing density and agonist distribution, examining how each affects platelet activation and thrombus growth *in vivo*. We asked whether regional differences in thrombus structure affect agonist movement and distribution, and, therefore, the extent of platelet activation. To test this hypothesis we developed a novel biosensor capable of measuring molecular transport *in vivo* in real time, and have used that biosensor in conjunction with a previously-developed thrombin biosensor [87] to compare transport rates and thrombin activity. The transport biosensor consists of albumin coupled to caged fluorescein molecules that uncage and fluoresce when flashed with 405 nm light. Subsequent loss of the fluorescence provides a direct measure of intrathrombus transport that we have combined with data generated by the thrombin biosensor and a thrombus porosity probe to produce a high resolution map of transport rates, thrombin activity and relative packing density within the thrombus.

Here we show that molecular transport in the gaps between platelets is orders of magnitude slower within the thrombus than in the overlying blood stream, and even slower in the core than in the shell. High-resolution mapping defines a low transport region coinciding with the region of greatest packing density and highest thrombin activity. Since greater packing density facilitates contact-dependent signaling between

adjacent platelets, we performed comparative studies in mice lacking Sema4D. These mice have a defect in contact-dependent amplification of collagen-induced platelet activation [88]. Collectively, the results establish a timeline in which initial platelet accumulation and the narrowing gaps between platelets serve as obstacles to molecular movement in what will become the thrombus core. This creates a region of reduced transport that facilitates local thrombin accumulation and greater platelet activation, while faster transport rates and greater instability within the shell help to limit thrombin accumulation and thrombus size. Thus, even the early stages of platelet accumulation produce an altered microenvironment that influences subsequent thrombus growth and, potentially, the impact of antiplatelet agents. In this and the following two chapters we use complementary experimental and computational approaches to test this model.

3.2 Materials and methods

3.2.1 Materials

CMNB-Caged Carboxyfluorescein SE and Alexa-fluor 488/568/647 monoclonal antibody labeling kits (Life Technologies, Grand Island, NY, USA). Bovine serum albumin (BSA, Jackson Immunological Research, West Grove, PA, USA). C57Bl/6J mice (Jackson Laboratories, Bar Harbor, ME, USA). Anti-CD62P (IgG, clone RB40.34) and anti-CD41 ($F(ab)_2$ fragment, clone MWReg30) (BD Biosciences, San Diego, CA, USA).

3.2.2 Synthesis of caged fluorescein (cAlb) conjugated to albumin (cAlb)

Bovine serum albumin was solubilized in 0.1 M sodium bicarbonate in PBS to a final concentration of 10 mg/mL. The CMNB-caged Carboxyfluorescein SE was dissolved in 100 µL of DMSO, and added to the solubilized BSA and mixed thoroughly. The reaction was incubated for 1 hour at room temperature, and then excess caged fluorescein was removed using 7kD MWCO desalting columns (Thermo Scientific, Pittsburg, PA, USA).

3.2.3 Hemostatic thrombus formation

Male mice 8-12 weeks of age were anesthetized with an intraperitoneal injection of sodium pentobarbital (90 mg/kg), and their jugular vein was cannulated for the introduction of cAlb (0.5 mg/mL), anti-CD41 AF-568, and anti-CD62P AF-647. The mouse cremaster was exposed, cleaned of connective tissue, opened, and prepared for viewing by intravital microscopy. The cremaster was maintained under a constant flow of bicarbonate buffer (37 °C) bubbled with 95%/5% N_2/CO_2. Mouse arterioles of 30-50 µm diameter were visualized with a BX61WI microscope (Olympus, St. Louis, MO, USA) with a 60X (0.9 NA) water immersion objective, and a CSU-X1 spinning disk confocal scanner (Yokogawa, Sugar Land, TX, USA). Fluorescence imaging was done using diode pumped solid state lasers (405 nm, 488 nm, 561 nm, 647 nm) with AOTF control as an excitation source (LaserStack, Intelligent Imaging Innovations, Denver, CO, USA), and images were captured using an Evolve digital camera (Photometrics, Tucson, AZ, USA). Endothelial cell ablation was performed with a pulsed nitrogen dye laser (SRS NL100, 440 nm) focused on the vessel wall through the microscope objective. The laser was fired between 1-10 times until red blood cells either escaped into the extravascular space or became trapped within the layers of the vessel wall. The University of

Pennsylvania Institutional Animal Care and Use Committee approved all procedures. In this and the two accompanying manuscripts, our focus is on the hemostatic response to injury and we have used the terms “hemostatic thrombus”, “hemostatic plug” and “thrombus” interchangeably.

3.2.4 Injury visualization

After injury the platelet deposition was monitored using anti-CD41 AF-568 fluorescence, and core development with anti-P-selectin (anti-CD62P). Background fluorescence was measured within the vessel for both anti-CD41 and anti-P-selectin, and subtracted from the images to determine the core and shell areas. In representative images of thrombi using anti-CD41, anti-P-selectin and thrombin sensor, the background fluorescence threshold is set and the results are displayed in binary mode unless otherwise noted in the figure legend.

cAlb fluorescence was visualized by un-caging the caged carboxyfluorescein with a 500 ms pulse of 405 nm light delivered through the microscope objective (Figure 1A and B). Immediately after the 405 nm light pulse cAlb fluorescence (ex: 488 nm), platelets (ex: 568 nm), and P-selectin (ex: 647 nm) were tracked for 15 frames. After 15 frames (~9 s) a new pulse was initiated. This sequence was repeated for 3 minutes. Separate studies determined that the observed rapid decay is not due to photobleaching, as only very mild photobleaching was observed using the experimental capture settings (Figure S3-8). Microscope control, image capture, and analysis was performed by Slidebook 5.0 (Intelligent Imaging Innovations, Denver, CO, USA).

3.2.5 Thrombin biosensor

Mouse thrombin sensitive antibody (mThS-Ab) was synthesized using a protocol previously described [87]. mThS-Ab was infused through the jugular cannula of the mouse prior to injury and was imaged every 10 seconds. Platelets and P-selectin were labeled with fluorescent anti-GPIbb (Emfret Analytics, Eibelstadt, Germany, Clone: Xia.C3) and anti-CD62P respectively, and were imaged once per second. Background fluorescence was measured within the vessel and subtracted from the mThS-Ab signal within the thrombus. Determining the location of the stable core at 20 minutes post-injury identified the low transport region (LTR), and mThS-Ab was quantified within the LTR and shell over time.

3.2.6 Analysis of cAlb data

For core and shell cAlb decay rates, the core and shell were masked using P-selectin staining as the marker for core. For each mask the cAlb decay curves were obtained once the region attained an area greater than 10 μm^2. The mean cAlb fluorescence intensity in the core and shell regions immediately prior to each 405 nm flash was defined as background fluorescence and subtracted from the cAlb images acquired subsequent to each flash. The mean cAlb fluorescence for each of the images acquired following each flash were then normalized to the cAlb fluorescence in the first image post-flash (representing the peak cAlb signal for each flash), resulting in a decay curve for each 405 nm flash. All the curves for a single injury were averaged to make a single decay curve, and curves for multiple injuries were averaged to generate the mean

curves with standard deviations reported. The curves were averaged over several injuries from at least 3 mice.

3.2.7 Sema4D-deficient mice

Sema4D null mice were back crossed onto C57Bl/6 were described previously [89]. All studies were performed using Sema4D$^{+/+}$ (WT) and Sema4D$^{-/-}$ littermates produced by crossing heterozygotes.

3.2.8 Porosity measurements

BSA labeled with AlexaFluor 488 (Invitrogen, Carlsbad, CA, USA) was infused into the mouse through a jugular cannula prior to injury. Fluorescence was measured continuously in the lumen, LTR, and shell during thrombus development. The lumen was assumed to have a porosity of 0.6 due to 40% hematocrit in the flowing blood, and the measured lumen fluorescence was used to calculate the plasma fluorescence with a porosity of 1. By normalizing the fluorescence within the shell and LTR to the plasma, we were able to calculate the porosity of each region over time.

3.3 Results

3.3.1 Measuring regional heterogeneity of intrathrombus transport

A necessary first step in this study was the development of a method to measure intrathrombus molecular transport rates *in vivo* in real time during hemostatic thrombus

formation. The injury model we have employed most frequently uses a laser or sharpened glass probe to produce a penetrating injury in the cremaster muscle microcirculation of a C57Bl/6 mouse [12]. Thus, in this and the two accompanying manuscripts, our focus is on the hemostatic response to injury and we have used the terms “hemostatic thrombus”, “hemostatic plug” and “thrombus” interchangeably. Confocal fluorescence microscopy with high speed video capture allows direct visualization of the response to injury and parameters such as platelet accumulation, platelet activation, packing density and thrombus porosity to be measured, the latter with stably-fluorescent albumin and dextran molecules [12]. To create a transport rate sensor for the present studies, albumin was labeled with caged fluorescein molecules (cAlb) that become stably fluorescent only after being uncaged by exposure to 405 nm light (Figure 3-1A). In the example shown in Figure 3-1B, pulses of 405 nm light uncaged the fluorophore within the field of view resulting in fluorescence that could be visualized within the thrombus. The rise and subsequent washout of fluorescence within the thrombus caused by a series of repeated light pulses separated by 10 seconds is shown in Figure 3-1C. Albumin-associated fluorescence in the lumen moves too rapidly for capture and analysis. Each thrombus was monitored for 3 minutes after injury, during which time multiple pulses and decay curves were generated (Figure 3-1D). Photobleaching contributed minimally to the decline in cAlb fluorescence during the period of observation between activating pulses (Supplemental Figure S1). Platelet deposition and surface P-selectin expression (an index of α-granule exocytosis) were recorded at the same time (Figure 3-2A and B).

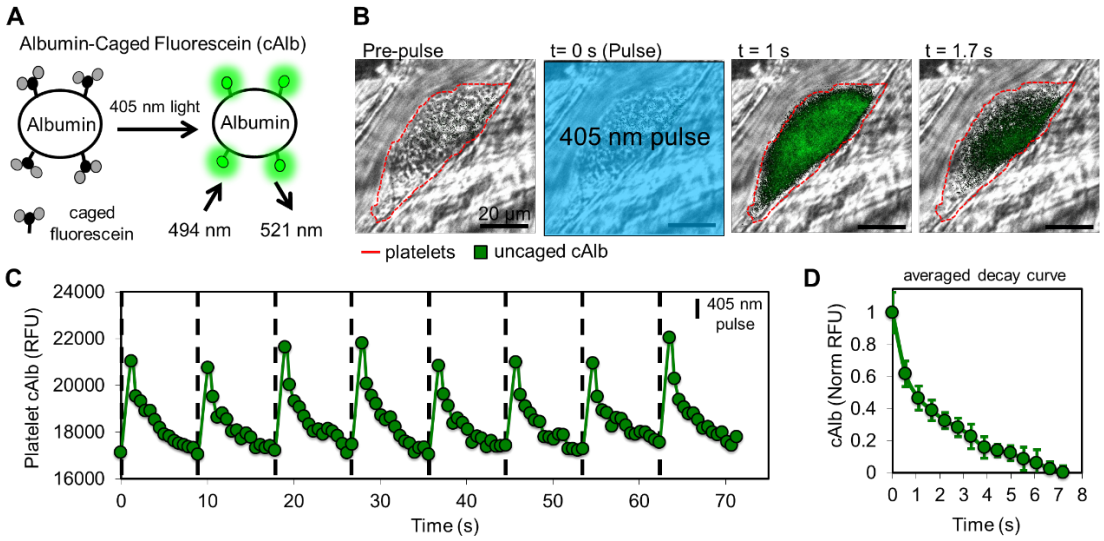

Figure 3- 1 Design of caged fluorescein-albumin biosensor (cAlb) for visualization of the molecular transport properties of thrombi generated in vivo.

(A) Bovine serum albumin was labeled with caged fluorescein (cAlb) which is uncaged using 405 nm light to induce fluorescence. (B) Intravital microscopy was used to observe cAlb *in vivo*. Infusion of cAlb into the blood stream was followed by laser-induced injury to the mouse cremaster muscle arterioles to induce thrombus formation. Periodic pulses of 405 nm light were used to uncage cAlb and the resulting fluorescence intensity and decay were monitored with fluorescent microscopy. The represented fluorescence intensity has had the background subtracted and then been scaled to demonstrate signal decay within the thrombus. (C) Quantification of the intrathrombus cAlb signal was measured over multiple pulses of uncaging light for thrombus in B. (D) An average intra-thrombus cAlb decay curve was generated by averaging the decay after each of 16 pulses taken over 3 minutes.

As reported previously, platelets accumulate rapidly in this injury model, reaching a peak 30-60 s after injury [12]. Surface P-selectin appears more slowly, becoming detectable within the thrombus core at 20 s and continuing to increase throughout the experiment with growth slowing after approximately 150 s (Figure 3-2B). To determine if molecular transport rates also show regional variation, cAlb decay was analyzed separately in the

P-selectin(+) core region and P-selectin(-) shell region of the thrombus. Average cAlb decay curves were generated for 13 injuries during the first 3 min post-injury for both regions (Figure 3-2C). We found that uncaged (i.e. fluorescent) cAlb was visible only within the thrombi. cAlb in the lumen of the vessel was traveling too fast to be flash-activated and observed. The core region had an average cAlb half-life of 2.6 s, which is approximately two-fold greater than the shell region's average half-life of 1.2 s. Detailed mapping showed that the slowest half-life recorded in the core was 8 s and the fastest in the shell was 0.5 s, yielding a maximum ratio of 16:1. Taken together these results demonstrate, first, that platelets retard the movement of soluble molecules in their vicinity and, second, the core and shell have differing transport properties, with the core retaining soluble proteins longer than the shell.

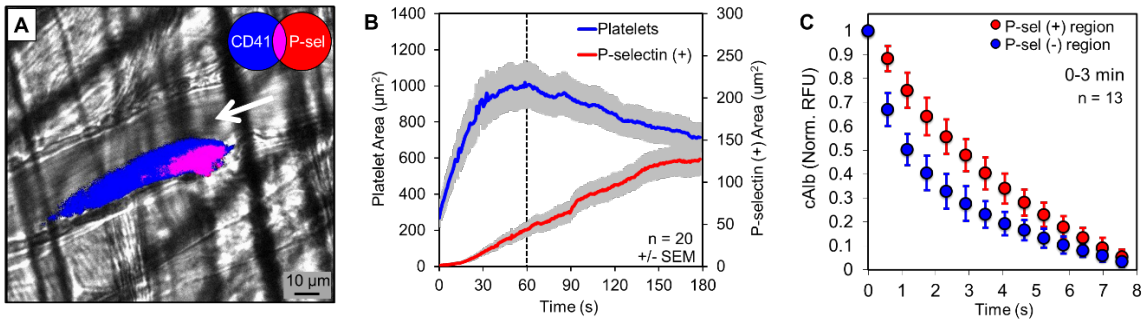

Figure 3- 2 Regional heterogeneity of cAlb transport properties.

(A) A representative image of a thrombus generated using a laser injury model in mouse cremaster arterioles (3 min post-injury). Thrombi were monitored for platelet deposition (blue), P-selectin exposure (red), and cAlb (not shown) for 0-3 min post-injury. (B) The growth of platelet (blue) and P-selectin(+) (red) areas were monitored over 3 minutes. The areas were measured by gating the images on either CD41(+) or P-selectin(+) pixels and then averaged across 20 injuries from 5 wild type mice. (C) Thrombus regions were defined as CD41(+)/P-selectin(+) and CD41(+)/P-selectin(-) for cAlb analysis. Pulses of 405 nm light were used to activate the cAlb infused prior to injury, and the

normalized decay curves for the P-selectin(+) (red) and P-selectin(-) (blue) regions were averaged over each pulse for 0-3 min post-injury (+/- SD).

3.3.2 Determining the kinetics of reduced intrathrombus transport and platelet packing

We hypothesized that slower molecular transport in the core leads to greater retention of soluble agonists, which in turn contributes to full platelet activation and α-granule secretion. If so, then reduced transport rates in the core region would precede P-selectin exposure on the platelet surface. To compare the kinetics of the development of regions of reduced transport with the kinetics of platelet activation, we identified a transition zone, defined as the region that is P-selectin(-) at 3 min, but becomes P-selectin(+) by 20 min (Figure 3-3A). Taking into account this definition of a transition zone, the shell region becomes the part of the thrombus that is neither core nor transition region. We found that the transition zone at 3 min post-injury, despite being P-selectin(-), had significantly slower cAlb transport than the shell (Figure 3-3B).

To generate a map of intrathrombus transport rates with the greatest possible resolution, we analyzed cAlb decay rates for single pixels within early thrombi (2-3 min post-injury), yielding high spatial-resolution cAlb $T_{1/2}$ heat maps for each thrombus (Supplemental Methods and Figure 3-3C). We observed a gradient of cAlb half lives extending from the region adjacent to the injury site showing the slowest transport. This region of low transport extended beyond the P-selectin(+) region into the transition zone (Figure 3-3C). Taken together the transition zone and the core form a *low transport region* (LTR), which has significantly reduced transport compared to the shell region (Figure 3-3C and

D). The appearance of reduced transport rates within the LTR preceding full platelet activation suggests a model in which transport heterogeneity regulates agonist distribution and platelet activation, which in turn affect platelet packing density and, therefore, local transport rates.

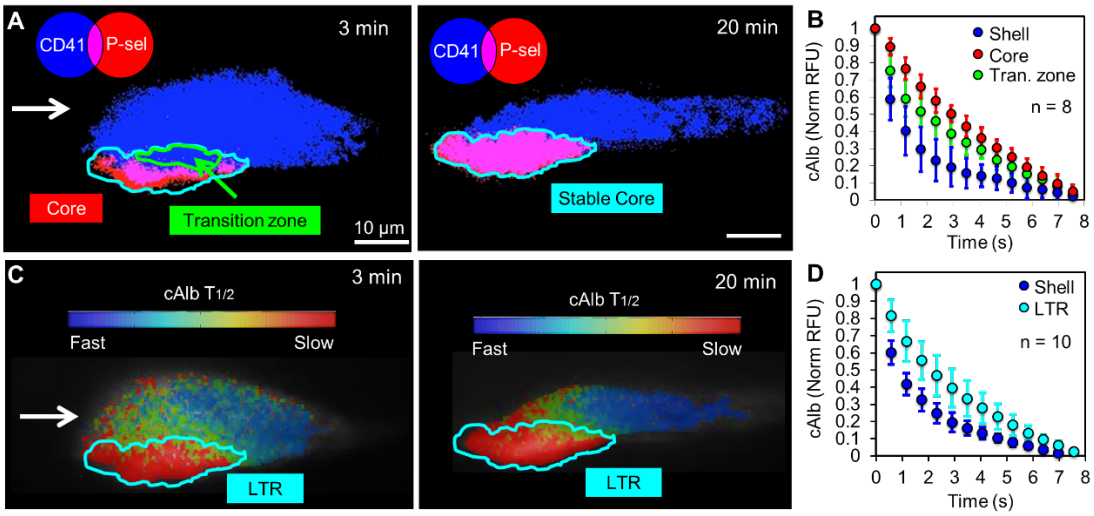

Figure 3- 3 Transport properties of the transition zone.

(A) A representative image of a thrombus at 3 min and 20 min post-injury showing platelet deposition (blue) and P-selectin exposure (red) at 3 min and 20 minutes. Also shown are the stable core (cyan outline) 20 min post-injury, and the transition zone (green outline) at 3 min post-injury. (B) Eight of the injuries had transition zones (green) large enough (> 10 μm^2) to be analyzed in addition to the core (red) and shell (blue) regions for their average cAlb decay curves (+/- SD). (C) For those same images in A the resulting cAlb $T_{1/2}$ time heat maps are shown with the low transport region (LTR) highlighted (cyan). The LTR is defined as the P-selectin(+) region plus the transition zone (i.e. the P-selectin(+) region at 20 minutes post-injury). (D) Analysis of the low transport region (LTR, cyan) transport compared to the shell (blue) transport properties using cAlb.

3.3.3 Measuring platelet packing dynamics within the low transport region

Within stable thrombi, the core maintains a higher platelet packing density, resulting in significantly decreased porosity [12]. We hypothesized that this high-density structure produces lower transport rates in the core by increasing steric hindrance between platelets, reducing permeability, and by increasing the tortuosity of the path cAlb needs to traverse to escape the core. To measure the dynamics of the increase in platelet packing density during early thrombus development, we infused albumin conjugated with stably-fluorescent (i.e. non-caged) AlexaFluor 488 and monitored changes in fluorescence within the low transport region and shell region. For reference, fluorescence was also measured outside of the thrombus in flowing blood, which consists of ≈40% hematocrit and a porosity of 0.6. By normalizing the fluorescence within the thrombus regions to the known value of the flowing blood, we were able to determine the porosity of each region within the thrombus (Figure 3-4). We found that porosity decreases rapidly in both regions as platelets accumulate following injury, with the low transport region achieving a significantly higher packing density than the shell by 60s after injury ($p < 0.05$). As reductions in both porosity and transport are observed prior to full platelet activation, this also supports our model of transport having a regulatory role in local platelet activation.

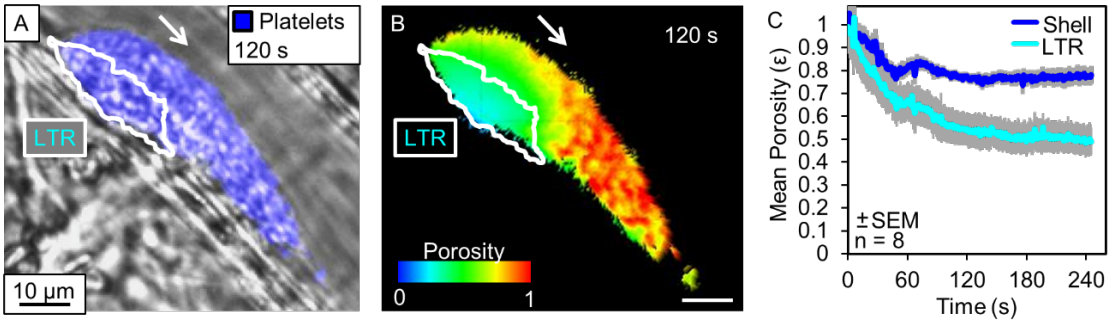

Figure 3- 4 Dynamics of thrombus regional porosity.

Albumin labeled with AlexaFluor 488 was infused into the mouse prior to injury and the fluorescence was monitored within the lumen, low transport region (LTR), and shell of the developing thrombi. (A) A representative image of platelets (blue) and LTR (white outline) 120 s post-injury. (B) For the same thrombus a pseudo colored image of the thrombus colored to represent the porosity based on the normalized fluorescence intensity. (C) Average porosity of the shell (blue) and LTR (cyan) of eight individual injuries over 240 s post-injury.

3.3.4 Regional heterogeneity of intrathrombus thrombin activity

To determine whether the altered structure and transport of the low transport region serve to concentrate agonists leading to increased platelet activation and eventual P-selectin exposure, we employed a recently developed thrombin activity sensor, designated mThS-Ab. The thrombin sensor consists of a FRET-based fluorogenic peptide thrombin substrate linked to anti-mCD41 to target it to the platelet surface [87]. Cleavage of the peptide by thrombin releases a quencher, allowing an increase in fluorescence. The resulting signal represents the spatial distribution of cumulative thrombin activity. Thrombin activity, platelet deposition, and P-selectin exposure were measured in developing (0-3 min after injury) and stable thrombi (20 min after injury)

(Figure 3-5A, Supplemental Movie M2). Consistent with our previous observation that fibrin deposition occurs only within the core region [12], we measured 6.5 times more thrombin activity within the low transport region than within the shell by 3 min after injury (Figure 3-5B). By 20 min even the minor signal in the shell was no longer detectable.

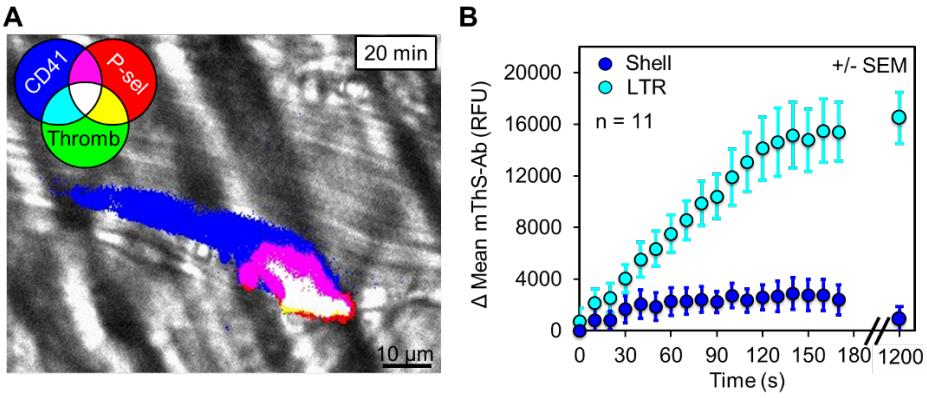

Figure 3- 5 Thrombin activity within the low transport region (LTR).

(A) A representative image of thrombin activity (mThS-Ab; green, binary mode) within a thrombus 20 min after injury also showing platelet deposition (blue) and core formation (red). Overlay of 3 channels is white. (B) The change in the mean mThS-Ab fluorescence was monitored within the low transport regions (cyan) and shell (blue) during the initial 3 minutes after injury and again at 20 min (+/- SEM).

3.3.5 Determining pathways which initiate and support low transport region formation

Since the data described so far show that the drop in transport rates within hemostatic thrombi precedes full platelet activation, we examined the effect of impairing platelet activation on transport rates. To do this, we selected Sema4D$^{-/-}$ mice, whose signaling

defect we have characterized previously [88,89]. Sema4D is a semaphorin family member on the surface of platelets that supports contact-dependent amplification of Syk activation downstream of the platelet collagen receptor, GPVI [88]. When studied after penetrating injury, Sema4D$^{-/-}$ mice show a defect in platelet accumulation and delayed P-selectin exposure during the first 3 min of thrombus development [12]. The studies in Figure 3-6 confirm this earlier observation. They also show that these mice have no significant defect in cAlb transport during this same period (Figure 3-6C and D). Thus, these results reinforce the idea that the drop in transport rates within the thrombus not only precedes full platelet activation (as defined in this case by α-granule exocytosis), but is at least partially independent of it.

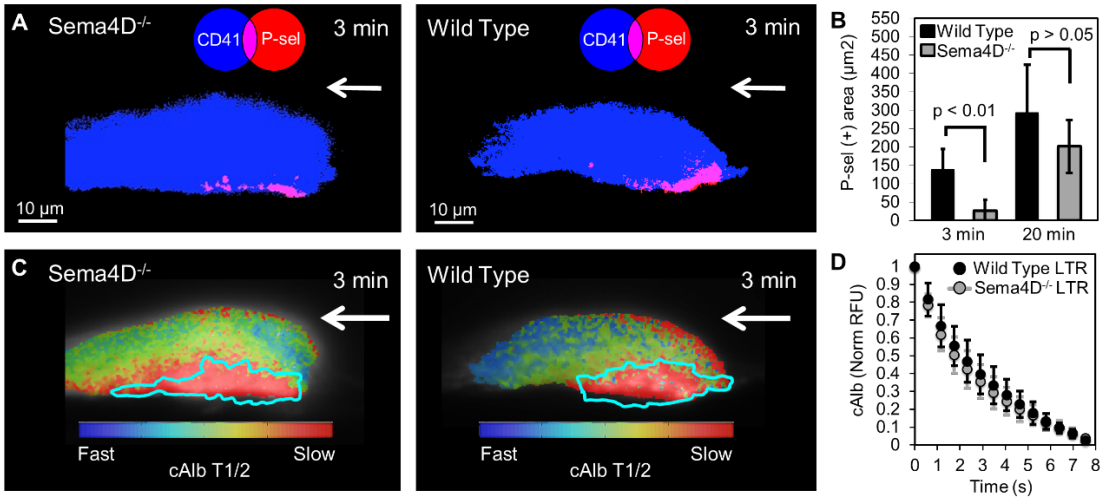

Figure 3- 6 The role of contact-dependent Sema4D signaling in LTR and core formation.

(A) Representative images of a thrombus generated in Sema4D$^{-/-}$ and wild type mice cremaster muscle arterioles showing platelets (blue) and P-selectin (red) at 3 minutes post-injury. (B) Quantification of the average P-selectin(+) area within Sema4D$^{-/-}$ and wild type thrombi at 3 and 20 min post-injury (n = 13 for both Sema4D$^{-/-}$ and WT; +/- SD)

showing a lag in P-selectin exposure in the knockout. (C) For each representative thrombus the corresponding cAlb half-life heat map is shown with the LTR highlighted (cyan). (D) The cAlb decay curves of the LTR of wild type (black) and Sema4D$^{-/-}$ (grey) thrombi (wild type n= 10, Sema4D$^{-/-}$ n= 14; +/- SD).

3.4 Discussion

Rather than being a homogeneous mass of equally-activated platelets uniformly interspersed with fibrin, studies in mouse models reveal that the hemostatic response to penetrating injuries shows considerable regional variation in the extent of platelet activation as judged by metrics such as the extent of α-granule exocytosis. In this and the following two chapters we have adopted a systems approach to understanding these events, combining observational, experimental and computational approaches to ask whether regional differences extend to other aspects of the hemostatic response and, if so, how such differences arise, contribute to thrombus growth and affect the benefits and toxicities of antiplatelet agents.

To do this, we developed a novel tool for measuring intrathrombus transport rates *in vivo* in real time and combined it with a recently-described thrombin activity sensor [87]. The results presented here show that regional differences in the extent of platelet activation are accompanied by differences in platelet packing density, intrathrombus molecular transport rates, distribution of at least one platelet agonist (thrombin), and deposition of fibrin. The results also show how these relationships evolve over time (Figure 3-7). High-resolution mapping based on confocal *in vivo* imaging studies transforms the transport data into a heat map and defines a hitherto unappreciated transition zone

between the thrombus core and shell. Within this zone are platelets that have not yet reached the point of α-granule exocytosis, but nonetheless retard the passage of solutes in the spaces between them. The transition zone plus the core of platelets that became P-selectin(+) early in the injury response form a low transport region that eventually becomes fully P-selectin(+).

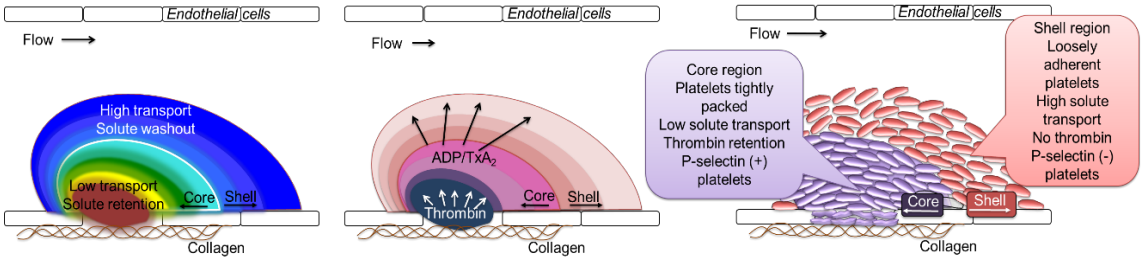

Figure 3- 7 Model of the role of transport on agonist distribution and thrombus architecture.

As platelets within a developing thrombus become activated they change shape, retract, and pack tightly together driving the formation of the low transport region. This leads to the retention of larger agonists, such as thrombin, within the low transport region. Smaller agonists, such as ADP and TxA_2, are able to diffuse more freely out of the low transport region. The localization of these agonist gradients drives continued platelet activation in the low transport region leading to core formation consisting of high platelet packing density, decreased solute transport, α-granule exocytosis, and fibrin deposition. The restriction of thrombin to the core contributes to the shell consisting of loosely adherent platelets, high solute transport, reduced platelet activation and no fibrin.

Changes in transport rates presumably reflect the increase in packing density as platelets grow closer to each other, increasingly hindering the movement of molecules in the gaps between platelets. Supporting this conclusion, we found that the distribution of thrombin activity within the thrombus mirrored the regions of slowest transport and

extended little, if at all, into the shell region of the thrombus where transport rates, although slower than in the remaining vascular lumen, were still faster than in the core. Data presented in Chapter 5 provide further support, showing that mice with a defect in $\alpha_{IIb}\beta_3$ outside-in signaling that impairs clot retraction form thrombi with increased transport in both the core and the shell, and decreased thrombin activity compared to wild type mice. Here we studied mice with a defect in contact-dependent signaling due to loss of the platelet surface ligand, Sema4D. These mice have a defect in core formation, but still developed a low transport region, supporting the idea that the reduced transport is not dependent on achieving full platelet activation.

The close relationship between the low transport region and the region of greatest thrombin activity is particularly informative. Others have also presented models suggesting that solute transport may play a key role in regulating thrombus growth by impacting coagulation factor access to the injury site as well as agonist escape from the thrombus [54,56]. These models have shown that limiting the gaps between platelets can greatly hinder transport and alter the movement of solutes through the thrombus [52,54,56]. Within this study we were unable to tease apart the contribution of fibrin in filling these gaps, but other investigators [53] have suggested fibrin doesn't have a large impact on protein transport. However, fibrin has been reported to decrease the permeability of platelet plugs [51], which may alter permeating flow and in turn protein transport.

We have previously shown that thrombin inhibitors prevent the formation of the core region [12]. Generation of thrombin *in vivo* begins with the exposure of tissue factor, but the local accumulation of thrombin is also governed by the availability of procoagulant

factors (including prothrombin), the exposure of negatively-charged phospholipids on the platelet and other membrane surfaces, the washout rates of thrombin from its original site of generation, and the ability of coagulation inhibitors such as TFPI and anti-thrombin to reach the site where thrombin and other coagulation factors are produced. Some coagulation proteins and inhibitors are contained within platelet α-granules and are eventually secreted at the site of platelet activation. Others are plasma-borne. To the extent that molecular transport becomes hindered in the region closest to the site of injury, secreted molecules will tend to accumulate and plasma-borne molecules will have difficulty gaining access. This means that as platelets begin to accumulate following vascular injury they participate not only by forming part of the hemostatic plug, but also by acting as obstacles to the free movement of molecules in the region closest to the injury.

Thus we propose that regional differences in platelet activation and in thrombus structure are closely related to each other and are both the driver for and the consequence of regional variations in agonist distribution and packing density. The data presented here plus our earlier studies with the thrombin sensor highlight the overlap between the region of greatest packing density, slowest transport and greatest thrombin activity [12,87]. We have previously shown that the size of the thrombus shell is dependent on signaling downstream of platelet $P2Y_{12}$ receptors for ADP [12]. At present, there is no way to detect ADP *in vivo* in real time. However, the vulnerability of the shell to $P2Y_{12}$ antagonists and the increase of shell size observed with a gain of function mutation in $G_{i2}\alpha$ [12] suggest that ADP concentration gradients extend further than do thrombin gradients. Therefore, it is a reasonable hypothesis that platelet recruitment initially

establishes a shell-like thrombus that is converted to the transition zone and core by thrombin. In a sense, the emergence of greater packing density within the core helps to create a molecular prison for thrombin that, along with the presence of thrombin inhibitors, limits the size of the core and, therefore, the overall size of the thrombus. It is also reasonable to propose that differences in the distribution of ADP and thrombin, as well as differences in the properties of the core and shell presage differences in safety and efficacy of $P2Y_{12}$ antagonists compared to PAR1 antagonists.

3.5 Supplemental Material

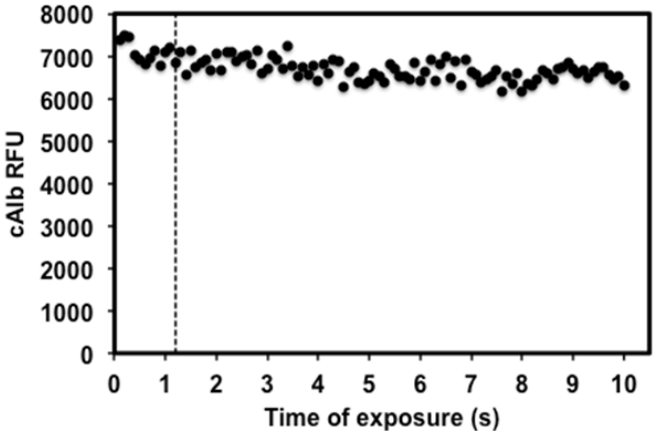

Figure 3- 8 Minimal photobleaching of cAlb.

The rate of cAlb photobleaching was measured by monitoring the fluorescence of pre-activated cAlb in a no-flow environment. The cAlb fluorescence was measured after 100 successive 100 ms exposures, which are the same as used during *in vivo* imaging. The dashed line indicates the time of exposure in between activated pulses *in vivo*.

3.5.1 Generation of cAlb heat maps

To generate the cAlb transport heat maps the raw acquired image captures typically consisted of 300 frames for each fluorescent channel, which were initially stored in a 4D matrix of size: “Total Number of UV flashes” x “Number of Image Captures between each UV Flash” x “Image Width” x “Image Height”. For the late-stage thrombogenesis images (20 min post injury), the whole duration of the image capture could be used for the analysis, since the thrombi were stable throughout the capture. Therefore, the albumin intensity channel matrix size was 20 x 15 x 456 x 508 for this case. That is, there were a total of 20 UV flashes with 15 image captures between each flash, and the resulting image sizes were 456 by 508 pixels. For the early-stage thrombus development, on the other hand, the clot structure was still evolving during the beginning of the capture, so only the last 6 flash periods (thrombi were observed to be sufficiently stable during this time) were used, resulting in matrix size of 6 x 15 x 456 x 508. Next, in order to improve accuracy, each dataset was averaged over the first dimension of the matrix, resulting in a mean flash period representation of size 15 x 456 x 508, for each dataset. Once normalized, the data was smoothed in 3D using the custom medfilt3 Matlab function (http://www.biomecardio.com/matlab/medfilt3.html), where the first two dimensions were the X and Y directions in the plane of the image, and the third one was time. The default 3 x 3 x 3 neighborhood was used for the median filtering. After that, the standard deviation of the pixel values over the 15 frame duration was calculated and the pixels that showed less than 20% deviation from their mean were excluded from the analysis. The reason for this was two fold: 1) pixels with negligible amount of albumin variation should not be taken into the consideration, because they could be representing a platelet, rather than albumin-filled voids between cells and 2) this resulted in significant computational savings, since the procedure effectively excluded the lumen and extra-vascular regions from the calculation. For similar reasons, the

CD41 mask was used to further exclude the non-thrombus pixels from the analysis. Finally, 1D piecewise cubic Hermite interpolation was used in order to estimate the half-life of the normalized albumin data for each pixel. A custom 2D median filter (ignores pixels previously excluded from analysis) with a tile size of 3 x 3 pixels was used to post-process the final results for noise reduction in the plane of the images. The resulting half-life "heatmap" (shown in color) was overlaid onto the mean thrombus representation shown in grayscale (CD41 channel image averaged over all frames). Peak half-life values were saturated at 4 seconds in order to highlight the differences between low and high albumin retention regions of the thrombi.

CHAPTER 4: A systems approach to hemostasis: 2. Computational analysis of molecular transport in the thrombus microenvironment

This research was originally published in *Blood*. Tomaiuolo M, Stalker TJ, Welsh JD, Diamond SL, Sinno T, Brass LF. *Blood*. 2014;124(11):1816-23. © the American Society of Hematology.

4.1 Introduction

Platelets are central to hemostasis, helping to form a hemostatic plug or thrombus at an injury site without occluding the vessel. Recent work has shown that hemostatic thrombi formed following penetrating laser or probe injury in the cremaster muscle microcirculation are heterogeneous with respect to important properties such as the extent of platelet activation, platelet packing density, porosity and the distribution of thrombin activity [12,87]. This heterogeneity is organized into a structure in which a core of highly activated platelets close to the injury site is covered by a shell of loosely adherent and less activated platelets [12]. In Chapter 3, we showed that the transport of plasma proteins in the gaps between platelets is also heterogeneous, being slower in the core than in the shell. These findings raise new questions about the origins of the thrombus architecture that we and others have observed.

Computational methods are useful for answering questions about complex systems, complementing experimental approaches and generating new hypotheses. Computational approaches have been used to model the hemostatic process (reviewed in reference [90]), but few have explicitly examined the impact of platelet packing density

or molecular transport through the hemostatic plug [52,53,56,91]. Here we propose that considering molecular transport leads to a more comprehensive understanding of how the internal organization of a hemostatic plug develops. Drawing on published studies [90] and Chapter 3 we have examined plasma velocity in a hemostatic plug modeled in two dimensions. To simulate solute transport, we have modeled hemostatic thrombi as a porous media comprised of regions with distinct physical characteristics that represent the core and shell. Using this computational framework we have reproduced experimental data, and then explored the role of the core by comparing solute transport through a simulated hemostatic thrombus with or without a core.

The results show that 1) once platelet accumulation begins, plasma velocity slows by orders of magnitude, and 2) relatively small number of platelets are sufficient to create a sheltered environment where diffusion, rather than convection, is dominant. Our results further emphasize that the core and shell are distinct physical microenvironments, and that the thrombus core acts as a selective molecular prison retaining some soluble agonists to increase their effective concentration. Predictions made based on this model are tested in Chapter 5.

4.2 Materials and methods

4.2.1 Model setup

We used two models to study intrathrombus transport. The first model, which was only used to study the flow characteristics inside the thrombus, is a 2D representation of a thrombus with platelets represented explicitly by ellipses and will be referred to as the

"explicit-platelet" model in the text. For this model we used computational fluid dynamics based on the Stokes equation to resolve the flow in the narrow gaps between platelets as well as in the lumen surrounding the thrombus (Figures 1-3). In the second model, the thrombus is represented as a two-compartment homogeneous porous medium; for this model, which includes species transport, we adopted a mathematical description similar to Kim et al. [53]. Here, we apply the Stokes equation for the lumen region and a Brinkman equation for the thrombus. These equations are coupled with convection-reaction diffusion equations to study solute transport in the thrombus (Figures 4-4 – 4-7). Both models were implemented and solved using COMSOL® version 4.3a.

4.2.2 Thrombus design for the explicit-platelet model

We designed a thrombus with size and geometry based upon *in vivo* images of stable thrombi (Figure S1). Each platelet was modeled as an ellipse with minor and major semiaxes of 0.6 μm and 1 μm. To investigate packing density we changed the dimensions of the ellipses without modifying their positions. We modeled the internal core-and-shell thrombus architecture by selectively changing the dimensions of a subset of platelets. Additional details may be found in the supplementary materials.

4.2.3 Solute transport

We used the "species transport in porous media package" in COMSOL® version 4.3a, solving the convection-reaction-diffusion equation: $\partial c/\partial t = D\nabla^2 c - u\nabla c + R$, where c is the concentration of chemical species of interest, D is the diffusion coefficient, u is the velocity vector field, and R describes sources of the various chemical species. We

imposed an initial uniform concentration of a tracer solute in the vessel, zero solute concentration at the influx boundary, and then ran the simulation until the concentration inside the thrombus regions decreased to zero. Additional details may be found in the supplementary materials.

4.2.4 Single parameter sensitivity analysis

The value of each of the six parameters (porosity, permeability and effective diffusion coefficient for the core and shell regions of the thrombus) was varied by 50% above and below its base case regressed value. For each variation, the transport simulation was run and the error between the simulation and experimental data evaluated. The sensitivity score with respect to each of the 6 parameters was calculated as the average of the root mean square error (RMSE) of the two simulations (+50% and -50%) relative to the RMSE of the base case fit.

4.2.5 Global sensitivity analysis

Each parameter was chosen randomly from a uniform distribution (Table 1). Each combination was chosen using a Latin hypercube sampling design. We simulated transport through the hemostatic thrombus and computed the RMSE between the simulation and the experimental data. We repeated this process 200 times with every simulation resulting from a different combination of parameters.

Table 4-1

Parameter value ranges used in the species transport simulations (Figures 4-7)

Parameter	Minimum	Reference	Maximum	Reference
Porosity − ε	>0	Minimum physically possible	1	Maximum physically possible
Permeability (m^2) − κ	10^{-18}	14	10^{-14}	14
Effective diffusion coefficient (m^2/s) − D	10^{-13}	Current paper	5×10^{-11}	11

4.3 Results

4.3.1 Model of in vivo thrombus formation

We began by examining the impact of thrombus size and packing density on plasma velocity within a hemostatic thrombus, the former by varying the number of platelets and the latter by varying the size of the gaps between platelets. To replicate results from the mouse injury model we considered a vessel 30 μm in diameter and designed growing platelet masses in which the smallest gaps were located in either the middle or the front of the mass. These manipulations were meant to reproduce a hemostatic thrombus growing (an increase in platelet number), consolidating (a reduction in gap size), or developing the characteristic core-and-shell architecture (heterogeneous gap distribution). Unless otherwise stated, all of the simulations had an inlet centerline velocity of 2 mm/s, typical of what is measured in similar size vessels under physiological conditions.

The results show that once a threshold is reached, the average plasma velocity within a hemostatic thrombus is minimally affected by the number of platelets within the thrombus. With as little as sixteen platelets, the average intrathrombus plasma velocity was approximately three orders of magnitude less than the bulk velocity (Figure 1A). Further increases in platelet number had only a minimal effect (Figure 1B-D). Using the largest thrombus geometry shown in Figure 1C, we examined how gap size and distribution affect molecular movement in a thrombus. The range of gap sizes that we considered was selected from electron microscopy studies in the literature [8]. We found that even when the minimum gap is as much as 400 nm, the average velocity within the thrombus is below 2 μm/s (Figure 2A). As gap size decreased, so did velocity, highlighting the ability of platelets to hinder flow.

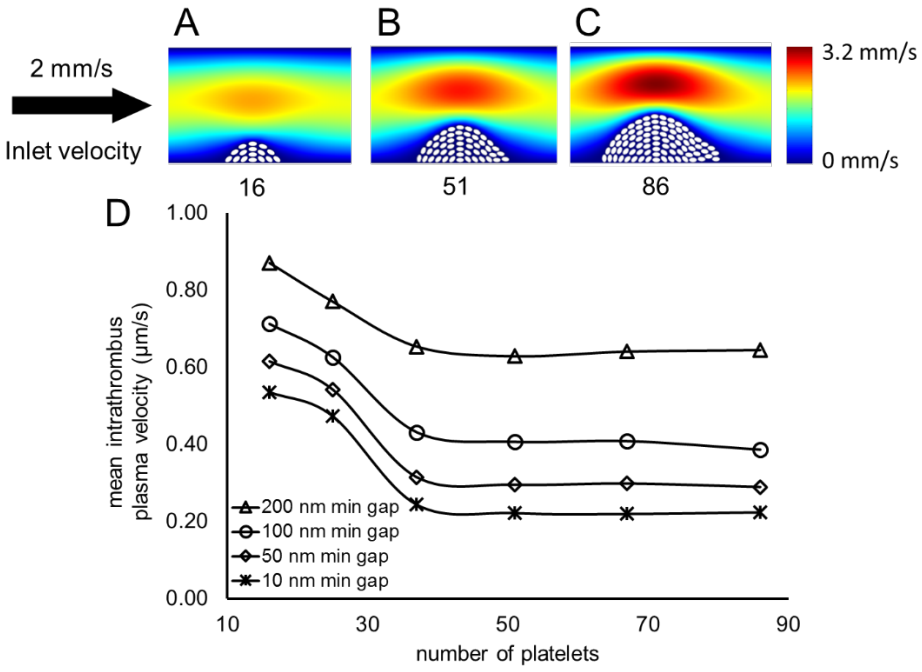

Figure 4- 1 Thrombus size does not determine intrathrombus plasma velocity.

(A-C) Successive stages of thrombus growth with corresponding number of platelets and bulk plasma velocity field. (D) The horizontal axis represents the number of platelets in

the hemostatic thrombus. The vertical axis shows the average plasma velocity computed between the platelets. In all cases the inlet vessel velocity is modeled as a pressure-driven parabolic profile with maximum velocity of 2 mm/s.

4.3.2 Convection Vs. diffusion

The relative impact of convection and diffusion is shown in Figure 2B, where minimum gap size is plotted against the Peclet number (see Methods), a value that estimates the relative contributions of convection and diffusion. A Peclet number of 1 indicates that convection and diffusion contribute equally, while a value <<1 indicates that diffusion dominates over convection. The results show that the small pore sizes within the thrombus produce a microenvironment in which molecular transport is dominated by diffusion. This effect was not substantially impacted by bulk plasma velocity. For instance even with a 4-fold increase in lumen velocity, from 2 to 8 mm/s, the intrathrombus velocity was still within the μm/s range (Figure 2C).

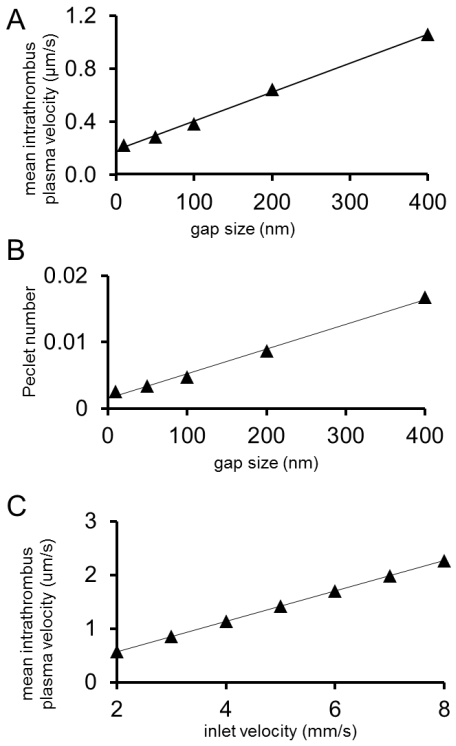

Figure 4- 2 Platelet gaps, plasma velocity and porosity in a hemostatic plug.

.

(A) The relationship of minimum gap size to mean intrathrombus plasma velocity. (B) The relationship between minimum gap size and the Peclet number shows that intrathrombus transport is dominated by diffusion. (C) The average velocity in a hemostatic thrombus increases linearly with the inlet velocity (slope = 0.28), but even when the velocity is quadrupled the velocity between platelets is still in the µ m/s range.

4.3.3 The impact of heterogeneous thrombus architecture

The presence of a tightly-packed thrombus core [12] was simulated by decreasing the minimum gap size between a subset of platelets from 200 to 10 nm (Figure 3, gray ellipses). The simulated core region was placed either in the front (Figure 3A and C) or

in the center (Figure 3B and D) of the platelet mass to determine whether the location of the core affected plasma velocity within the mass. Figure 3E illustrates how the plasma velocity is affected by the presence of platelets. The velocity of the plasma near the vessel wall immediately upstream of the thrombus is about 0.5 mm/s. Between platelets this falls to 1 μm/sec, decreasing even further where the narrowest gap between platelets is 10 nm. Notably, the location of the core had little effect (Figure 3F).

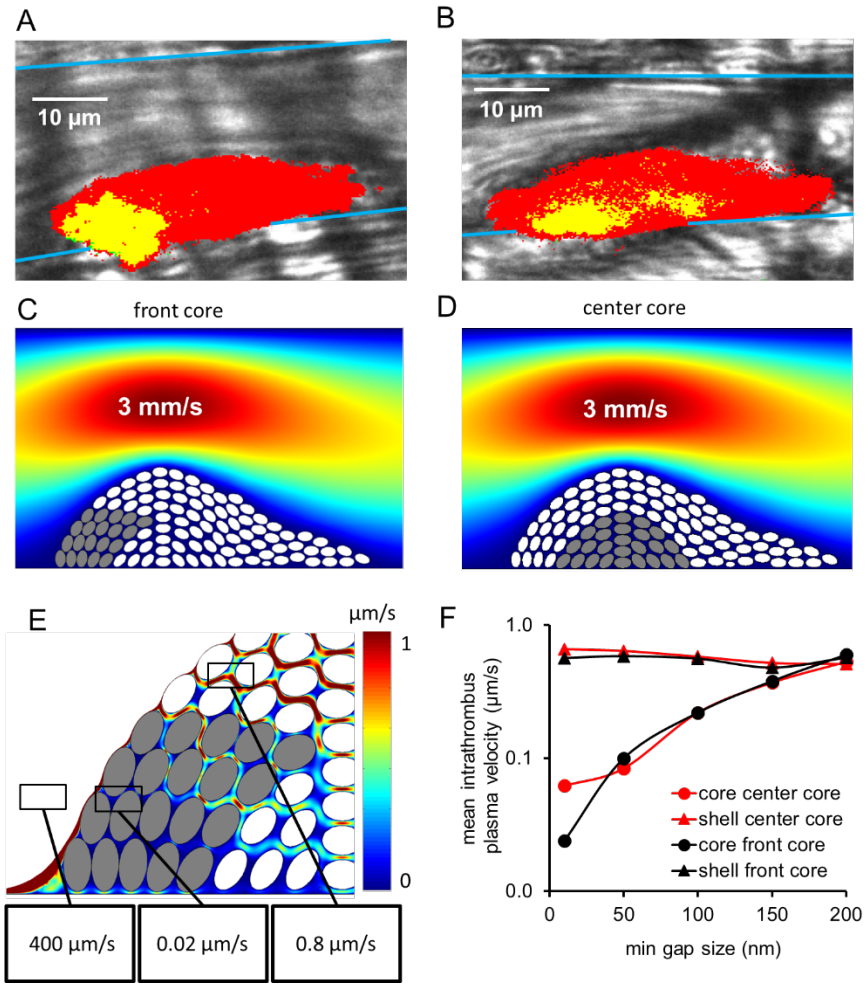

Figure 4- 3 Heterogeneous gap size distribution. Based on experimental data.

(A, B) Two different architectures were designed with a subset (the core) of more tightly packed platelets at the front (C) or in the center (D) of the hemostatic plug. The smallest

gaps are 200 nm and 10 nm between white and gra y platelets respectively. In all cases the inlet vessel velocity is modeled like a pressure driven parabolic profile with maximum velocity of 2 mm/s. E) Sample regions in a pre-thrombus area, behind core platelets (gray) and shell platelets (white) with their respective computed velocity magnitudes. F) Average intrathrombus plasma velocity computed for geometries with the core in the front (black) or in the middle (red). Platelet packing density, but not the core location, determines the average velocity between platelets.

4.3.4 Solute transport within the hemostatic plug

In the first manuscript in this series [22], we provide experimental evidence that solute transport rates are slower in the core than in the shell. Solute transport measures how molecules move in the complex geometry of a hemostatic plug. Particle movement in the absence of obstacles and convection is described by Brownian motion (i.e. the diffusion coefficient). The diffusion coefficient of albumin [92] is $6x10^{-11}$ m^2/s, which given similarity in mass, resembles that of thrombin [93] ($8x10^{-11}$ m^2/s), but is much lower than non-protein agonists such as ADP [94] ($50x10^{-11}$ m^2/s). We next asked whether the observed differences in transport can be reproduced assuming that the core and shell are characterized by microenvironments with different transport properties, as opposed to being just two distinct geographical regions.

To do this, we designed a thrombus with size, shape and architecture based on the *in vivo* observations. Because the model that we used to study flow characteristics places large computational demands when trying to resolve flow features in the narrow gaps between individual platelets, we modeled the thrombus as two homogeneous regions with physical characteristics described by three parameters: porosity, permeability and

the effective diffusion coefficient (Figure 4A). Porosity represents the fraction of empty space in the mass, with larger gaps corresponding to larger porosity values. Permeability is the ability of a porous material to allow fluid to pass through, thus describing pore connectivity. The effective diffusion coefficient represents how a molecule of a certain size diffuses through a porous material. The presence of solid boundaries within a porous media hinders molecular movement, and as a result the effective diffusion coefficient is smaller than the free diffusion coefficient. Note that these material characteristics are independent. Thus, it is possible for two materials, or two hemostatic plug regions, to have the same porosity but different permeability or diffusion coefficients, and *vice versa*.

Porosity values for the core and shell were obtained *in vivo* [12]. Permeability values were obtained *in vitro* [51] and do not distinguish between core and shell regions. These experimental estimates served as an initial guide for our simulations. We assumed the existence of a core and a shell, and in both regions assigned a value for each of the three parameters. Thus, each simulation is specified by six parameters, and the value of a parameter for the core cannot be larger than the value of the corresponding parameter for the shell. We simulated the transport through the hemostatic plug, computed the average concentration in each region over time, and compared it to the experimental data (see Methods). We found a set of parameters for which there is a good agreement between the simulation and experimental data (Figure 4A). Thus, by hypothesizing that the core is more densely packed than the shell, we found a combination of parameters (Table 2) that reproduces the experimental data. Assuming instead that the core is as densely packed as the shell, does not lead to a good agreement between experimental data and simulations (Figure 4B).

Table 4-2

Parameter values used in Figure 4A

Parameter	Core	Shell
Porosity − ε	0.2	0.4
Permeability (m^2) − κ	10^{-17}	10^{-16}
Effective diffusion coefficient (m^2/s) − D	4×10^{-12}	10^{-11}

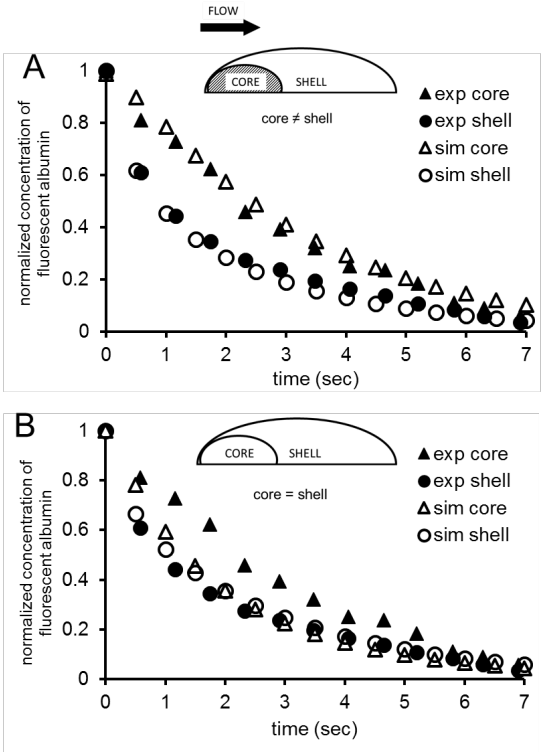

Figure 4- 4 Solute transport can be computationally reproduced.

The diagram of the geometry used to simulate the solute transport process is shown above each graph. The hemostatic plug is designed as a combination of two homogeneous regions, denoted as “core” and “shell”, in which physical characteristics

such as packing density and fibrin content are defined by porosity, permeability and effective diffusivity. The graphs show data (from Welsh at al., 2014) and simulations of caged fluorescent albumin transport. The vertical axis shows the normalized concentration of fluorescent albumin from experimental data (filled symbols –exp) and simulations (empty symbols – sim). Solute transport is faster in the shell (triangles) than in the core (circles) in vivo. These phenomena can be computationally reproduced only by assuming that the core and the shell have different packing densities (A) and not otherwise (B).

Due to the multidimensional nature of the parameter space it is possible for multiple combinations of parameters to fit the data equally well. Since it is not feasible to investigate all possible combinations, we used sensitivity analysis to determine the impact of each parameter on solute transport. Two complementary approaches were used, single-parameter and global sensitivity analysis. Single parameter analysis reveals how sensitive the simulation output is to the change of a single parameter. The model is sensitive to the effective diffusion coefficient and, to a lesser degree, porosity (Table 3). Conversely, the model is insensitive to the choice of the permeability value. The large sensitivity to the effective diffusion coefficient fits well with the results obtained in the previous section where we observed that the intrathrombus microenvironment is diffusion dominated. The global sensitivity analysis was performed by running simulations using different parameter combinations. We found a nonlinear trend with a well-defined minimum for the effective diffusion coefficient (Figures 5A and B). This shows that choosing the correct value for the effective diffusion coefficient results in a good fit to the data regardless of other parameter values. This confirms the results of the single-parameter sensitivity analysis. Moreover the minimum in the scatter plots represents a theoretical estimate of the effective diffusion coefficient values in a hemostatic plug (compare the minima in Figure 5 with the values shown in the bottom

row of Table 2). In contrast, the same analysis applied to porosity and permeability shows no pattern (Figure S5), confirming our previous conclusion that molecular movement in the thrombus is dominated by diffusion.

Table 4-3

Single parameter sensitivity analysis

	Sensitivity score	
Parameter	**Shell**	**Core**
D (diffusion)	3.02	0.43
ε (porosity)	0.82	0.06
κ (permeability)	0.0006	0.0004

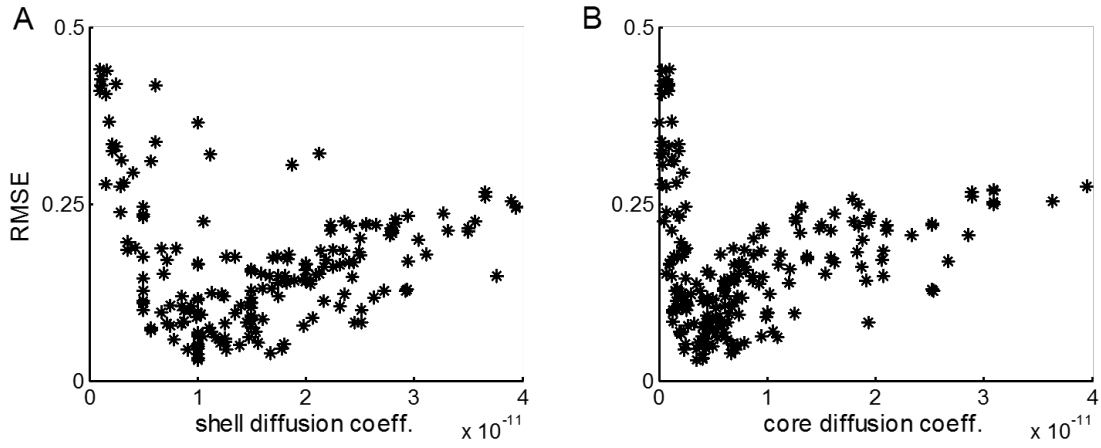

Figure 4- 5 Global Sensitivity analysis.

We implemented global sensitivity anal ysis performing 200 simulations, each with a different combination of parameters, and evaluated the fit (RMSE value) to the experimental data describing the transport of caged fluorescent albumin. We plot the

values sampled for the effective diffusion coefficient in the shell (A) and in the core (B) with the corresponding RMSE value. The effective diffusion coefficient values show a robust signal with respect to the fit, independently of the choice of the other parameter values. From this we estimate the effective diffusion coefficient to be 1x10-11 and 4x10-12 m2/s for core and shell respectively.

4.3.5 Release of soluble agonists from the injury site

Potent platelets agonists, such as thrombin, are primarily produced in close proximity of the injury site [12,87]. We examined how a closely-packed core region affects the distribution of thrombin-like solutes that are produced in a small region under the core of the hemostatic plug. Parameter values estimated in the previous section (porosity, permeability and effective diffusion coefficient) were used to describe the physical characteristics of the core and the shell. We simulated the constant release of a substance with the same diffusion coefficient as albumin from a 1 μm patch on the vessel wall under the core. We ran the simulation until it reached steady state (usually at about 30 seconds) and computed the average concentrations of the solute in the simulated core and shell, comparing a model in which packing density is greater in the core than the shell (which is what we observe *in vivo*) with a model in which packing densities are equal in the core and shell.

The results are summarized in Figure 6 with the computed concentrations normalized to the value calculated in the core when the packing densities are equal. Having a densely packed core increases the effective concentration of soluble agonists in the core approximately 4.5-fold (Figure 6 *lower left*). In contrast, the concentration attained in the shell was 10- to 20-fold lower than in the core, regardless of whether the core and shell

were consider as having equal or unequal packing density (Figure 6 *lower right*). The core is thus acting as a selective molecular prison, where molecules may get 'trapped' in a gap size dependent manner. Conceivably, as platelets transition to a state of full activation and fibrin polymerization fills the available spaces within the core [12], the core becomes a prison for an even broader set of molecules.

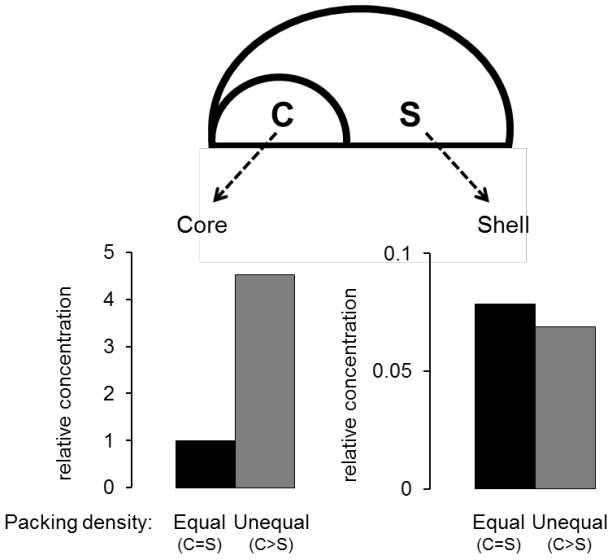

Figure 4- 6 The core is retentive.

Relative concentrations in a simulated core (C) and shell (S) were calculated when a substance with the same diffusion coefficient as albumin was released from a 1 μm patch under the core. Simulations were run until steady state was reached, comparing two scenarios in which the packing density in the core was either equal to or greater than the shell. Calculated concentrations were normalized to the value attained in the core when the packing densities are equal. The graph on the lower left shows steady state concentrations in the core, which are higher when density in the core is greater than the shell. The graph on the lower right shows steady state concentrations in the shell, which are lower than in the core and unaffected by having core density greater than the shell.

4.3.6 Testing model predictions

The simulations described so far show that packing density dictates transport rates. We hypothesized that a decrease in packing density would modify the thrombus architecture by reducing the size of the core and total platelet accumulation. This would happen because: 1) larger average gaps between platelets decrease the effective concentration of agonists, especially in the core, which is where we have shown [12,87] that most of the thrombin is found; 2) the decrease in agonist concentration reduces platelet activation, leading to a smaller core; and 3) fewer fully activated platelets diminish the paracrine effects of agonists such as ADP and TxA_2 released from activated platelets, causing a decrease in total platelet accumulation.

We tested this hypothesis using data obtained with mice carrying a substitution of phenylalanine for two tyrosine residues in the cytoplasmic domain of the β subunit of the $\alpha_{IIb}\beta_3$ integrin. This diYF mutation impairs integrin outside-in signaling and slows clot retraction *in vitro* [95]. In the following chapter [96], we show that this mutation also impairs retraction *in vivo*, suggesting that hemostatic thrombi in these mice will have larger gaps between platelets compared to wild type. Figure 7A shows the comparison of caged fluorescent albumin transport experiments in control and diYF mice (from Chapter 5, Figure 5-2). Consistent with our hypothesis, transport in both the core and the shell is faster in the diYF mice.

We modeled conditions in the diYF mice using the parameter values listed in Table 2, changing only the value of the effective diffusion coefficient in both the core and the shell

to simulate the looser platelet packing. We used the RMSE to estimate the fit to the data. We found a good agreement with the experimental data (Figure 7B) when the value of the effective diffusion coefficient was doubled in both the core and shell (D_c = 8x10^{-12} m^2/s; D_s = 2x10^{-11} m^2/s). These results illustrate that we can reproduce the experimental observations of solute transport in diYF mice by modeling a thrombus with decreased packing density compared to wild-type.

Next we utilized the parameter set that provided the best fit to the diYF data to simulate the constant release of an agonist from the vessel wall and compared the results with the wild type simulation (Figure 7C). This simulation demonstrates that when the gaps between platelets become larger, as in the diYF mice, the concentration of thrombin-like agonists is decreased in the core and in the shell. This supports our hypothesis that a reduction in the size of the core in diYF mice is due not to the inability of platelets to be activated or to a decrease in agonist production, but to an increase in the size of the gaps between the platelets.

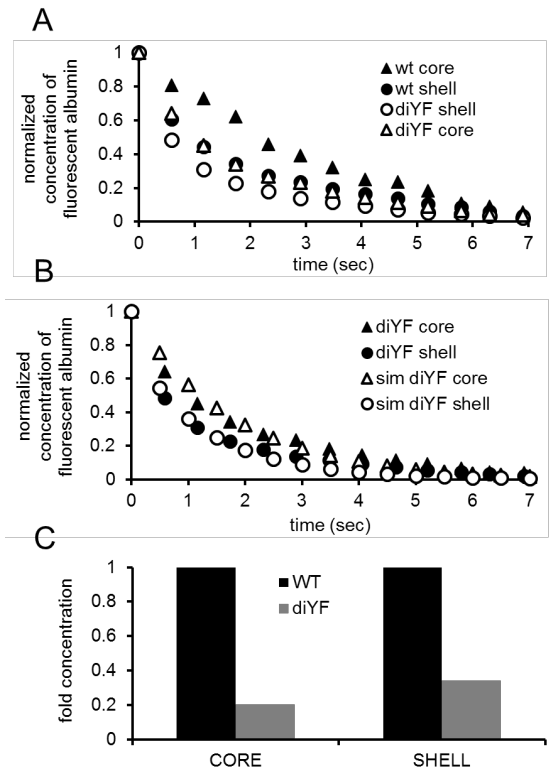

Figure 4- 7 Larger gaps predict faster solute transport and decreased platelet activation.

A) Solute transport, as measured by caged fluorescent albumin, is faster, both in the core (circles) and in the shell (triangles), of diYF mice (empty symbols) compared to WT mice (filled symbols) (experimental data are from Chapter 5, Figure 5-2). B) Simulations (empty symbols) predict measured solute transport data, for both the core (circles) and the shell (triangles) of diYF (filled symbols) mice. C) Simulation of solute release from a wall region under the core predicts that the average concentration at steady state will be lower in both regions in the diYF mice.

4.4 Discussion

The hemostatic response requires platelets to adhere to the vessel wall and then to each other, forming part of a plug that prevents further bleeding and fostering the local

production of thrombin and fibrin. Here we have considered platelets from a different perspective, focusing on their ability to alter their local environment by obstructing the free flow of plasma-borne molecules into the region of injury and the free flow of platelet-derived molecules out of the region. Our goal was to understand how the physical attributes of a platelet-enriched thrombus impact the hemostatic response, an idea previously examined by Kim, et al. using data obtained *in vitro* [53]. To accomplish this goal, we utilized experimental solute transport data [22] to inform numerical simulations.

The results show that by acting as obstacles platelets can retard plasma flow by orders of magnitude. Our estimates for intrathrombus velocity are in agreement with *in vitro* estimates [51] and 3D simulations [4]. A further reduction in plasma velocity is achieved by decreasing the size of the gaps between platelets. The end result is the formation of a sheltered microenvironment where diffusion, rather than convection, becomes the dominant mechanism for molecular movement. Using simulations benchmarked on experimental evidence we estimate the effective diffusion coefficient for an albumin-like substance to be five times smaller in the shell than in the vessel lumen, and even smaller in the core. We expect the effective diffusion coefficient of thrombin to be even smaller given its binding kinetics.

Solute transport within a hemostatic mass has recently received attention. Hindered protein transport through a fibrin cap has been considered [53], with results suggesting that the cap limits thrombus growth. Hindered transport was also considered as a mechanism capable of stopping thrombus growth [54,56]. In a previous study from our group, transport through a reconstructed 3D thrombus was examined[4]. The results show that a protein-sized solute released from the bottom of the thrombus will escape from the

sides. Thus, a variety of experimental and theoretical approaches have reached similar conclusions. This speaks to the generality of hindered transport as a mechanism to limit thrombus growth following injury in order to achieve hemostasis while avoiding unnecessary vascular occlusion. Hemostasis begins with platelets being recruited at a site of injury, stably-attached platelets becoming progressively more activated by potent agonists, such as thrombin, which are produced primarily at the site of injury [12,87]. As platelets become more activated, the gaps between them shrink and soluble agonists can either be trapped (i.e. thrombin), or prevented from penetrating in quantities sufficient to drive excessive platelet activation and fibrin deposition (i.e. prothrombin and other coagulation factors) [54,59].

As in any model, certain simplifications and assumptions are necessary. In the explicit-platelet model (Figures 1-3), where only fluid flow was examined, platelets were assumed to be ellipsoids with semi-axes of 1 and 0.6 μm. However, our results suggest that intrathrombus flow is governed primarily by gap size and not by the details of platelet shape. Platelet shape change, variability in platelet size, or the presence of larger cells such as leukocytes would all alter the flow, but we assume that such effects are captured implicitly by varying the gap size distribution. The effect of gap size distribution on flow is illustrated in Figure 1. Intrathrombus velocity is progressively decreased as the gap size decreases. For all gap size distributions considered the flow is always in the regime of low Reynolds, Peclet and Womersley numbers (see supplementary materials). Under the physiological conditions we examined we can expect constant laminar flow in the lumen and diffusion to be dominant in the thrombus.

The homogeneous species transport model, which is based on a porous medium representation of the thrombus, is parameterized using measurements obtained *in vivo*

(Chapter 3 and 5). The parameters in the homogeneous transport model (diffusivity, permeability and porosity) implicitly capture the macroscopic details such as platelet packing density or shape change and fibrin content, or any combination of the two. Our species transport simulations (Figures 4-7) depend, therefore, on an effective diffusivity derived from experimental data.

The solute transport data (Figure 4) show the loss of fluorescence over time in a 2D thin slice (~0.5 μm) of the thrombus taken with a confocal microscope. The caged fluorescent albumin, however, elutes from the thrombus in a 3D volume, thus it can take paths that cannot be accounted for in a 2D model. Macroscopically, 2D simulations assume that transport in the 3rd dimension is not important, or that the thrombus is "long" in the neglected dimension. While this is obviously a simplification, the 2D results remain meaningful for analyzing the effects studied here. In the Supplementary Materials we show that in a 3D diffusion-only version of the thrombus where the depth-to-length aspect ratio approaches 0.5, the 2D simulation results become a good approximation to the 3D simulations (Figure S7B).

An increasing amount of *in vivo* evidence is consistent with the model we propose. Porosity measurements indicate that the differences between core and shell are size selective [12]. Thrombin activity can be detected only in the core [12,87]. Full platelet activation, as measured by P-selectin expression, occurs only in the core, whose size is neither by eliminating ADP signaling nor enhanced by boosting it [12]. Artificially increasing plasma prothrombin concentration does not increase total platelet accumulation in an arterial injury model [97], suggesting that increasing the concentration of thrombin precursor does not lead to increased thrombin production or increased platelet

recruitment. Finally, our model predicts that changing the dynamics of transport changes the effective concentration of agonists and thus thrombus architecture. We verified this prediction experimentally in an *in vivo* mouse model characterized by a defect in platelet retraction. We found that thrombi with larger gaps developed smaller cores and accumulated less fibrin [96].

Taken together, this study and the accompanying chapters demonstrate the importance that gap size has in shaping molecular transport and platelet activation status. Although others have addressed the potential importance of gaps [98] or estimated gap sizes [53,99,100], this is the first effort of which we are aware that combines observational and computational approaches to understand the effect of gap size on thrombus growth. In 3D one can expect that some platelets, or portions of platelets, may be in direct membrane-membrane contact (0 nm), or in indirect contact mediated by protein-protein interactions (tens of nm), integrin-fibrinogen-integrin interactions (less than 100 nm) [101] or GPIb/IX-VWF interactions (possibly ≥100 nm) [102]. In this microstructure it is important to know the gap size distribution, because that is what ultimately determines transport rates.

In conclusion, the results presented here demonstrate that the interactions between platelet biology and molecular transport are important in shaping thrombus architecture and determining platelet activation status. These interactions have already been partially unmasked by *in vivo* data [12] indicating that the outer, less closely-packed region of a hemostatic thrombus is driven primarily by platelet-derived highly-diffusible molecules such as ADP, and is therefore most susceptible to $P2Y_{12}$ antagonists. In contrast, the tightly-packed core region is primarily driven by the less diffusible thrombin and is more

susceptible to thrombin inhibitors. The effects of intrathrombus transport should therefore be considered when designing new and improved antiplatelet agents.

4.5 Supplemental materials

4.5.1 Thrombus design.

To investigate plasma velocity we designed a thrombus with size and geometry based upon *in vivo* images of stable thrombi formed following penetrating laser-induced injuries in mouse cremaster arterioles (Figure S1). Each platelet was modeled as an ellipse with minor and major semiaxis measuring respectively 0.6 μm and 1 μm. To investigate packing density we changed the dimensions of the ellipses without modifying their positions. The minimum gap size allowed corresponds to the minimum distance between two ellipses stacked vertically; this metric is correlated with, but does not always correspond to, the absolute minimum gap size in the entire thrombus. The gap size distribution shown in Figure S2A depends on the minimum gap size; increasing the minimum gap size also increases the average gap size (Figure S2B) and the porosity (Figure S2C). These results show that the minimum gap size is an appropriate variable for controlling changes in the internal gap size distribution. To ensure that the particular thrombus geometry we chose (Figure S1) does not introduce bias, we also generated randomly packed semicircular 'thrombi', using ellipses of the same dimensions, where the minimum allowed gap was the same minimum gap we used in our design (Figure S3A and B). A similar gap size distribution was found (Figure S3C). Finally we modeled the internal core-and-shell heterogeneous thrombus architecture by selectively changing

the dimensions of a subset of platelets to reproduce images of thrombi formed *in vivo* following penetrating injuries in the microcirculation [12].

4.5.2 Computational Fluid Dynamics.

We used COMSOL® version 4.3a (a commercial finite element fluid dynamics solver) to simulate the flow of fluid in a blood vessel. In the cremaster vasculature, under physiological conditions, the blood flow is slow (i.e. Reynolds number ~ 0.01) and thus one can use the Stokes equations to simulate the fluid flow. For our explicit platelet model (Figure 1) we solved the Stokes equations: $\nabla^2 u - \nabla p = 0$; $\rho \nabla \cdot u = 0$, where η is the dynamic viscosity, u is the velocity, ρ is the fluid's density, and p is the pressure. In this model the hemostatic plug is represented explicitly by a collection of ellipses (platelets) variable in size and number, with gaps between them, placed at the bottom of a 30 μm vessel.

For the homogenous porous media model, in which the platelets are replaced by an effective homogeneous medium, we computed the intrathrombus fluid velocity using the Brinkman equation: $\eta/\varepsilon \nabla^2 u - \nabla p - \eta/k\, u = 0$; where k denotes the permeability of the porous medium, and ε is the porosity. The Brinkman equation is a semiempirical adaptation of Darcy's law and, given the slow flow velocity, can be applied inside the thrombus. The effective viscosity term present in the Brinkman equation, is defined as viscosity/porosity (η/ε) and incorporates the effects of thrombus porosity and tortuosity on fluid viscosity. In this model the hemostatic plug consists of two homogeneous porous media regions each characterized by three parameters: porosity (ε), permeability (κ) and

effective diffusion coefficient (D). The initial parameter values were chosen from the literature: the initial value for porosity was chosen to be 0.6 for the shell and 0.4 for the core, based on earlier *in vivo* measurements [12] while the initial value for permeability [51] was taken to be 10^{-18} m^2. We simulated a fluid having properties similar to water, with constant density of 1000 kg/m^3 and viscosity of 0.0008 Pa s. To estimate the relative contribution of diffusion and convection in our designed thrombus we defined a Peclet number as follows: Pe = (average diameter of an intrathrombus pore) x (average intrathrombus velocity) / (value of the bulk diffusion coefficient). In both models (explicit platelet and homogeneous porous media) we chose a pressure drop of 3 Pa that corresponds to a centerline velocity of a typical cremaster blood vessel as measured from velocimetry (i.e. 2 mm/s). No-slip boundary conditions were applied at the vessel walls and platelet walls. From the numerical solvers embedded in COMSOL we used PARDISO [103] with a relative tolerance of 10^{-4}. Other solvers (i.e. MUMPS and SPOOLES) were tested with similar tolerance levels, minor differences were observed in the solution time, but not in the solution result. The simulation time was 2 minutes using an Intel i7 with 8 cores and 12 GB of RAM.

4.5.3 Solute transport

Solute transport was simulated using the species transport in porous media in COMSOL® version 4.3a using the convection-reaction-diffusion equation: $\partial c/\partial t = D\nabla^2 c - u\nabla c + R$, where *c* is the concentration of chemical species of interest, D is the diffusion coefficient, *u* is the velocity vector field, R describes sources of the chemical species (e.g. ADP from platelet dense granules). The albumin diffusion coefficient in the

bulk is $6x10^{-11}$ m^2/s [104], the corresponding effective diffusion coefficient values for albumin in the core and shell regions were estimated in this study from the caged fluorescent albumin transport data reported in chapter 3. To simulate the transport of caged fluorescent albumin we set an initial uniform concentration of a tracer solute in the vessel, imposed a zero concentration at the influx boundary and ran the simulation until the concentration inside the thrombus regions was zero. We imposed zero diffusive flux ($n \cdot \nabla c = 0$) boundary conditions at the outlet boundary and no flux boundary conditions at the vessel walls. From the numerical solvers embedded in COMSOL we used MUMPS [105] with a relative tolerance of 10^{-3} and an absolute tolerance of 10^{-6}. The simulation time was approximately 1 hour using a maximum step size of 10^{-3} seconds. To assess the fit to the experimental data we computed the average concentration in each region over time and the root mean square error (RMSE), which we computed as follows: for each experimental data point available we calculated the square deviation from the simulated point and then computed the average of all such points.

4.5.4 3-dimensional species transport simulations.

Here we asked if the parameters estimated in the 2D model are a good approximation for a 3D representation of the model. The experimental data (Figure 4) shows the loss of fluorescence over time in a 2D image of a thin (~0.5 μm) longitudinal slice of the thrombus taken with a confocal microscope. In reality however, the caged fluorescent albumin elutes from the thrombus in a 3D volume, and thus can take paths to escape that cannot be represented explicitly in a 2D model. In other words, in a 2D model it is implicitly assumed that the 3rd dimension is long enough that edge effects do not

influence the dynamics in the middle. Here we examined the influence of the 3rd dimension by comparing transport in simplified 2D and 3D models.

We started by comparing the 2D homogeneous porous media model used in the main text (which included fluid flow in the lumen) with a simplified model using the same 2D geometry but without explicit consideration of the flow in the lumen. In this new model, we only need to specify 2 parameters for each homogeneous porous media region (core and shell), namely the porosity and the diffusion coefficient (both as in Table 2). No-flux boundary conditions were applied at the base of the thrombus and zero concentration at the outer boundary of the thrombus. The latter boundary conditions simulate the rapid disappearance of a solute leaving the thrombus via flow in the lumen. We set an initial uniform concentration of a tracer solute in the thrombus and ran the simulation until the concentration inside the thrombus regions was zero. We computed the average concentration over the entire thrombus at each time point and compared it to a simulation where fluid flow in the lumen was explicitly considered. The results show that the simplified 2D model is a good approximation of the full system, at least when only considering the overall average concentration (Figure S6).

Next we compared the simplified 2D model results with a 3D representation. We considered the aspect ratio between the length and the depth of a thrombus (Figure S7, upper insert). For each aspect ratio examined we used the same parameter values, initial conditions and boundary conditions as in the 2D diffusion model. We ran the simulations and determined the ratio between the diffusion coefficient in the 3D model and the diffusion coefficient in the 2D model ($D_{3D} \,/\, D_{2D}$) needed for the 3D simulation results to match the 2D simulations (Figure 7B). We found that when the aspect ratio is

greater than about 0.5, the 2D model is a meaningful comparison to the 3D model. This suggests that the estimates we obtained from our homogeneous porous media 2D model are a good approximation for the 3D case if the geometry of the thrombus is such that the depth of the thrombus is at least about half its length.

4.5.5 Non-dimensional parameters.

To compute the Reynolds and Womersley numbers we used a diameter of 30 μm, matching that of the arterioles we use in our experiments, and a heart rate of 600 beats per minute to compute the angular frequency of the oscillations (i.e. 10 Hz). The value for the blood dynamic viscosity at 37 degrees C, and at a shear rate of 100 s^{-1}, was taken from Rosenson et al. [106].

Reynolds number:

$$R_e = \frac{uL}{\nu} = \frac{(2 * 10^{-3}\ m\ s^{-1})(30 * 10^{-6}\ m)}{10^{-6} m^2\ s^{-1}} = 0.06;$$

where u is the velocity, L is the characteristic length and ν is the kinematic viscosity.

Womersley number (mouse arteriole):

$$\alpha = R\left(\frac{\omega}{\nu}\right)^{1/2} = 15 * 10^{-6} m * \left(\frac{10\ s^{-1}}{10^{-6} m^2 s^{-1}}\right)^{\frac{1}{2}} = 0.0474;$$

where R is the radius, ω is the angular frequency of the oscillations and ν is the kinematic viscosity.

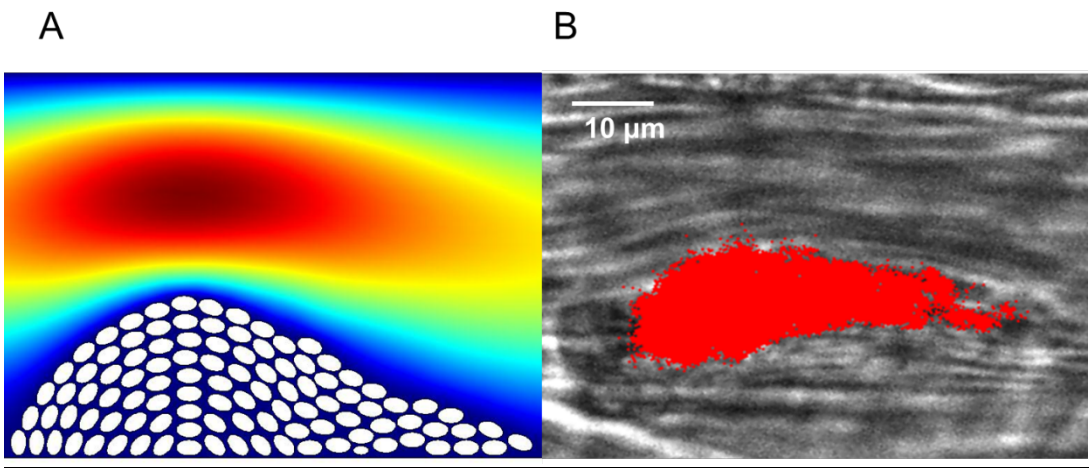

Figure 4- 8 Geometry used in the simulations.

(**A**) Geometry used in the simulations is based on thrombus in vivo image (**B**).

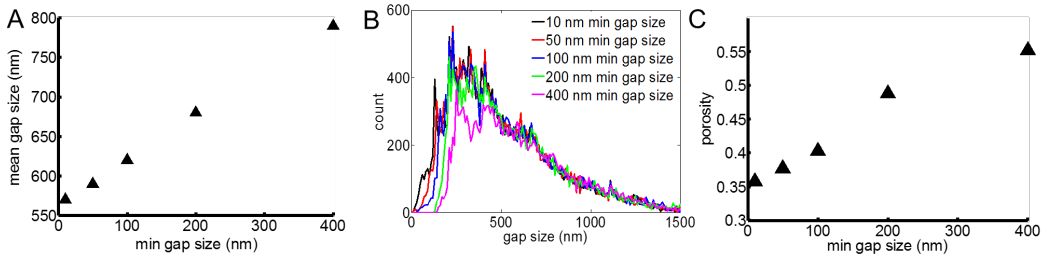

Figure 4- 9 Relation between minimum gap size and mean gap size.

A) Relation between minimum gap size and mean gap size. **B**) Distributions of gap size between platelets using different minimum gap sizes (10 nm bins). **C**) Relation between minimum gap size and porosity, computed as the fraction of empty space in the 2D geometry.

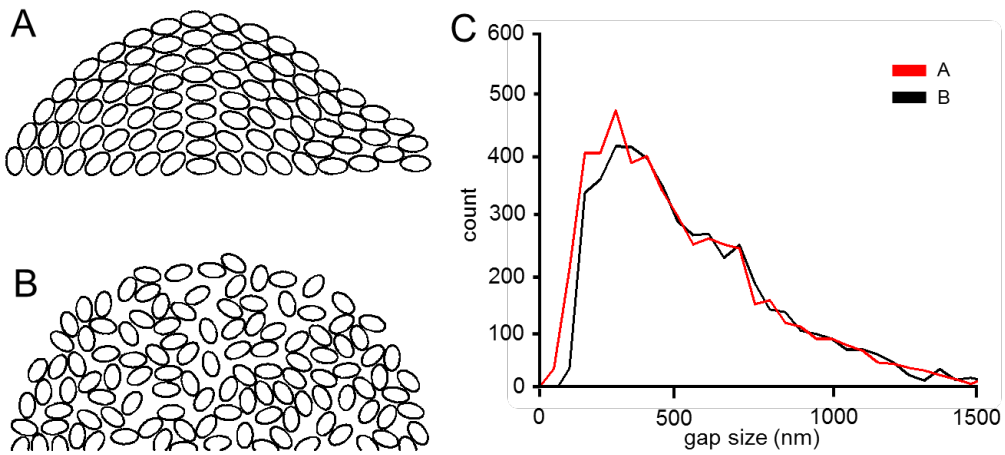

Figure 4- 10 Thrombus simulation architecture.

A) Thrombus used for simulations in main text with minimum gap size of 100 nm. **B)** Sample thrombus generated by a random packing algorithm with minimum gap size of 100 nm. **C**) Comparison between the distributions of gap sizes of A and B (50 nm bins).

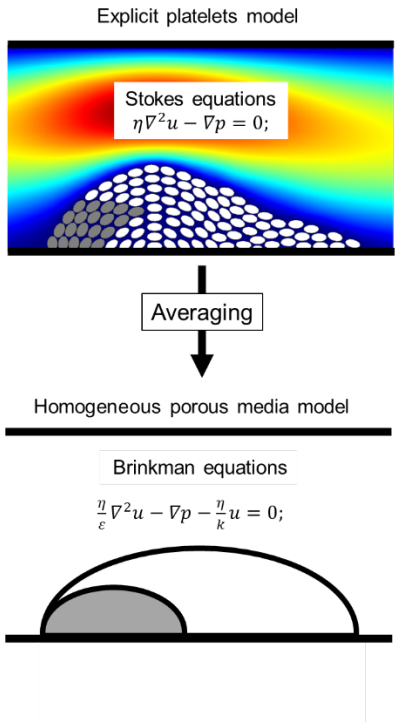

Figure 4- 11 Schematic illustration of the relationship between the explicit platelet and homogenous porous media models.

The velocity fields are computed using the Stokes equation in the model with explicit platelets, and using the Brinkman equation in the model with homogenous porous media.

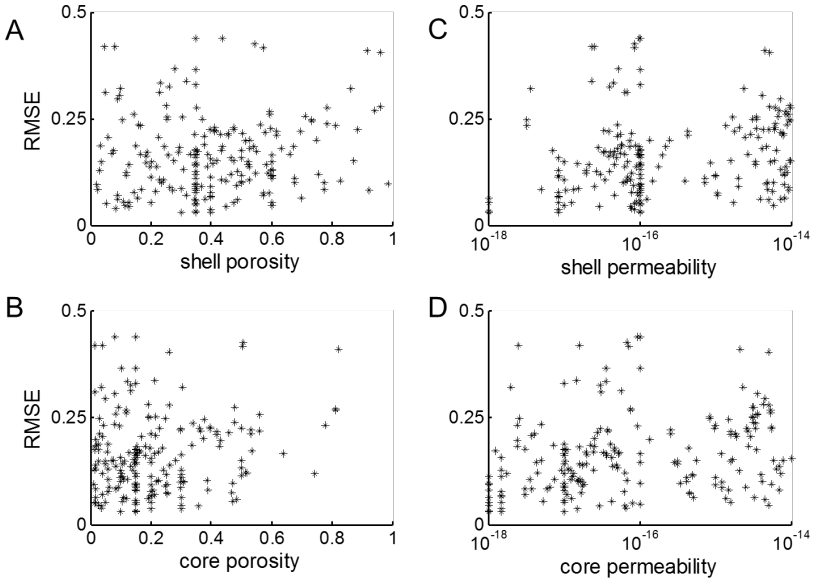

Figure 4- 12 Global sensitivity analysis.

A) Global sensitivity analysis simulations evaluated as the fit (RMSE value) to the experimental data describing the transport of caged fluorescent albumin. We plot the values sampled for the porosity in the shell (**A**) and in the core (**B**), and for the permeability in the shell (**C**) and in the core (**D**), with the corresponding RMSE value. No correlation is found for any of the parameters, or for any of the regions, illustrating that the choice of these parameters does not influence the fit to the experimental transport data.

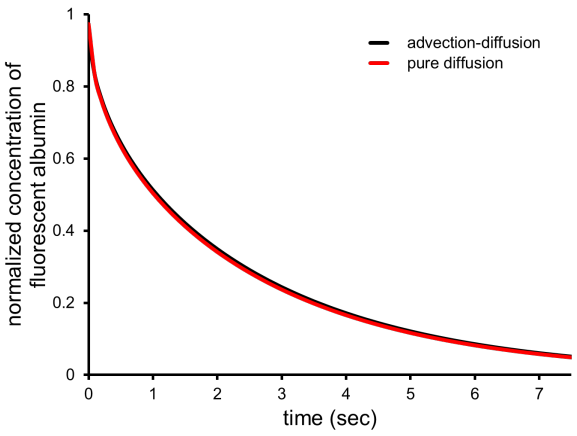

Figure 4- 13 Comparison between 2D advection-diffusion and 2D diffusion model inside of the thrombus.

Average concentration computed over the entire thrombus using advection-diffusion in a homogeneous porous media (black line) is compared to a model with only diffusion (red line). For both models we used the parameter values listed in Table 2 for porosity and diffusion coefficient.

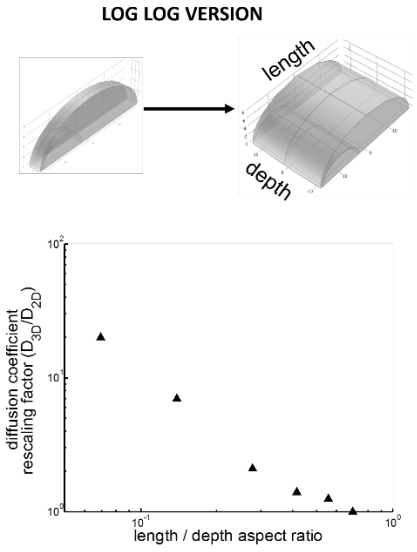

Figure 4- 14 3D core and shell homogeneous porous media diffusion model.

The x-axis shows the aspect ratio between the depth and the length (see upper insert). The y-axis shows, on a log scale, the ratio between the 3D and the 2D diffusion coefficient value for which the 3D results closely match the 2D results. When the depth-to-length aspect ratio is greater than about 0.5, the 2D simulation becomes a good approximation to the 3D model.

CHAPTER 5: A systems approach to hemostasis: 3. Thrombus consolidation regulates intrathrombus solute transport and local thrombin activity

This research was originally published in *Blood*. Stalker TJ, Welsh JD, Tomaiuolo M, Wu J, Colace TV, Diamond SL, Brass LF. *Blood*. 2014;124(11):1824-31.

5.1 Introduction

In previous studies, we and others have shown that the extent of platelet activation during the hemostatic response to penetrating injuries is heterogeneous, resulting in a distinctive thrombus architecture that consists of a core of fully-activated platelets immediately adjacent to the site of injury overlaid by a shell of minimally activated platelets[12,80,81,107-109]. We have also shown that different signaling pathways within the platelet signaling network predominate in different regions of the thrombus, with ADP/$P2Y_{12}$ signaling being critical for platelet recruitment and retention in the shell, while thrombin signaling drives full platelet activation and firm adhesion in the core[12]. These findings show how partially overlapping gradients of soluble agonists emanating from the site of injury can support platelet accumulation, promote platelet activation and produce the characteristic thrombus architecture.

Regional differences within hemostatic thrombi are not limited to the extent of platelet activation. There are physical differences as well. Most notably, our previous studies showed that the core region has reduced porosity and decreased plasma molecule penetration compared to the shell, indicative of increased platelet packing density in the

core[12]. Solute transport in the gaps between platelets is also slower in the core than in the shell, both of which are orders of magnitude slower than in the remaining vessel lumen[110]. The drop in transport rates occurs soon after platelet accumulation begins, preceding full platelet activation as detected by the appearance of P-selectin on the platelet surface. A computational analysis based on these observations indicates that diffusion, rather than convection, governs the movement of plasma and platelet-derived molecules in the small gaps between platelets found in the core, and suggests that the observed difference in transport rates is sufficient to confine the accumulation of thrombin to the core[111].

Based on these findings, we now propose an extended model for hemostasis in which 1) greater platelet packing density in the thrombus core helps to determine local thrombin activity by providing a microenvironment in which thrombin can accumulate, and 2) active regulation of platelet packing density contributes to thrombus growth and stability by helping to determine where thrombin is generated and fibrin accumulates. Here we have tested this model by perturbing platelet packing density and measuring its effects on intrathrombus solute transport, localization of thrombin activity and platelet activation. Doing so required the development of a novel method to measure thrombus consolidation in real time *in vivo* in mice with a defect in clot retraction. Prior studies have demonstrated that following initial platelet accumulation at a site of vascular injury, the platelet mass rapidly consolidates via platelet-mediated retractile processes[112,113]. Law *et al.*[114] showed that substituting Phe for Tyr747 and Tyr759 (diYF) in the cytoplasmic domain of the β subunit of $\alpha_{IIb}\beta_3$ inhibits outside-in signaling through the integrin and impairs clot retraction without affecting integrin activation and fibrinogen

binding. Here, we have tested the same diYF mice following vascular injury using a newly-established method for assessing molecular transport in the gaps between platelets[110]. The results show that the diYF mice have a defect in thrombus mass consolidation and that this defect is accompanied by the increase in transport rates and a decrease in fibrin accumulation in the thrombus core predicted by the computational modeling. Taken together, these studies reveal a novel role for outside-in signaling in the regulation of platelet mass consolidation and intrathrombus solute transport in the gaps between platelets. They also show that physical properties such as platelet packing and molecular transport are integral components of the hemostatic response, helping to determine agonist distribution and platelet activation within an evolving platelet mass.

5.2 Materials and methods

5.2.1 Mice

DiYF mice were described previously[114,115]. They were originally generated in the laboratory of Dr. David Phillips at Portola Pharmaceuticals (San Francisco, CA) and were obtained by us from Dr. Tatiana Byzova at the Cleveland Clinic Foundation (Cleveland, OH). They are backcrossed on to the C57Bl/6 background at least 7 times[115], and were therefore compared with C57Bl/6 mice from Jackson Laboratories (Bar Harbor, ME) as controls. Male mice 8-12 weeks of age were used for intravital microscopy experiments. The University of Pennsylvania Institutional Animal Care and Use Committee approved all animal procedures.

5.2.2 Laser-induced injury in mouse cremaster arterioles

The laser-induced thrombosis model as performed here was described in detail previously[12]. Additional information is provided in the Supplementary Materials.

5.2.3 Platelet mass consolidation

Platelet mass consolidation was measured using an approach modified from Ono et al[112]. Blood was drawn from a donor mouse via cardiac puncture using heparin as the anticoagulant and diluted 1:1 with modified Tyrode's buffer (4 mM HEPES, pH 7.4, 135 mM NaCl, 2.7 mM KCl, 3.3 mM NaH_2PO_4, 2.4 mM $MgCl_2$, 0.1% glucose and 0.1% BSA). Platelet rich plasma (PRP) was obtained by centrifugation at 150 g for 7 minutes. Alexa-fluor 568 labeled anti-CD41 $F(ab)_2$ was added for 15 minutes, followed by gel filtration of the platelets to remove plasma proteins and unbound labeling antibody. Approximately 50 million gel filtered platelets in 200 µl sterile Tyrode's buffer were infused into a recipient mouse prepared for intravital microscopy using standard procedures via a jugular vein cannula. The donor platelets were easily distinguished from the recipient's endogenous platelets via their fluorescent label, and they were incorporated into laser-induced thrombi normally. To assess platelet mass consolidation, time-lapse image captures of thrombus formation were analyzed offline. Stably adherent donor platelets were identified based on their Alexa-fluor 568 label, and the center of each donor platelet was marked manually frame-by-frame using the Manual Tracking procedure in Slidebook image analysis software (Intelligent Imaging Innovations, Denver, CO). Once marked, the straight line distance from where a platelet first firmly adhered to its final position at the conclusion of the timelapse (3 minutes post-injury) was calculated using

Slidebook and is reported as the end displacement. Multiple platelets were tracked in each thrombus and multiple thrombi from several mice were studied.

5.2.4 Intrathrombus solute transport

Intrathrombus solute transport was measured using caged fluoroscein coupled to albumin (cAlb) as described in detail in Welsh *et al* [110]. A detailed description is provided in the Supplementary Materials.

5.2.5 Computational simulation of solute transport

A detailed description of computational methods including model design and parameter description is included in an accompanying manuscript[111]. Additional information is provided in the Supplementary Materials.

5.2.6 Flow cytometry

Mouse blood was obtained via the inferior vena cava using heparin as the anti-coagulant, diluted 1:1 in modified Tyrode's buffer and centrifuged at 150 g for 7 minutes to obtain PRP. Alexa-647 fibrinogen, anti-P-selectin and Annexin V were added to separate samples, and the platelets were stimulated with either PAR-4 agonist peptide (AYPGKF, Bachem, Torrance, CA) for fibrinogen binding and P-selectin expression studies or the combination of AYPGKF and convulxin for Annexin V binding studies. Platelets were incubated for 15 minutes at 37˚C, diluted 5-fold with PBS and

fluorescence immediately measured using a BD FACS Calibur flow cytometer with subsequent analysis using FlowJo flow cytometry software.

5.2.7 Statistics

For data obtained from intravital microscopy experiments, statistics were calculated using the Mann-Whitney test for non-parametric data using GraphPad Prism 6.0 software.

5.3 Results

5.3.1 Role of β3 integrin tyrosine phosphorylation in platelet mass consolidation

Mice in which the two tyrosines in the β3 cytoplasmic domain have been mutated to Phe (diYF) were described previously, and showed a defect in integrin function, but the exact mechanism of this inhibition is unclear [114]. Platelets from diYF mice have normal $\alpha_{IIb}\beta_3$ integrin inside-out activation and ligand binding, but ligand binding induced β3 tyrosine phosphorylation is absent [114]. Outside-in signaling pathways that require β3 phosphorylation are thus impaired, resulting in unstable platelet aggregate formation and impaired fibrin clot retraction [114].

Previous reports have used intravital microscopy to observe consolidation of the platelet mass during the early stages of thrombus formation in vivo[112,113]. Although distinct from fibrin clot retraction in vitro, some of the same signaling mechanisms have been shown

to play a role in both processes, including myosin dependent platelet retraction[112,113]. Since diYF platelets were previously shown to have a defect in fibrin clot retraction, we sought to determine whether platelet mass consolidation was impaired following vascular injury in diYF mice. To accomplish this goal, we employed a single platelet tracking approach in which the movement of individually labeled platelets is tracked as the entire platelet mass consolidates towards the site of injury. In this case, platelets are removed from donor mice, labeled with Alexa-568 anti-CD41 $F(ab)_2$ fragments, and then infused into a syngeneic recipient mouse in numbers that result in labeling of a small percentage of the circulating platelet pool (described in the Methods section). Penetrating injuries were inflicted in cremaster muscle arterioles using a laser fired through the optics of the microscope[116]. We have previously shown that the response to laser injury is similar to the response observed when injuries are inflicted with a sharpened glass pipette[12].

Using this combination of injury and tracking techniques in wild-type mice, individual platelets within the platelet mass may be observed to move toward the site of injury as the mass consolidates with a mean end displacement of 4.2±0.27 μm (mean±SEM, Figure 1A-B, supplemental video 1). The bulk of the consolidation occurred during the first 60-90 seconds post-injury. Inward movement was reduced by approximately 50% in thrombi formed in diYF mice, which had a mean end displacement of 2.1±0.27 μm ($p<0.0001$ vs. WT, Figure 1B, supplemental video 2). These findings demonstrate that platelet mass consolidation is decreased in diYF mouse thrombi.

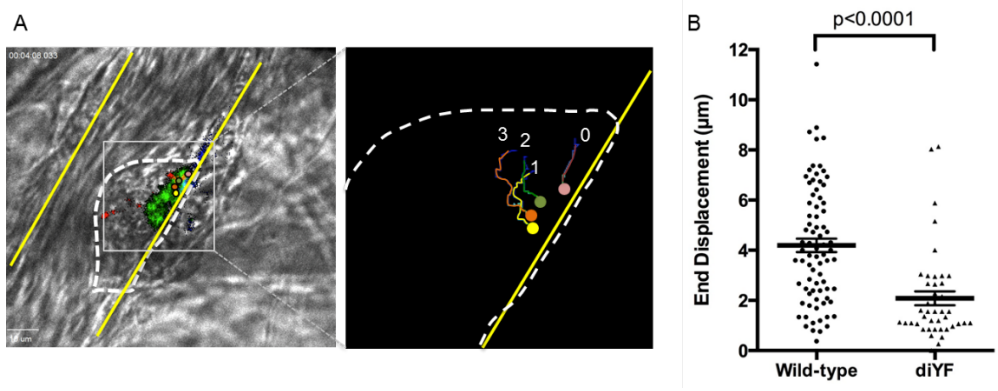

Figure 5- 1 Loss of β3 integrin tyrosine phosphorylation attenuates platelet mass consolidation following vascular injury in vivo.

Platelet mass consolidation was monitored by tracking the movement of individual platelets following adhesion to a developing thrombus, as described in Methods. A) Photomicrographs show representative thrombus from a wild-type mouse. The panel on the left shows 4 fluorescently labeled platelets within the platelet mass (outlined by the dotted line). The panel on the right shows the region in the left panel outlined by the gray box. The movement of the four platelets was tracked over time using image analysis software, and the tracks of each platelet in the image can be seen. B) The movement of individual wild-type and diYF platelets during laser-induced thrombus formation is reported as the end displacement (total distance along a straight line from platelet starting point to endpoint). Horizontal line and error bars indicate the mean±SEM. For wild-type, n=78 platelets from 14 thrombi and for diYF n=43 platelets from 12 thrombi. Statistics were calculated using the Mann-Whitney test.

5.3.2 Intrathrombus solute transport

One possible consequence of impaired platelet mass consolidation in diYF thrombi is altered plasma and solute transport in the narrow spaces between platelets. Intrathrombus solute transport is a critical regulator of platelet activation and thrombus evolution as it determines how far soluble molecular species generated at the injury site (e.g. thrombin) may distribute from their source before they are washed out[111]. Solute

transport was measured during hemostatic thrombus formation *in vivo* using caged fluorescein molecules conjugated to albumin (cAlb) as described in the Methods section. Following a flash of 405 nm laser light, the washout of the cAlb may be quantified over time to generate decay curves as a measure of solute transport within a platelet mass as a whole or in specific subregions (i.e. core and shell regions; Figure 2A-B). Consistent with the findings reported in Welsh et al[110], we found that in wild-type mice cAlb washout (i.e. solute transport) was substantially slower in the core region of thrombi as compared to the shell region (Figure 2B). This result is consistent with our previously reported finding of decreased porosity (i.e. increased platelet density) in the thrombus core vs. shell regions[12]. Interestingly, solute transport was increased relative to controls in both regions of the diYF thrombi, with transport in the core region of diYF thrombi similar to transport in the shell region of wild-type thrombi (Figure 2B). This finding suggests reduced platelet packing throughout thrombi in diYF mice, consistent with the impaired ability of diYF platelets to retract and consolidate the platelet mass as described above.

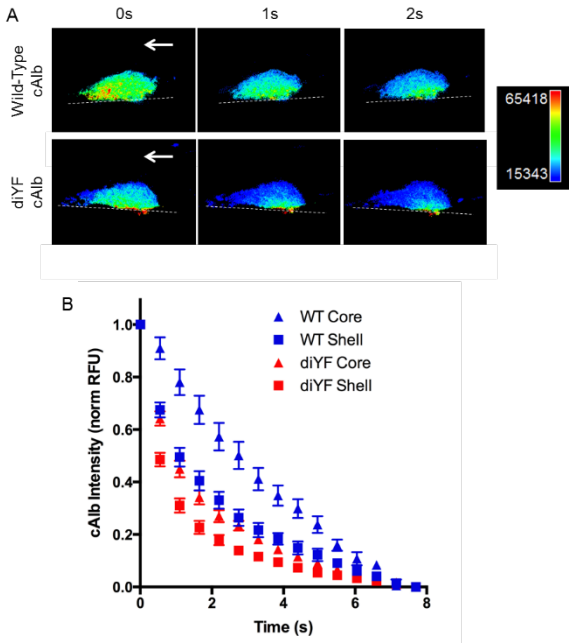

Figure 5- 2 Molecular transport is increased in diYF thrombi.

Caged fluorescent albumin (cAlb) was used to calculate molecular transport in thrombi formed following laser-induced injury in cremaster arterioles of wild-type and diYF mice. A) Photomicrographs show caged-FITC albumin fluorescence within a representative wild-type and diYF thrombus. The fluorescence is shown in pseudocolor to indicate relative concentration (blue is low, red is high). From left to right, panels show the same wild-type (top row) or diYF (bottom row) thrombus immediately following a flash of 405 nm laser light to uncage the cAlb in the thrombus (0s), followed by images captured 1 sec and 2 sec after the flash. The decrease in albumin fluorescence from 0-2 seconds is due to washout of the albumin from the platelet mass. Note the albumin is retained longer in the core region of the thrombi. B) Graph shows cAlb washout in the core (P-selectin positive, triangles) and shell (P-selectin negative, squares) regions of wild-type (blue) and diYF thrombi (red). Quantification and normalization procedure is described in Methods. Values are mean ±SEM for n=11 wild-type and n=12 diYF thrombi.

5.3.3 Computational simulation of agonist distribution in diYF thrombi

To investigate the impact of altered intrathrombus solute transport on platelet agonist distribution within a thrombus, we used computational modeling to simulate the physical conditions present within wild-type vs. diYF thrombi. Specifically, we examined the impact of the physical microenvironment on the distribution of a protein-sized solute released from the vessel wall at the base of a simulated platelet mass to mimic thrombin generation at a site of injury in vivo. The Navier-Stokes equations (COMSOL v4.3a) were used to resolve the flow field in a simulated 30 μm diameter blood vessel with a centerline velocity of 2 mm/s (i.e. mimicking a mouse cremaster arteriole). The Brinkman equations[117] were used to solve the velocity field in the thrombus modeled as a porous media and the advection-reaction-diffusion equation was used to simulate the transport of solutes in a porous media describing the hemostatic mass. To simulate the core and

shell architecture of wild-type and diYF thrombi, two regions were created in which the porosity, permeability and effective diffusion coefficient were varied by region to reproduce the solute transport conditions observed in vivo[111] (Figure 3A). Next, the constant release of a protein-sized solute from a 3 μm patch below the core region was simulated until a steady state was reached. The concentration of the solute in the core region of diYF thrombi was significantly reduced compared to its concentration in the core of wild-type thrombi (Figure 3B). The solute concentration was also significantly reduced in the shell of diYF thrombi compared to wild-type, although it should be noted that very little solute was retained in the shell region in both cases (note the difference in y-axis scale between Figure 3B and C). Thus, these computational simulations suggest that structural differences between the core and shell region can account for the heterogeneity of platelet activation observed in wild-type mice in vivo, and further predict that altered molecular transport within diYF thrombi will result in reduced local thrombin activity.

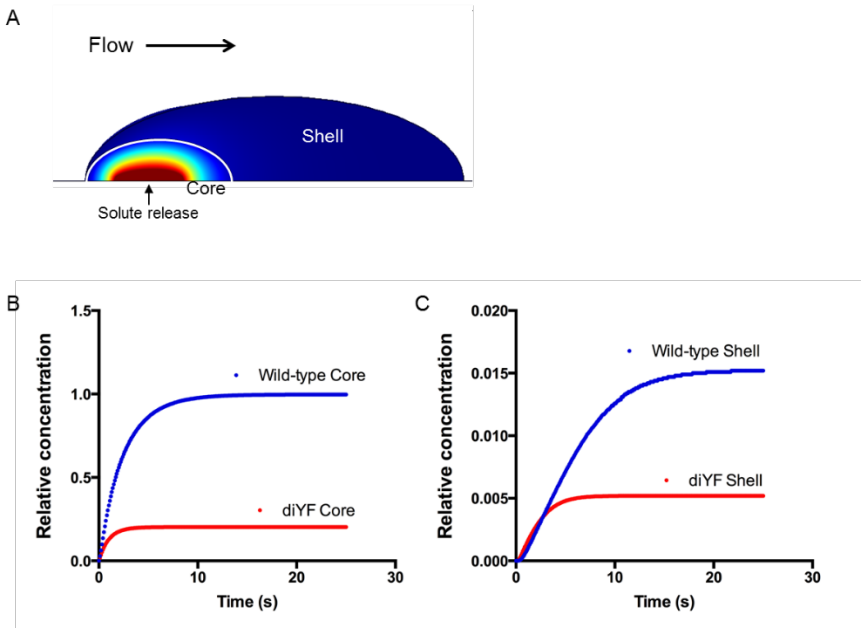

Figure 5- 3 Computational modeling studies demonstrating the impact of impaired platelet mass consolidation on solute distribution within a thrombus.

A) A snapshot of the simulation at steady state showing the core and shell regions, as well as the relative concentration of a solute released at a constant rate from a 3 μm patch on the vessel wall beneath the core region (shown in pseudocolor – red is high, blue low concentration). B and C) Graphs depict relative concentration in the core (B) and shell (C) regions of a solute released at a constant rate from the vessel wall beneath the core region. The core and shell regions were defined by values for porosity, permeability and effective diffusion coefficient that were chosen based on their ability to fit the transport data for wild-type and diYF mice shown in Figure 2.

5.3.4 Laser injury-induced platelet accumulation, activation and fibrin formation in diYF mice

The above results indicate that $\alpha_{IIb}\beta_3$ outside-in signaling mediated by β3 integrin tyrosine phosphorylation helps to regulate thrombus architecture and solute transport. Thus, diYF mice serve as a good model to test our hypothesis that thrombus structure and intrathrombus solute transport are key regulators of agonist distribution and subsequent platelet activation at sites of vascular injury in vivo. We quantified total platelet accumulation, P-selectin expression and fibrin deposition in diYF mice compared to wild-type controls following laser-induced injury in mouse cremaster arterioles. Total platelet accumulation was moderately reduced in diYF mice as compared to wild-type controls (Figure 4A-C), although peak platelet accumulation was not significantly different between the two strains (Figure 4C). In both cases the kinetics of platelet accumulation were comparable to prior reports using this thrombosis model [12,39,116]. In contrast, the number of P-selectin positive platelets was significantly reduced in thrombi

formed in diYF mice (Figure 4D-F), indicating decreased full platelet activation following vascular injury in vivo in the absence of β3 integrin tyrosine phosphorylation.

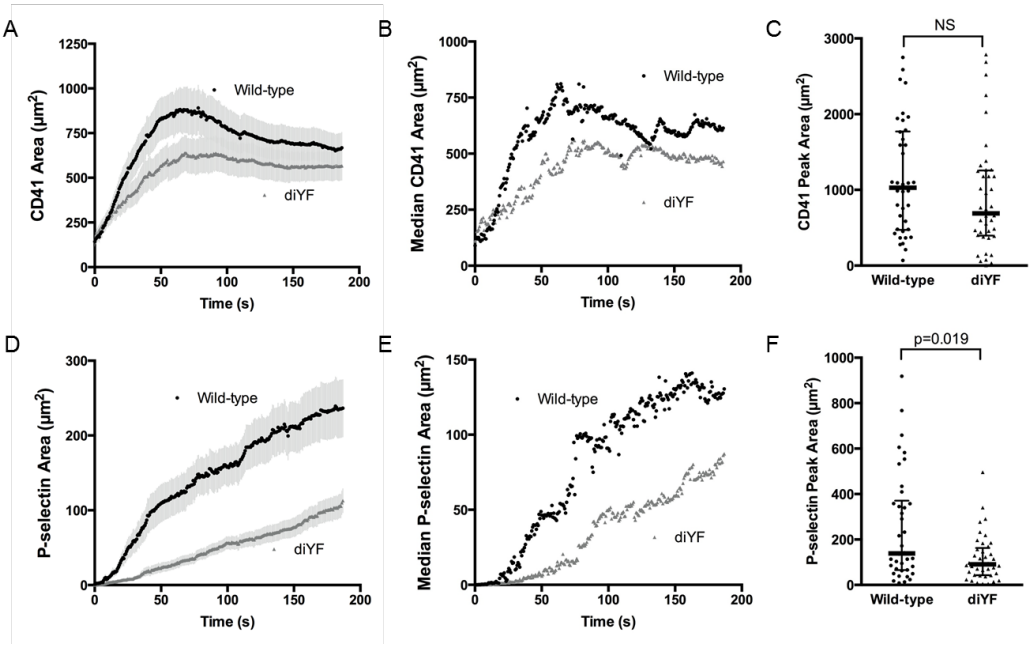

Figure 5- 4 Loss of β3 integrin tyrosine phosphorylation attenuates platelet activation following vascular injury in vivo.

Total platelet accumulation and α-granule secretion were monitored following laser-induced injury in mouse cremaster arterioles using fluorescently tagged antibodies against mouse CD41 and P-selectin, respectively. The graphs in A/B and D/E show total platelet accumulation (CD41 positive area; A mean±SEM, B median) and α-granule secretion (P-selectin positive area; D mean±SEM, E median) over time in wild-type (black circles) and diYF mice (gray squares). Graphs in C and F show peak thrombus (C) and P-selectin positive (F) areas for wild-type and diYF mice. The horizontal line and error bars indicate median and interquartile range. For wild-type, n=38 thrombi from 7 mice and for diYF n=41 thrombi from 6 mice. Statistics were calculated using the Mann-Whitney test for non-parametric data.

In agreement with prior findings[114], fibrinogen binding by individual diYF platelets in response to the PAR-4 agonist AYPGKF was normal (Figure 5A), demonstrating that the

attenuated platelet accumulation and activation *in vivo* is not related to a direct effect of the diYF mutation on inside-out $\alpha_{IIb}\beta_3$ activation. Further, the ability of diYF platelets to secrete their α-granules and express P-selectin in vitro as assessed by flow cytometry was normal (Figure 5B), as was their ability to mobilize P-selectin to the surface of platelets spread on immobilized fibrinogen (Figure 5C-D). These findings indicate that the defect in P-selectin expression observed *in vivo* was not due to reduced P-selectin levels in diYF platelets or a direct effect of β3 tyrosine phosphorylation-dependent signaling on α-granule secretion.

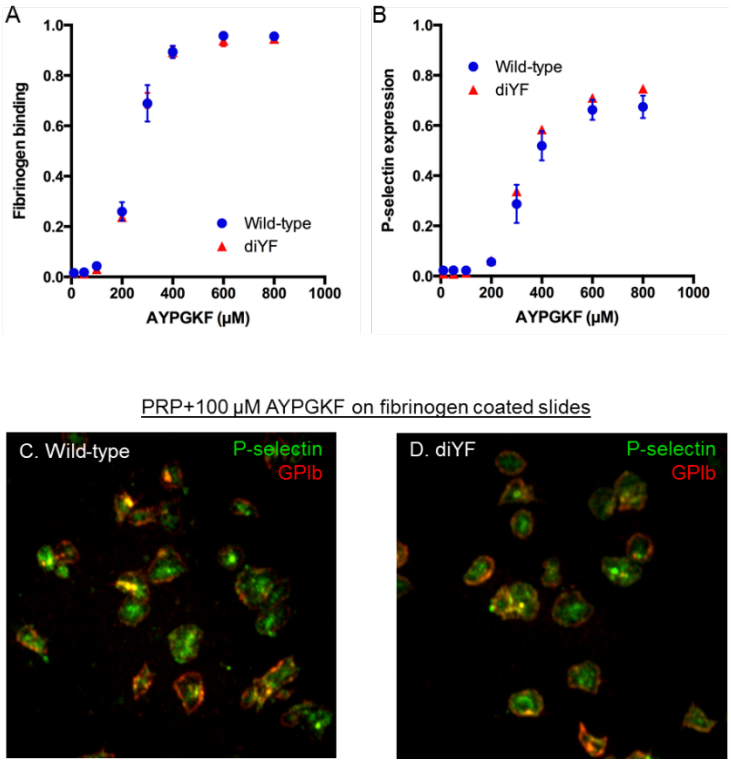

Figure 5- 5 Fibrinogen binding and P-selectin expression are normal in diYF platelets.

A-B) Flow cytometry analysis of fibrinogen binding (A) and P-selectin expression (B) in wild-type and diYF platelets. Platelets were stimulated with the indicated concentrations of the PAR-4 agonist AYPGKF. Data are expressed as the percentage of positive cells (mean±SEM, n=3). C) Representative photomicrographs from wild-type and diYF platelets showing GPIb (red) and P-selectin (green) expression by immunofluorescence. Platelets were stimulated with 100 μm AYPGKF and allowed to spread on immobilized fibrinogen for 45 minutes at 37˚C. The cells were fixed and stained with anti-GPIb and anti-P-selectin without permeabilization to assess surface protein expression.

5.3.5 Fibrin deposition

Prior studies have demonstrated that full platelet activation and α-granule secretion in the laser-induced injury model as used here are primarily due to thrombin-dependent platelet activation[12,39,108,118]. To determine whether there was reduced thrombin activity in diYF mice, we measured fibrin deposition during thrombus formation. We found that the total area of fibrin deposition was significantly attenuated in diYF mice as compared to wild-type (Figure 6A-C). Further, the fibrin specifically colocalized with platelets was significantly reduced (Figure 6D-F), suggesting attenuated local thrombin activity within the platelet mass. Importantly, the decrease in fibrin area corresponded to decreased total fibrin accumulation, as quantification of fibrin fluorescence intensity mirrored the results obtained by analyzing fibrin area (Supplemental Figure 1A-C). This reduced thrombin activity was not a result of impaired ability of diYF platelets to expose phosphatidylserine on the outer leaflet of the plasma membrane, as annexin V binding to diYF platelets was normal (Supplemental Figure 1D). Thus, it is likely that the reduced thrombin activity observed in diYF mice is attributable to decreased thrombin retention

within the platelet mass as a result of impaired platelet packing and increased intrathrombus solute transport.

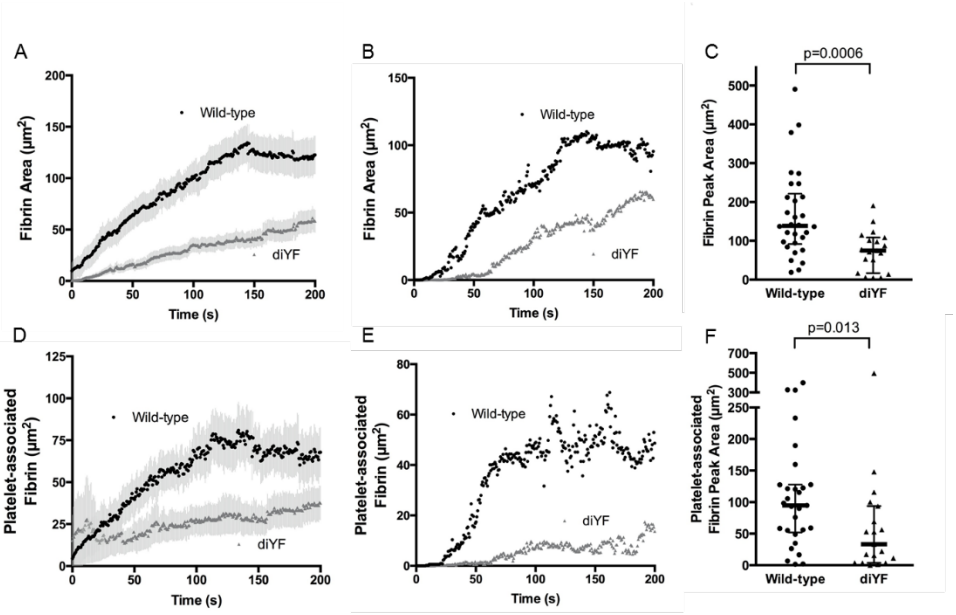

Figure 5- 6 Loss of β3 integrin tyrosine phosphorylation attenuates fibrin formation following vascular injury in vivo.

(A-C) Total fibrin accumulation was monitored following laser-induced injury in mouse cremaster arterioles using a fluorescently tagged antibody that specifically recognizes mouse fibrin. The graphs in A and B show total fibrin area (A, mean±SEM; B, median) over time. Panel C shows peak fibrin area for wild-type and diYF mice. The horizontal line and error bars indicate median and interquartile range. D-F) Platelet-associated fibrin was defined as the area that was positive for both fibrin and CD41 fluorescence. The graphs in D and E show platelet associated fibrin area (D, mean±SEM; E, median) over time. Panel F shows peak platelet-associated fibrin area for wild-type and diYF mice. For wild-type, n=30 thrombi from 6 mice and for diYF n=19 thrombi from 4 mice. Statistics were calculated using the Mann-Whitney test for non-parametric data. E) Flow cytometry analysis of Annexin V binding to wild-type and diYF platelets. Platelets were stimulated with 100 μM PAR-4 agonist AYPGKF and the indicated concentrations of convulxin. Data are expressed as the percentage of positive cells (mean ±SEM, n=3).

5.4 Discussion

Platelet accumulation at a site of vascular injury is a dynamic process that requires assimilation of chemical and physical cues regarding the extracellular environment to promote a cellular response that is coordinated in both time and space to achieve optimal hemostasis. Extensive studies of platelet intracellular signaling pathways over the past several decades have greatly enhanced our understanding of platelet function. Still, it is only by examining platelet function in the complex milieu of an intact vasculature that we can begin to understand how these multiple signaling components are integrated along with contributions from other cells, the vessel wall and local hemodynamic conditions in order to generate a hemostatic plug. In this regard, the current study sought to investigate how a platelet signaling pathway ($\alpha_{IIb}\beta_3$ outside-in signaling), physical characteristics of the platelet mass (platelet mass consolidation), and local molecular transport within the microenvironment of a platelet mass, interact with each other during hemostatic plug formation *in vivo*. The data demonstrate that each of these components contributes to platelet accumulation and particularly platelet activation following vascular injury. They show that as platelets begin to accumulate at a site of injury they act as physical obstacles, limiting the movement of molecules through the spaces between them. As more platelets accumulate and become activated, outside-in signaling resulting in $\beta3$ phosphorylation contributes to the regulated consolidation of the platelet mass and increased platelet packing density. The increase in packing density results in reduced solute transport within the platelet mass, particularly in the core region. This region of reduced molecular transport provides a protected microenvironment where soluble species such as thrombin generated at the site of injury

are retained, leading to robust, irreversible platelet activation (Figure 7). Thus, the platelet response is dictated by the interaction of local conditions impacting agonist distribution and concentration with the platelet signaling network.

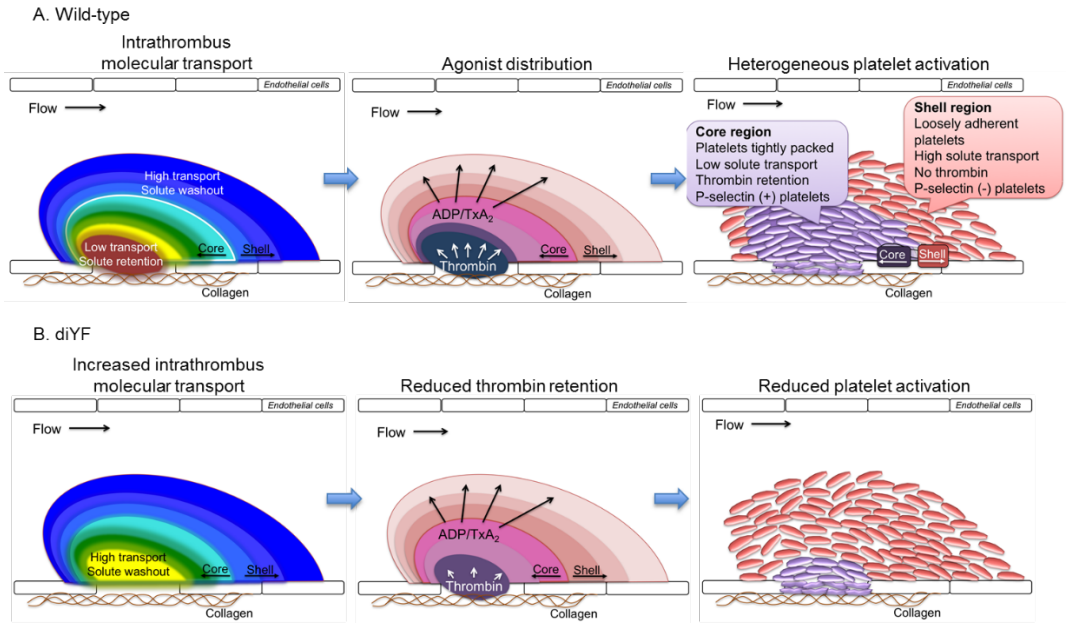

Figure 5- 7 A model for the role of intrathrombus molecular transport in the regulation of agonist distribution and platelet activation.

A) Diagrams show relative gradients of intrathrombus molecular transport rates (left), platelet agonist distribution (middle), and platelet activation (right) following vascular injury in vivo. B) The impact of impaired beta 3 integrin phosphorylation is shown.

Prior studies have demonstrated that platelet mass consolidation is critical for ensuring the stable accumulation of platelets at a site of injury in vivo[112,113]. Consolidation is mediated by platelet retraction, as demonstrated by the attenuation of this process by a myosin IIa inhibitor. However, Ono et al[112] found that this process is independent of fibrin formation and therefore distinct from platelet-mediated fibrin clot retraction. In the

present study, we found that mice in which the two β3 cytoplasmic tail NxxY tyrosines are mutated to phenylalanine (diYF) have impaired platelet retraction during platelet accumulation *in vivo*, resulting in a more loosely packed platelet mass. Thus, β3 integrin tyrosine phosphorylation is a critical upstream signaling component necessary for efficient platelet mass consolidation *in vivo*. As primary platelet activation events (including inside-out $\alpha_{IIb}\beta_3$ activation, fibrinogen binding and granule secretion) are normal when diYF platelets are studied *ex vivo*, diYF mice provide a unique model in which the role of platelet packing density and platelet mass architecture may be studied independently of direct effects on primary platelet activation pathways.

In conjunction with the impaired platelet mass consolidation seen in diYF mice, we found that intrathrombus transport was increased, allowing molecules to elute out of the platelet mass faster in diYF mice. The importance of solute transport through a thrombus or blood clot has been proposed in several prior studies using combinations of *in vitro* and theoretical approaches[56,59,63,119,120]. In general, these studies predicted that the presence of a platelet/fibrin plug will substantially impact solute transport, including movement of coagulation and fibrinolytic enzymes, at a site of vascular injury. In one recent example, Kim et al[53] demonstrated that the density of a fibrin network overlaying a platelet plug has a significant impact on the permeability of solutes moving through the network. They found that denser networks reduced permeability such that a larger layer of solute may develop at the boundary between the shell and core regions. This study and others[52,91] relied on computational models based on thrombus architectures observed using confocal imaging to simulate solute transport. In the first manuscript of this series[110], we provide for the first time a description of molecular transport measured

directly within a platelet mass in vivo, and relate dynamic changes in intrathrombus molecular transport to changes in platelet mass architecture, thrombin distribution and platelet activation. The results of that study indicated that irreversible platelet activation is preceded by a decrease in solute transport in the same region of the platelet mass that will become P-selectin positive (i.e. the core region). These results are consistent with the finding that porosity of the core region is significantly reduced compared to the shell region with similar kinetics to the platelet mass consolidation observed here. Taken together with the results of studies from the diYF mice, a model emerges in which regulated changes in platelet mass consolidation, dictated at least in part by β3 tyrosine phosphorylation dependent platelet retraction, contribute to an altered hemodynamic microenvironment within the core region of the platelet mass in which molecular transport is slowed and solutes are retained to promote platelet activation (Figure 7).

Several factors determine the movement of molecular species within and/or around a pile of platelets, including the size of the pores (plasma volume) between platelets, how well connected are the pores as well as their spatial distribution, the tortuosity of the pore space, the plasma velocity and the size of the solute. In the second manuscript in this series[111], computational modeling studies were performed to examine the importance of each of these variables in determining molecular transport within a platelet mass, as well as the likely impact of interplatelet molecular transport on the distribution of soluble species generated at a site of injury, such as thrombin. Those studies demonstrate that as platelets accumulate and become tightly packed, molecular movement is primarily determined by the effective diffusion of the molecular species. In other words, the small gaps between platelets within a hemostatic plug or thrombus,

particularly in the core region where they are most tightly packed, provide a microenvironment where soluble species are protected from washout. Further, differences in physical factors between the core and shell regions suggest that retention of soluble species within the core region not only has the potential to promote platelet activation in that region, but may also provide a mechanism to limit the extension of hemostatic plug. The data in the present study indicate that platelet mass consolidation is a critical component regulating molecular transport within a platelet plug, as reduced consolidation in diYF mice resulted in increased solute transport during platelet plug formation. They further provide evidence supporting a model in which the consequences of increased solute transport include reduced concentration/distribution of bioactive molecules, as demonstrated by the finding of decreased thrombin activity and decreased platelet activation in diYF thrombi. It should be noted, however, that while we have ruled out several possibilities for direct effects of the diYF mutation on platelet activation, we cannot at present rule out the possibility that other, currently unappreciated effects of the diYF mutation could also contribute.

While we have not explicitly considered the contribution of fibrin(ogen) to solute transport in this study, it likely plays an important role. Indeed, the contribution of fibrin to solute transport is captured in our in vivo measurements, as fibrin is present within the developing platelet mass. Similarly, the physical properties used to define our computational model included the contribution of fibrin as these were based on our in vivo measurements where fibrin was present. With regard to solute transport, the expected impact of fibrin formation would be similar to platelet retraction shrinking the spaces between platelets, e.g. decreased pore volume and increased tortuosity. In addition, several pro- and anti-coagulant proteins (including thrombin itself) bind to fibrin,

further impacting their distribution within a platelet mass. Additional approaches are required to tease out the precise contribution fibrin, but are beyond the scope of the current study.

In conclusion, we have demonstrated a novel role for $\alpha_{IIb}\beta_3$ outside-in signaling in the regulation of platelet mass consolidation in vivo. Further, we provided evidence that the extent of platelet packing in a hemostatic plug regulates interplatelet molecular transport, agonist distribution and subsequent platelet activation. Taken together, these observations demonstrate that optimal hemostatic plug formation results from the interaction of physics, biochemistry and cell biology.

5.5 Supplemental Materials and Methods

Laser-induced injury in mouse cremaster arterioles was performed essentially as described previously[12]. Alexa-fluor 568 anti-CD41 $F(ab)_2$ (clone MWReg30, BD Bioscience, San Jose, CA) was used to label platelets, Alexa-fluor 488 anti-P-selectin (clone RB40.34, BD Bioscience) used to label activated platelets that had secreted their α-granules, and Alexa-647 anti-fibrin antibody (clone 59D8, a generous gift from Dr. Hartmut Weiler and Dr. Rodney Camire) was used to label fibrin, which serves as a surrogate for thrombin activity. There was no significant difference in the diameter of arterioles selected for laser injury studies between wild-type and diYF (33.84±0.78 μm vs 31.92±0.76 μm, respectively). Similarly, centerline red blood cell velocities were not significantly different in cremaster arterioles of wild-type and diYF mice (3.6±0.5 mm/s vs. 3.4±0.8 mm/s, respectively).

Intrathrombus solute transport was measured using caged fluoroscein coupled to albumin (cAlb) as described in detail in Welsh *et al*[110]. The cAlb was infused intravenously via the jugular vein cannula following preparation of mice for intravital microscopy. The cAlb was flash activated using a 500 ms pulse of 405 nm laser light to uncage the fluorophore during image acquisition following laser-induced injury. Each flash was followed by FITC fluorescence image acquisition for 15 frames (approximately 10 seconds) at which time a new flash was initiated. This sequence was repeated continuously for 3 minutes post-injury. The FITC fluorescence is observed as a peak of fluorescence immediately following the 405 nm flash, followed by a rapid decay as the cAlb is washed out of the thrombus and field of view. Pilot studies determined that the observed rapid decay is not related to photobleaching, but rather reflects cAlb transport. cAlb decay curves were generated for each thrombus by averaging each of the normalized decay curves for that thrombus. The cAlb decay curves of multiple thrombi were then averaged to generate a mean decay curve for each genotype (wild-type and diYF) as a measure of intrathrombus molecular transport.

Computational simulation of solute transport: A detailed description of computational methods including model design and parameter description is included in chapter 4. Briefly, the thrombus is represented as a two-compartment homogeneous porous medium. We apply the Stokes equation to solve the flow field in the lumen region and a Brinkman equation for the flow field in the thrombus. We used the "species transport in porous media package" in COMSOL® version 4.3a, solving the convection-reaction-diffusion equation: $\partial c/\partial t = D\nabla^2 c - u\nabla c + R$, where *c* is the concentration of chemical species of interest, *D* is the diffusion coefficient, *u* is the velocity vector field, and *R*

describes sources of the various chemical species. We imposed an initial uniform concentration of a tracer solute in the vessel, zero solute concentration at the influx boundary, and then ran the simulation until the concentration inside the thrombus regions decreased to zero.

Chapter 6: More than just stopping red cells: how hemostatic thrombi limit extravasation of plasma- and platelet-borne molecules

6.1 Introduction

Recent reports show that hemostatic thrombi formed after vessel damage in vivo in mice, and ex vivo using human blood, develop a heterogeneous structure[13,36,80,81,121] in which a core of fully-activated platelets and fibrin is overlaid by a shell of less-activated platelets [12]. A prominent characteristic of the core is that it consists of densely-packed platelets, with increased packing density driven by contraction of cross-linked platelets through $\alpha_{IIb}\beta_3$ integrin-dependent outside-in signaling [12,95,96]. We have shown that tight platelet packing restricts molecular transport within the core, producing a region with a corresponding increase in local thrombin activity and platelet activation. Based on studies in cremaster muscle arterioles, we have previously proposed that this heterogeneous architecture is important for regulating the distribution of soluble agonists within the thrombus and, therefore, thrombus growth and core formation. Here we extend those observations into venules and test the hypothesis that thrombus architecture is also a key to understanding how hemostatic thrombi prevent the loss of plasma as well as the escape of red cells.

After a penetrating injury red cells and plasma permeate through the injury site and into the extravascular space, driven by the pressure differential between the vessel lumen and the surrounding tissue. Thrombus formation at the injury site resists the movement of plasma and red cells out of the vessel, and restricts the transport of molecules within and across the thrombus microenvironment [51,55,120]. Previously we have shown that

thrombi formed from human blood flowing over a collagen/tissue factor surface have a Darcy permeability ($\kappa = 2x10^{-14}$ cm^2), approaching that of an intact endothelium [13]. Put differently, hemostatic thrombus formation in theory serves not only to halt the escape of red cells, but also to alter the transport of plasma-borne and platelet-derived molecules from the lumen and thrombus microenvironment into the extravascular space [22,52,56]. Since plasma and platelets are the source of numerous coagulation factors [63,122,123], growth factors [124-127] and mediators of inflammation [128,129], transport properties at the site of vascular injury are potentially an important regulator of wound healing and recovery in the surrounding tissues. Thus we propose that the complex architecture of fully hemostatic thrombi is needed in part to limit the loss of soluble molecules and further propose that achieving "plasma stasis" may require attributes that are not precisely the same as those required to stop red cell loss.

Here we have tested these ideas, first developing a novel method for quantifying plasma protein extravasation at the site of penetrating injuries in the mouse microvasculature in real time and then using it to examine the relationships between thrombus architecture and plasma protein loss following penetrating injuries in mouse cremaster muscle venules. By infusing albumin labeled with a caged fluorophore (cAlb) into mice we used intravital microscopy to measure the kinetics of plasma protein escape concurrently with markers of thrombus formation. A combination of pharmacologic and genetic approaches resolved the relative contributions of platelets, fibrin, clot retraction and thrombus architecture in vessel sealing.

The results show that the core-and-shell architecture observed in arterioles is largely recapitulated in venules. The studies with cAlb show that while red cell escape after

small penetrating injuries can be stopped by only a few platelets, a larger, more stringent structure is required to limit plasma protein extravasation. We found that the rate of plasma protein extravasation is highly sensitive to small changes within the platelet mass, including changes in platelet packing density, but not the accumulation of fibrin. Plasma stasis is especially sensitive to inhibition of ADP-dependent signaling. Defects in clot retraction, especially when combined with defects in platelet accumulation, cause a large increase in plasma protein extravasation. Together with previous studies, this helps to explain how a fully competent hemostatic thrombus structure matures over time to eventually halt not only the loss of red cells, but also the outflow of soluble plasma-borne molecules into the extravascular space. It also shows how members of two widely-used classes of antiplatelet agents ($P2Y_{12}$ and $\alpha_{IIb}\beta_b$ antagonists) can prolong the escape of plasma-borne molecules by delaying formation of an effective vascular seal in the microvasculature.

6.2 Methods and Materials

6.2.1 Mice.

Male mice 8-12 weeks of age were used for all intravital experiments. C57Bl/6 mice (Jackson Laboratories, Bar Harbor, ME) were used for experiments utilizing anti-platelet agents, and were compared to diYF mutant mice that had been backcrossed on to the C57Bl/6 background at least 7 times. DiYF mice were originally generated in the laboratory of Dr. David Phillips at Portola Pharmaceuticals (San Francisco, CA [95]) and were obtained by us with his approval from Dr. Tatiana Byzova at the Cleveland Clinic Foundation (Cleveland, OH). $G_{i2}\alpha$(G184S) mutant mice were provided by Dr. Richard

Neubig (Michigan State University). The mice used in this study were heterozygous for the mutant allele ($Gnai2^{G184S}$), which we have previously showed confers a gain of function in their platelets in vitro and in vivo [130]. Their wild-type littermates were used as controls.

6.2.2 Caged albumin synthesis.

As described previously [22], bovine serum albumin (BSA, Jackson Immunological Research West Grove, PA, USA) was labeled with CMNB-Caged Carboxyfluorescein, SE (5-Carboxyfluorescein-Bis-(5-Carboxymethoxy-2-Nitrobenzyl) Ether, β-Alanine-Carboxamide, Succinimidyl Ester) (Life Technologies, Frederick, MD, USA). Briefly, the BSA was solubilized in 0.1 M sodium bicarbonate in phosphate buffered saline to a final concentration of 10 mg / mL. Concurrently, 1 mg of CMNB-caged carboxyfluorescein was solubilized in 100 μL of dimethyl sulfoxide and was thoroughly mixed with the BSA solution. The reaction was incubated for 1 hour at room temperature before purified over a 7 kDa molecular weight cutoff desalting column from Thermo Scientific (Waltham, MA, USA).

6.2.3 Intravital microscopy and injury generation.

Mice were anesthetized with sodium pentobarbital (90 mg/kg) through an intraperitoneal injection. The mouse jugular vein was cannulated to allow for the infusion of fluorescent markers and pharmaceutical agents. The cremaster muscle was then exposed and prepared for viewing by confocal microscopy. The cremaster muscle was under

continuous flow of bicarbonate buffer maintained at 37°C and bubbled with 95%/5% N_2/CO_2. Venules with a diameter of 30-50 μm were utilized, and injury was induced with a pulsed nitrogen dye laser (SRS NL100, 440nm). The laser was fired until red blood cells escaped the vessel indicating sufficient vessel wall damage. The area was then visualized with a BX61WI microscope (Olympus, Center Valley, PA, USA) with a 60X (0.9 NA) water immersion objective, and a CSU-X1 spinning disk confocal scanner (Yokogawa, Sugar Land, TX, USA). Fluorescence imaging was performed using a diode optic tunable filter control as an excitation source (LaserStack; Intelligent Imaging Innovations, Denver, CO, USA). Images were captured with an Evolve digital camera (Photometrics Tucson, AZ, USA).

Platelets were visualized by anti-GPIbβ (clone Xia.C3; Emfret Analytics, Eibelstadt, Germany) labeled with Alexa-568, or anti-CD41 (F(ab)2 fragment, clone MWReg30, and anti-CD62P (P-selectin; IgG, clone RB40.34) labeled with Alexa-647 obtained from BD Biosciences (San Jose, CA, USA), and Alexa-647 anti-fibrin antibody (clone 59D8, a generous gift from Dr. Hartmut Weiler and Dr. Rodney Camire) was used to label fibrin.

Plasma protein extravasation (L(t)) was measured by the extravasation of caged albumin (cAlb), which was uncaged every 15 fames by exposure of 405 nm light and then quantified by the resulting increase in fluorescence excitation at 488 nm (Supplemental Figure S1B). Thrombus formation was modified by the addition of Cangrelor (a generous gift from The Medicines Company, Parsippany, NJ, USA), Hirudin (a gift from Dr. Sriram Krishnaswamay, Children's Hospital of Philadelphia) or eptifibatide (Integrilin; purchased from Schering Plough).

In pilot studies plasma protein extravasation was measured in both arterioles and venules. Although similar extravasation dynamics were observed in both, only venule data were used for the studies reported here because the thicker walls of the arterioles resulted in some of the leaked plasma being retained within the wall in a pseudo-aneurysm that interfered with extravasation measurements.

6.2.4 In vitro thrombus permeability measurements.

A sidearm microfluidic chamber was used to generate thrombi ex vivo as previously described [13]. Briefly, re-calcified (10 mM) citrated whole blood, from wild type and diYF mice, was perfused over a collagen/tissue factor surface to induce thrombus formation. Blood flow was maintained at a shear rate of 200 s^{-1}, and a transthrombus pressure drop of 15 mmHg. Platelet and fibrin deposition were monitored for 10 min, and then Texas Red fluorophore (Life Technologies) was infused and dynamically imaged to measure the thrombus permeability as described [13,51].

6.3 Results

6.3.1 Thrombus formation and maturation limits plasma protein loss from the site of injury.

As we have previously shown in mouse arterioles [12], laser injury of healthy mouse venules results in the formation of a non-occlusive hemostatic thrombus, which

differentiates into a P-selectin(+) core region and a P-selectin(-) shell region over the first few minutes after injury (Figure 1A-C). To measure plasma protein loss from the injury site in real time, we infused albumin conjugated with caged carboxyfluorescein (denoted “cAlb”) prior to injury. After injury we used pulses of 405 nm light to flash-activate any cAlb that escaped into extravascular tissue planes (Figure 1A and Supplemental Figure S1A). By measuring the gain in extravascular cAlb fluorescence at 15 s time intervals, we quantified relative cAlb extravasation (L(t)) over time for as long as 20 minutes (1200 seconds) after injury (Supplemental Figure S1B and S1C).

The results show a rapid initial loss of plasma protein after injury, followed by a gradual decrease in cAlb extravasation over 3 minutes (Figure 1A and D). We monitored cAlb extravasation concurrently with red cell loss, platelet accumulation, fibrin deposition and P-selectin exposure, allowing us to compare the kinetics of each of these events. As in arterioles, we found that red cell loss ended within the first few seconds of injury. Fibrin and platelet accumulation continued after that point, peaking at approximately 60 s. cAlb extravasation continued well after the peak in platelet accumulation, but continued to gradually decline to a level above background (pre-injury) escape. The continued decline in cAlb escape is informative, suggesting that ongoing structural changes within the thrombus contribute to plasma protein retention (Figure 1B-D). At 200 s after injury, relative cAlb extravasation rates were ~60% less than at 15 s, but not a total cessation of plasma protein extravasation (Figure 1E and Supplemental Figure S1C). These data demonstrate that in response to vascular damage in the microvasculature few platelets are required to achieve hemostasis, however plasma protein extravasation continues beyond stable thrombus formation and beyond 20 minutes post-injury (Supplemental Figure S1).

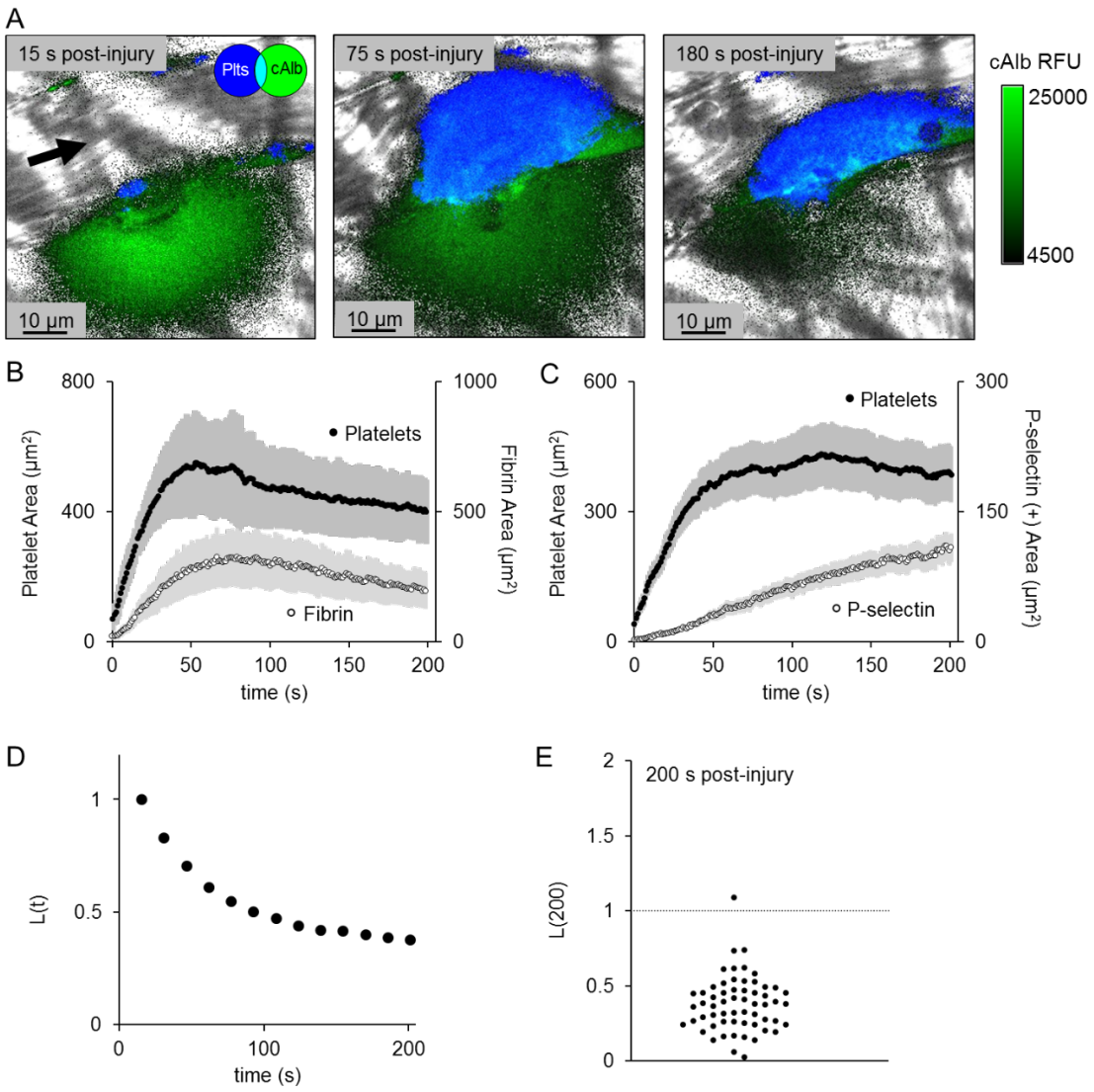

Figure 6- 1 Measuring plasma protein extravasation in vivo.

(A) Representative images of a thrombus formed in a mouse cremaster venule showing platelets (blue) and flash-activated cAlb (green). Each image is taken directly after an activating-pulse of 405 nm light. (B) Time course of average platelet (black) and fibrin (white) area (n=24; +/- SEM). (C) For a separate data set we tracked average platelet area (black) and P-selectin positive area (white) (n=23; +/- SEM). (D) Time course of the average relative cAlb extravasation (L(t)). (E) A dot plot of the relative cAlb extravasation for each injury at 200 s post-injury (n=47; +/- SEM).

6.3.2 The relative contributions of platelets and fibrin to vessel sealing.

The initial rapid decrease in plasma protein extravasation (~60 s post-injury) coincided with initial platelet deposition and fibrin accumulation. To determine how each of these events contributes to vessel sealing, we infused the integrin $\alpha_{IIb}\beta_3$ antagonist, eptifibatide (20 mg/kg) [131], to inhibit platelet cohesion and decrease platelet accumulation (Figure 2A-C). Eptifibatide treatment led to a ~70% decrease in peak platelet area ($p< 0.001$), but had no impact on peak fibrin formation ($p = 0.79$) (Figure 2A-C). Eptifibatide-treated thrombi were still hemostatic with no increase in red cell escape observed, but had a large increase in plasma protein extravasation post-injury (Figure 2DE&F). When we examined the dynamics of cAlb extravasation over 200 s post-injury, we observed a significant portion (36%) of the eptifibatide-treated thrombi showed cAlb extravasation had increased from 15-200 s post-injury, in contrast to vehicle treated thrombi which all had decreased cAlb extravasation, suggesting that the eptifibatide-treated thrombi were not stable and weakened over time (Figure 2F).

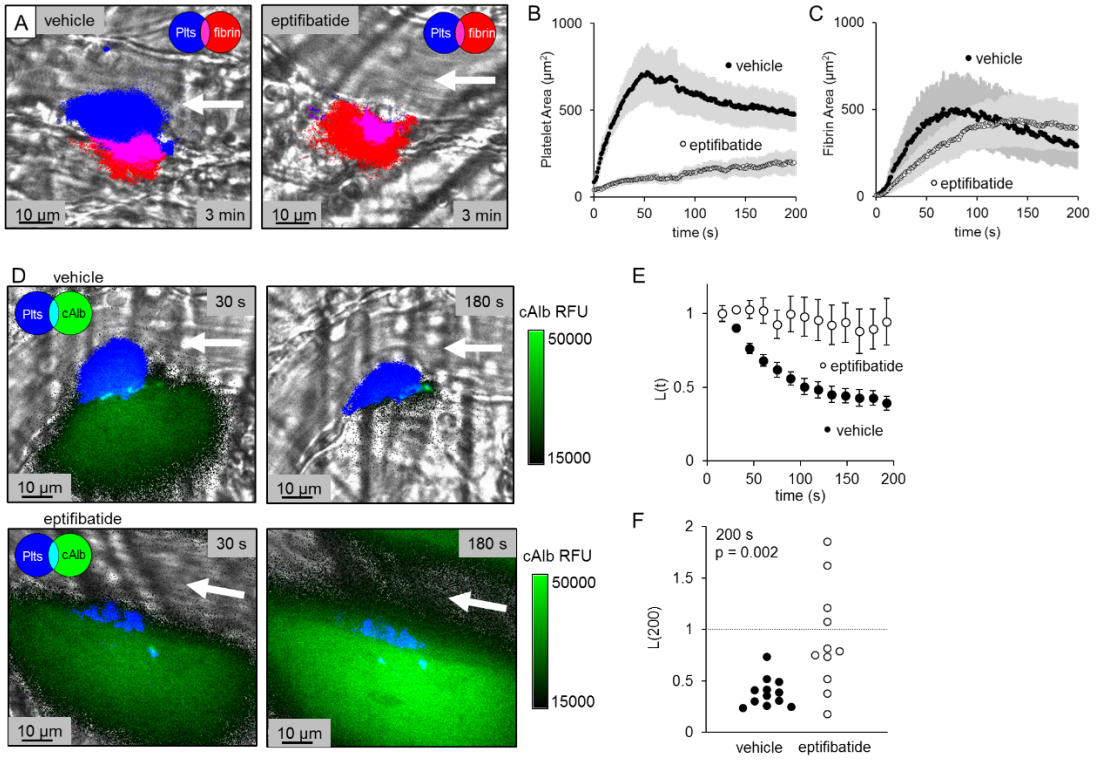

Figure 6- 2 Inhibition of αIIbβ3 integrin reduces platelet accumulation and vessel sealing.

(A) Representative images of thrombi formed in the presence of either vehicle or eptifibatide (20 mg/kg), showing both platelets (blue) and fibrin (red) 3 minutes post-injury. (B) Average platelet area and (C) fibrin area for both the vehicle-treated (black) and eptifibatide-treated (white) thrombi (+/- SEM). (D) Representative images of cAlb extravasation (green) at both 30 and 180 s post-injury for vehicle and eptifibatide treated thrombi (blue). (E) Time course and (F) dot plot of relative cAlb extravasation for vehicle (black) and eptifibatide (white) treated thrombi (vehicle n=12, eptifibatide n=11; +/- SEM).

Given the eptifibatide results, which highlight the contribution of platelets to achieving plasma stasis, we tested whether increased thrombus size would further reduce plasma protein extravasation, or if thrombus driven vessel sealing is largely maximized. To test

this hypothesis we used Gi2α(+/G184S) mice whose platelets show an increase in responsiveness to ADP because of resistance to signal termination by RGS proteins downstream of Gi2-coupled $P2Y_{12}$ receptors. As we have previously reported [12], laser injury induced 72% larger thrombi in the Gi2α(+/G184S) mice than in paired wild type control mice (Supplemental Figure S2A-B). However, this increase in platelet accumulation had no effect on the dynamics of vessel sealing, implying that normal sized thrombi reflect the limit to how much platelets can restrict plasma protein transport (Supplemental Figure S2C).

6.3.3 Platelet retraction contributes to vessel sealing.

In previous studies we demonstrated the importance of platelet packing density in limiting intrathrombus solute transport. To test the hypothesis that platelet retraction helps to limit plasma protein extravasation, we compared cAlb extravasation in wild type mice with cAlb extravasation in mice in which two critical tyrosines in the cytoplasmic domain of the β subunit of integrin $\alpha_{IIb}\beta_3$ were replaced with phenylalanine residues (denoted diYF). The platelets from these mice show normal integrin activation, but have a defect in outside-in signaling that leads to delayed clot retraction in vitro and reduced thrombus consolidation in vivo [95,96].

Consistent with the studies in arterioles, we observed no defect in either the kinetics of platelet accumulation or the total area of the platelet mass in the diYF mice (Figure 3A). For the first 60 seconds (the period of greatest platelet accumulation), there was also no difference between diYF and matched control mice in their ability to slow the

extravasation of cAlb (Figure 3B and C). After 60 seconds, however, extravasation in the diYF mice remained elevated compared to the controls. This suggests that after initial platelet recruitment, platelet retraction drives intrathrombus remodeling to further seal the injury site (Figure 3B). The lack of retraction in the diYF mice led to a 54% increase in relative cAlb extravasation at 200 s post-injury (Figure 3C). We saw a similar difference in Darcy permeability measurements performed ex vivo using wild type and diYF mouse blood in a microfluidics device (Supplemental Figure S3). Taken together, these results suggest that initial vessel sealing is driven by the rapid accumulation of platelets, while continued sealing is driven in part by the same integrin $\alpha_{IIb}\beta_3$-mediated retraction that increases platelet packing density and decreases thrombus permeability. Thus cAlb extravasation is highly sensitive to small changes in the intrathrombus structure, although the differential impact of retraction on plasma protein permeation and diffusion remains unresolved.

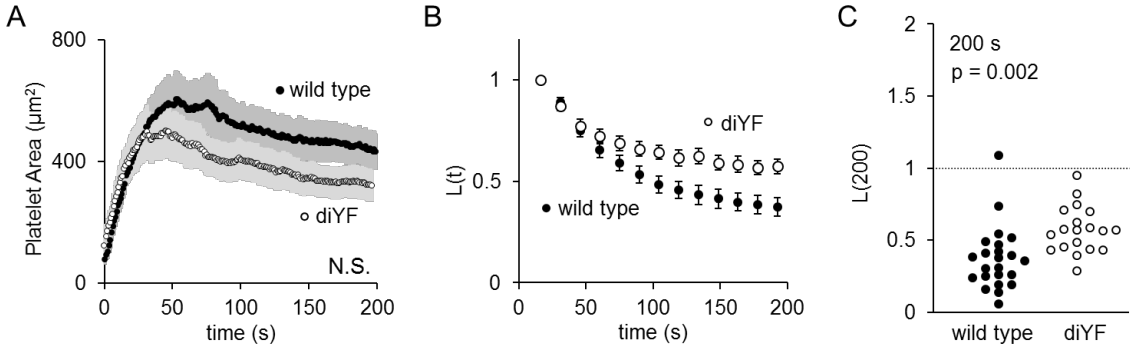

Figure 6- 3 Outside-in signaling drives platelet retraction and vessel sealing.

(A) The average platelet area for wild type (black) and diYF thrombi (white) (+/- SEM). (B) Time course and (C) dot plot of cAlb extravasation for wild type (black) and diYF (white) thrombi (wild type n=24, diYF n=19; +/- SEM).

6.3.4 The role of fibrin accumulation, ADP and thrombus architecture in restricting plasma protein loss.

In our prior studies on arterioles, we found that fibrin accumulation after penetrating injuries is restricted to the thrombus core, as is detectable thrombin activity [12,87]. Addition of a direct thrombin antagonist, such as hirudin or bivalirudin, abolished fibrin accumulation and caused a decrease in the size of the thrombus core as well as a reduction in overall thrombus size. In the present studies, we found that hirudin also causes a reduction in overall thrombus size in venules, but did not alter platelet activation measured by P-selectin exposure (Figure 4). Fibrin accumulation was essentially abolished (Figure 4C). Despite these changes, hirudin had no significant effect on plasma protein extravasation (Figure 4E and F). This suggests that fibrin accumulation plays no role in preventing the extravasation of plasma proteins in this injury model.

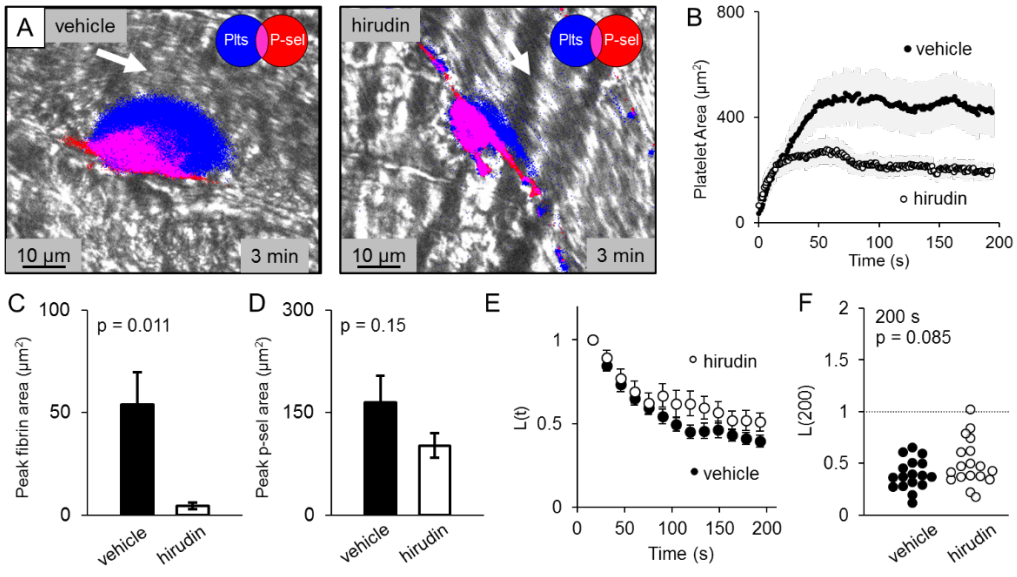

Figure 6- 4 Thrombin inhibition decreases fibrin accumulation and thrombus size, but not vessel sealing.

(A) Representative images of thrombi formed either in the presence of vehicle or thrombin inhibitor Hirudin (2 μm) showing platelets (blue) and P-selectin (red) 3 minutes post-injury. (B) Quantification of average platelet area, (C) fibrin area, and (D) peak P-selectin area for both vehicle-treated (closed) and hirudin-treated (open) thrombi (+/- SEM). (D) Time course of average cAlb extravasation and (E) dot plot of cAlb extravasation at 200 s for both vehicle-treated (closed circle) and hirudin treated (open circle) thrombi (vehicle n=17, Hirudin n=18; +/- SEM).

The results with hirudin contrast with those obtained with the direct-acting $P2Y_{12}$ antagonist, cangrelor. Like hirudin, cangrelor caused a decrease in overall thrombus size, and had no effect on platelet activation measured by P-selectin exposure (Figure 5A-B). However, cangrelor-treated thrombi showed a significant increase in plasma protein extravasation (Figure 5C-D). Combining hirudin and cangrelor had an effect on extravasation that was similar to adding cangrelor alone, despite having an even greater effect on platelet deposition and P-selectin exposure (Figure 5E-H). Taken together these results suggest that ADP is crucial for driving decreased thrombus permeability. This is consistent with previous observations that in human thrombi, ADP and thromboxane A2 are the major drivers of retraction in the absence of thrombin [51]. The results also suggest that P-selectin exposure, while informative about α-granule exocytosis, is not directly tied to formation of a tight vascular seal limiting plasma protein extravasation.

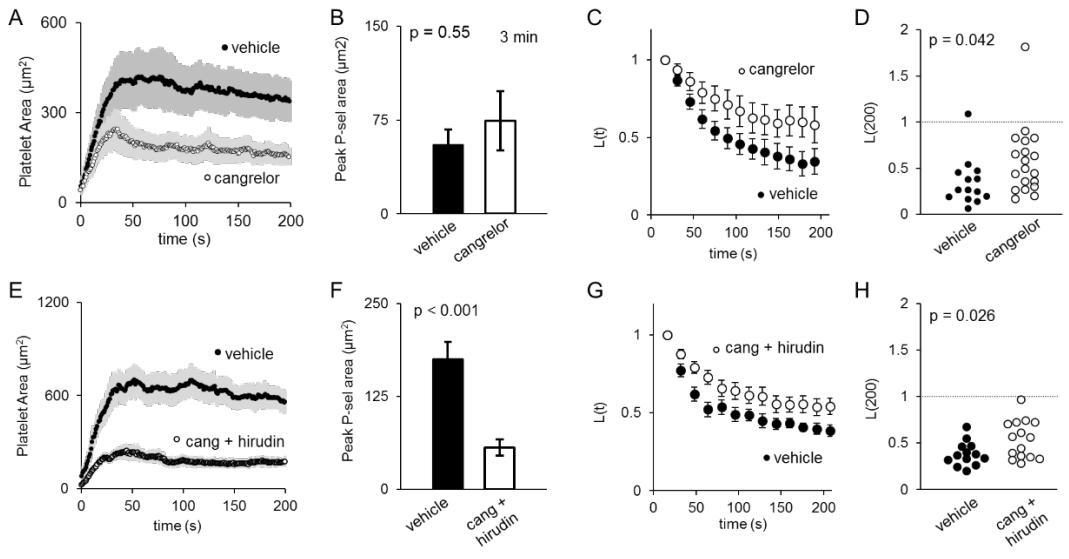

Figure 6- 5 ADP drives fully competent core formation and shell recruitment.

(A) Quantification of average platelet area and (B) peak P-selectin positive area of vehicle (black) and cangrelor-treated (white) thrombi. (C) Average cAlb extravasation time course and (D) dot plot of relative cAlb extravasation at 200 s post-injury (vehicle n=15, Cangrelor n=20; +/- SEM). (E) The average platelet area and (F) peak P-selectin positive area for vehicle (black) and cangrelor / hirudin (white) treated thrombi (+/- SEM). (G) Time course of relative cAlb extravasation, and (H) dot plot of cAlb extravasation at 200 s post-injury (Vehicle, black n = 13; Cangrelor / hirudin, white n = 15).

6.3.5 Plasma protein accumulation in the extravascular space.

Lumenal proteins will accumulate in the extravascular space when the rate of delivery out of the vessel exceeds the rate at which proteins disperse into the surrounding tissue. To measure the dispersion rate of cAlb we observed the rate of cAlb fluorescence decay (ΔF(decay)) between fluorescence-activating pulses of 405 nm light. The decay of fluorescent cAlb correlates to the rate at which extravascular fluorescent cAlb molecules

disperse within the surrounding tissue (Supplemental figure S4A and B). We found that the cAlb dispersion rate was greatest initially, peaking 60 s after injury, which is approximately the same time that peak platelet accumulation is achieved (compare Supplemental Figure S4C with earlier figures). Despite the higher initial rate of dispersion the extravasation of cAlb into the extravascular tissue greatly exceeded the dispersion during the first 60-75 s post-injury, causing substantial cAlb accumulation (Figure 6A). However, after sufficient thrombus growth to limit cAlb extravasation below the rate of dispersion, leading to a gradual but consistent decline in fluorescent extravascular cAlb (Figure 6A).

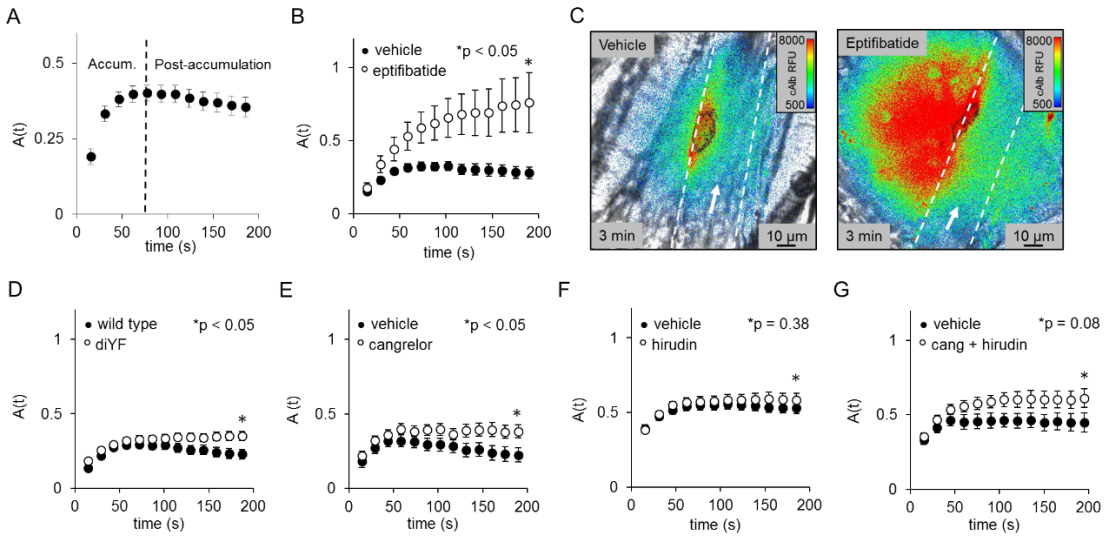

Figure 6- 6 cAlb accumulation in the extravascular space.

(A) cAlb accumulation (A(t)) was measured by the relative fluorescence remaining 15 s after each activating light pulse for 200 s. (B) cAlb accumulation was measured for Eptifibatide-treated thrombi (open) and vehicle-treated thrombi (closed). (C) A pseudo-colored image of cAlb intensity 3 min post-injury with the vessel shown in white and platelets outlined in black. (D) cAlb accumulation for diYF and wild type thrombi, (E) cangrelor-treated, (F) hirudin-treated, and (G) cangrelor/hirudin treated, vs vehicle treated thrombi.

Perturbations in thrombus structure that impacted cAlb extravasation similarly affected cAlb accumulation. Eptifibatide-treated injuries showed no change in average cAlb fluorescence decay rates compared to vehicle, suggesting that the dispersion rate is independent of the extravasation rate (Supplemental Figure S4D). However, since the extravasation rate remained elevated (Figure 2), there was greater extravascular cAlb accumulation (Figure 6B). This led to a continuously increasing gradient of cAlb in the tissue surrounding the injury site, while vehicle treated thrombi had shrinking cAlb gradients by 200 s post-injury (Figure 6C). Thrombi formed in diYF mice also allowed for moderate accumulation of cAlb (Figure 6D), as did thrombi formed in the presence of cangrelor (Figure 6E). Consistent with the hypothesis that cAlb accumulation is primarily driven by to extravasation rates, we observed no effect of hirudin alone on cAlb accumulation (Figure 6F).

Taken together these results demonstrate that hemostatic thrombi are able to achieve a level of vessel sealing that limits plasma protein extravasation to rates less than the rate at which plasma protein dissipates into the surrounding tissue, preventing the continued concentration of plasma proteins in the surrounding tissue. Thus, small changes in the structure of the thrombus that impair vessel sealing can produce a larger than normal gradient of potentially bioactive molecules at the site of injury.

6.4 Discussion

It has been well established that soluble plasma-borne and platelet-derived molecules play a role in post-injury inflammation and wound healing [124-129,132]. It is less clear how

the delivery of these molecules is constrained following injury. It has also been well established through computational [53,55,56] and experimental [22,51,59,96,120] examination that thrombi are capable of acting as a molecular sieve altering the transport of proteins and small molecules through dense platelet packing and fibrin formation. Here we tested the idea that thrombus structure plays a regulatory role in protein extravasation, just as we have previously shown it contributes to the local accumulation of thrombin and ADP, the deposition of fibrin, and the cessation of red cell loss. To investigate this hypothesis we designed a novel sensor able to measure plasma protein extravasation in real time, allowing us to correlate changes in plasma protein transport and intrathrombus structure. We found that following small penetrating injuries in the microcirculation in healthy mice, hemostatic thrombus formation significantly reduces the rate of plasma protein extravasation, just as it brings an end to red cell escape. However, we found that plasma protein loss continues beyond the time when red cell escape ends, persisting for at least 20 minutes after injury, an observation that suggests that maintaining molecular exchange between the circulating blood and surrounding tissue may be beneficial, or at least not harmful, for achieving an optimal for post-hemostatic responses.

In addition to providing information about the kinetics of vascular sealing, our results demonstrate that platelets, not fibrin, are primarily responsible for limiting the loss of soluble proteins. Data obtained with inhibitors of platelet activation and cohesion, and with the retraction-deficient diYF mice show that both total platelet accumulation and platelet retraction are involved. However, there appears to be a limit to how much platelet accumulation alone can reduce plasma protein movements. Thus, although considerably larger thrombi formed in mice expressing the Gi2α(G184S) gain of function

allele, we found no difference in extravasation rates. The inability of fibrin to significantly block plasma protein extravasation is consistent with observations in human blood demonstrating the limited effect of fibrin on clot permeability [13,51]. Together these observations demonstrate that platelet accumulation and organization are the driving events for resisting molecular permeation into the extravascular space.

The ability of a thrombus to restrict plasma protein extravasation is defined by the size and structure of the thrombus microenvironment. Therefore, the differential effects of the inhibitors that we employed are informative in examining how specific pathways shape the physical structure of the thrombus microenvironment. We found that both hirudin and cangrelor decrease thrombus size to a similar extent without effecting P-selectin exposure. However, hirudin treatment had no effect on plasma protein extravasation, while cangrelor treatment induced a significant increase in plasma protein extravasation. This suggests that ADP inhibition, but not thrombin, alters the structure of the resulting thrombus microenvironment allowing for increased protein extravasation. These results also confirm that fibrin accumulation, which is ablated in the presence of hirudin, contributes little to preventing plasma protein extravasation, at least in the acute setting.

Notably, while having a greater impact on overall platelet accumulation, the combination of cangrelor and hirudin had no greater impact than cangrelor alone on plasma protein extravasation. Therefore, we suggest that the impact of ADP receptor inhibition on the intrathrombus microenvironment is likely limited to the region immediately adjacent to the injury site. Thus, further decreasing platelet deposition in the case of combined cangrelor-hirudin treatment does not increase plasma protein extravasation. Interestingly, the combined cangrelor-hirudin treatment also significantly decreased P-

selectin exposure. However, the extent of P-selectin exposure, which we have previously used as a marker to define the thrombus core region did not correlate with plasma protein extravasation. Even though antagonizing platelet $P2Y_{12}$ receptors alone has no effect on P-selectin expression in either arterioles (our previous studies [12]) or venules (the present data), it clearly affects transport properties. Thus, the two processes (α-granule exocytosis and vessel sealing) are not irrevocably linked.

Finally, our results also show that thrombus formation is capable of limiting plasma protein extravasation sufficiently to prevent the continuous accumulation of plasma borne protein within the local tissue. Since extravasated cAlb dispersed into surrounding tissues at a relatively steady rate, accumulation was primarily dependent upon the delivery rate of cAlb through the thrombus. Directly after vessel injury rapid plasma protein extravasation leads to local cAlb accumulation until progressive vessel sealing slows the rate of plasma protein extravasation below the rate of dispersion causing a net decrease in the concentration of cAlb in the local area (Figure 7). Within the sequence of events, platelet retraction drives the transition from plasma protein accumulation to dispersion.

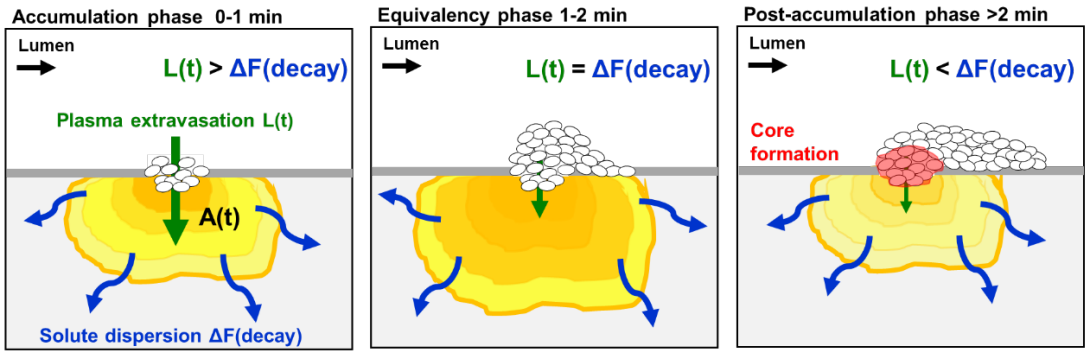

Figure 6- 7 Model of plasma-stasis in mouse cremaster venules.

A model depicting the evolution of plasma-stasis during thrombus formation. From 0-1 minute post-injury plasma protein extravasation (L(t)) is greater than the rate of plasma protein dispersion (ΔF(decay)) into the tissue resulting in increasing accumulation (A(t)). From 1-2 minutes thrombus formation limits L(t) to be equal to ΔF(decay) bringing A(t) into a steady state. Finally, after 2 minutes post-injury L(t) becomes slightly less than ΔF(decay), causing a slight but steady decrease in A(t).

In conclusion our study demonstrates a novel method for both measuring the transport of luminal proteins into the extravascular space and evaluating the integrity of thrombi forming in vivo. The results show that the hemostatic response produces a core-and-shell structure in venules that resembles the response in arterioles, but is less dependent thrombin. We have previously suggested that the core-and-shell architecture is needed in part to allow local differential accumulation of platelet agonists [22,55,96]. The results obtained here refine our understanding of the implications of thrombus structure, showing that the pace of achieving plasma stasis is much slower than for halting red cell loss and the structural requirements are greater. While red cell loss in this model ceases after very few platelets have accumulated, halting plasma protein escape requires greater platelet accumulation, ADP-dependent signaling and increased platelet packing density, thus providing another reason for the complex architecture observed in fully hemostatic thrombi. Formation of a vascular seal appears not to require fibrin accumulation. We assume, but have not shown here, that the delivery of soluble platelet-derived molecules, including growth factors and cytokines, is subject to the same constraints as the delivery of plasma-borne molecules. Finally, the results obtained in the presence of members of two widely-used classes of antiplatelet agents ($P2Y_{12}$ and

$\alpha_{IIb}\beta_3$ antagonists), show how these drugs can prolong the escape of plasma-borne molecules by delaying formation of an effective vascular seal.

6.5 Supplemental materials

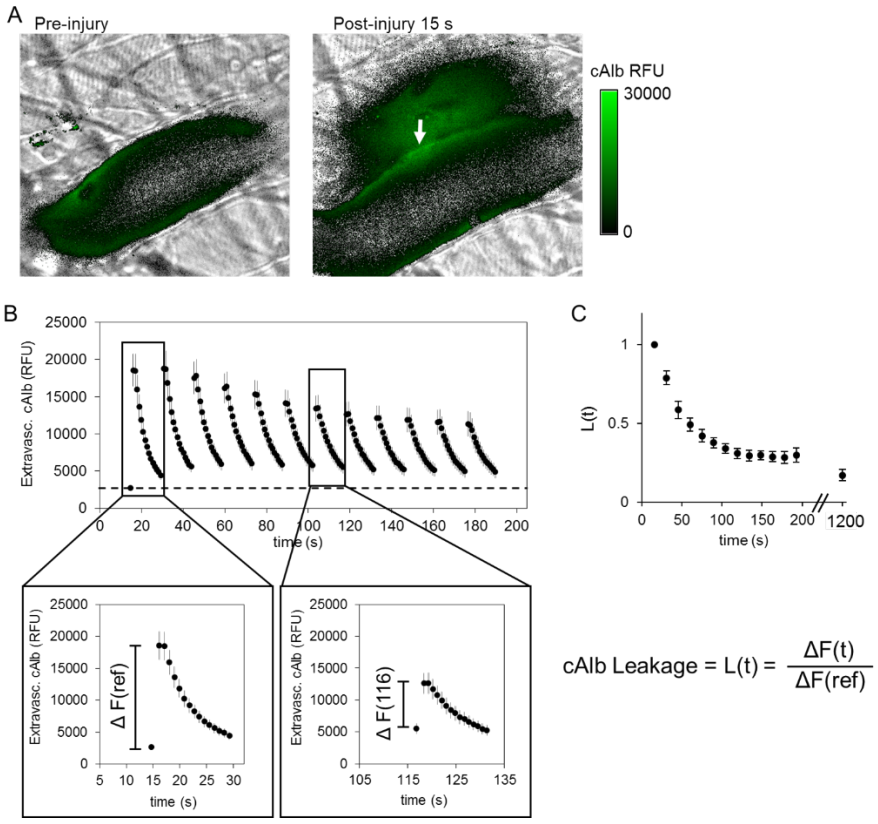

Figure 6- 8 Using cAlb to measure plasma protein extravasation in real time.

(A) A representative image of cAlb localization before and after laser-induced vascular injury (white arrow). Both images were captured immediately following an activating pulse of 405 nm light. (B) The mean cAlb fluorescence measured in the extravascular space, and how the gain and loss are measured following a light pulse every 15 s. (C) Time course of cAlb extravasation from wild type venules from 15-1200 s post-injury.

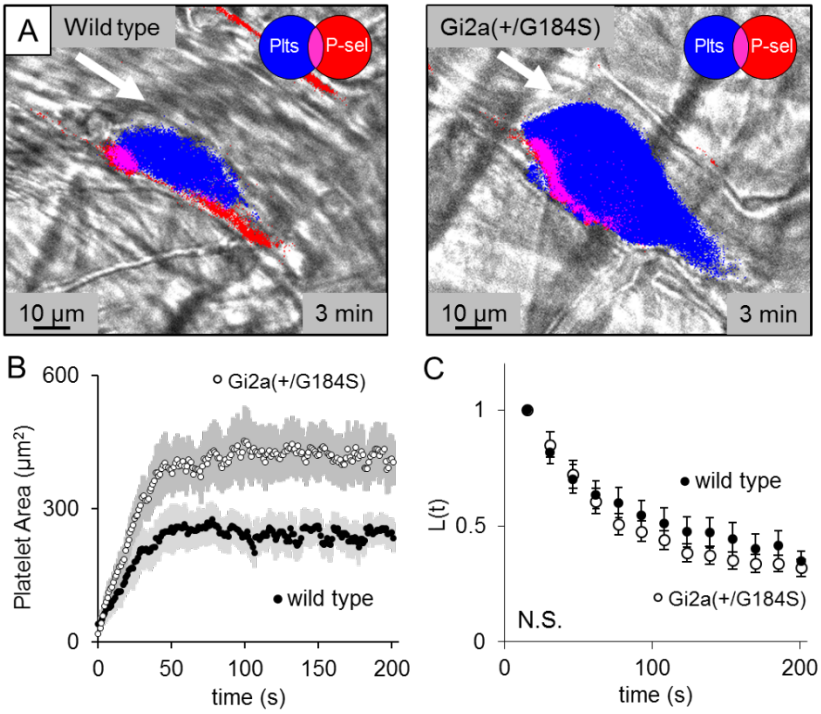

Figure 6- 9 Increased shell formation does not increase vessel sealing.

(A) Representative images of thrombi formed in wild type and RGS-resistant $G_{i2\alpha}$(+/G188S) mice showing platelet deposition (blue) and P-selectin exposure (red) at 200 s post-injury. (B) The area of platelet deposition and (C) cAlb extravasation was quantified over time for both the wild type (closed circle) and $G_{i2\alpha}$(+/G188S) (open circle) thrombi (wild type n=13, Gi2 n=23; +/- SEM).

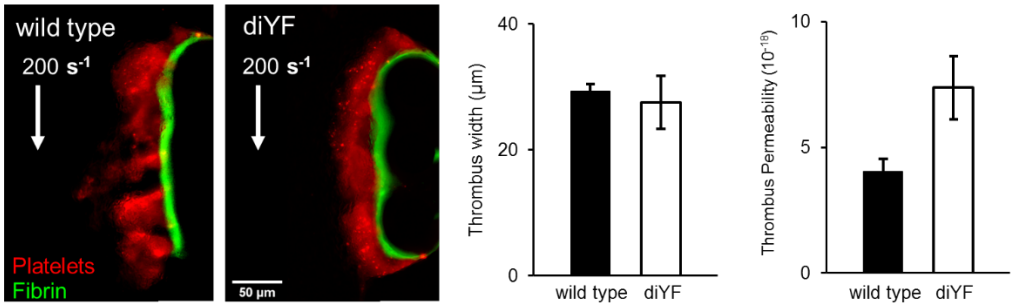

Figure 6- 10 Permeability of wild type and diYF thrombi.

(A) Representative images of thrombi formed in a side-arm microfluidic chamber showing platelets (red) and fibrin (green) formed using re-citrated blood drawn from wild type and diYF mice (n=3). (B) Average thrombus width after 10 minutes of blood flow. (C) Quantification of the average thrombus permeability at 10 minutes.

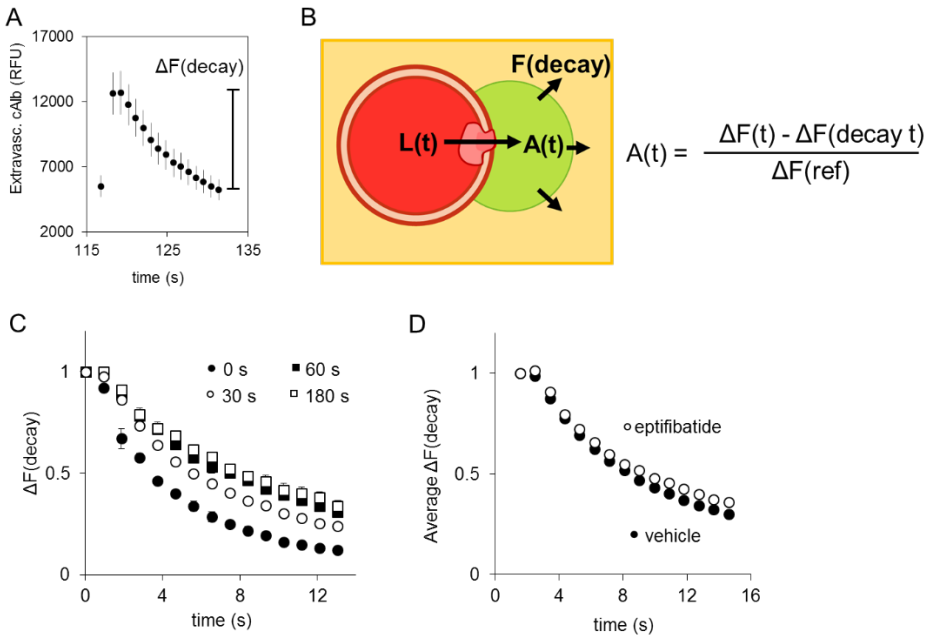

Figure 6- 11 Extravascular cAlb transport and accumulation.

(A) The accumulation (A(t)) of extravascular cAlb was measured by calculating the differences between the delivery (ΔF(t)) and the dispersion (ΔF(decay)) of cAlb normalized by ΔF(ref). (B) A schematic representation of extravascular cAlb transport. (C) The rate of extravascular cAlb dispersion was measured by quantifying the relative decay rate of fluorescent cAlb between activating light pulses. Shown are the average cAlb decay curves a 0s (closed circle), 30 s (open circle), 60 s (closed square), and 180 s (open square). (B) The total average extravascular cAlb decay for both vehicle and eptifibatide-treated thrombi.

Chapter 7: Real time intravital imaging of thrombus formation in the mouse femoral artery reveals critical differences from events in the microvasculature

7.1 Introduction

Following vascular injury hemostatic thrombi must prevent blood loss without obstructing vessel flow and causing ischemic injury. Hemostatic thrombi formed in the mouse microvasculature and in microfluidic devices using human blood, form a characteristic architecture with a core of densely packed and highly activated (P-selectin (+)) platelets forming at the site of injury [12,13]. The core is covered with a shell of loosely packed and less activated (P-selectin (-)) platelets. The core is also differentiated from the shell by the presence of fibrin deposition which is limited to the extravascular space and the core. In the mouse microvasculature platelets rapidly accumulate at the site of injury, and thrombin activity drives stable platelet accumulation and eventual α-granule exocytosis and fibrin deposition within the core region [12]. Concurrently, ADP and TxA2 released during thrombus formation extend beyond the core and recruit platelets which make up the shell region [12]. We have also presented a model in which dense platelet packing within the core region regulates thrombin localization shaping local platelet activation, fibrin deposition, and thrombus development [22,55,96]. Here we aim to extend these observations to the mouse macrocirculation, namely the femoral artery and vein, and determine the relative contribution of various agonists to thrombus growth and development.

Clinically relevant thrombosis often occurs within the macrocirculation, and the large blood volume within these vessels makes occlusion especially damaging. The macrocirculation differs from the microcirculation significantly in vessel wall biology and architecture [46,49,50,133-136], and local hemodynamics [47,137]. These differences affect the underlying molecular mechanisms driving platelet activation and thrombus formation. While platelet adhesive proteins, such as $\alpha_{IIb}\beta_3$ and GPIb-α, are universally important the mechanisms of platelet activation and thrombus development vary between vascular beds and injury type [33-35,40]. To further understand how variations in vessel biology and physics impact thrombus formation we developed a method to image thrombus formation in response to laser injury in the mouse femoral artery and vein. We then compared thrombus architecture development and agonist contributions in the femoral artery and vein to previous observations in the cremaster arteriole and venules.

Our results demonstrated that hemostatic thrombi formed in the femoral artery develop an architecture of a highly activated P-selectin(+) core covered by a less activated P-selectin(-) shell, similar to what is observed in the microvasculature. However, the relative rate of core formation is significantly slower in the femoral artery. Also similar to observations in the microvasculature, $P2Y_{12}$ inhibition resulted in embolization of the shell region, and thrombin activity drove core formation. However, inhibition of thrombin, which leads to 80-90% reduction of thrombus size in the microvasculature, had no impact on total platelet deposition in the femoral artery, suggesting a separate mechanism behind stable platelet accumulation. Histological analysis of tissue factor distribution showed that, consistent with previous observations [57], in both the cremaster arterioles and the femoral artery tissue factor is predominately localized to the vessel

adventitia. However, this results in tissue factor being 10-fold further from the vessel lumen in the femoral artery, which may delay thrombin generation.

Taken together our results present a model in which there are several key similarities and differences between thrombus formation in the macro- and microcirculation. Platelets rapidly deposit at the injury site to stem bleeding, and accumulate into the lumen and downstream driven by ADP recruitment. After an initial lag phase, thrombin activity drives further platelet activation and P-selectin exposure creating a core-shell architecture. These results demonstrate a new technique to get high-resolution imaging of thrombi formed in the mouse macrocirculation, provide evidence of how vessel architecture impacts agonist production, and demonstrate the conservation of the previously described core-shell architecture.

7.2 Material and Methods

7.2.1 Materials

C57Bl/6J mice 8-12 weeks old were used for all experiments (Jackson Laboratories, Bar Harbor,ME, USA). Thrombus formation was visualized using anti-CD62P (IgG, clone RB40.34) and anti-CD41 (F(ab)2 fragment, clone MWReg30) (BD Biosciences, San Diego, CA, USA). Fluorescent fibrinogen conjugated to AlexaFluor 488 provided information about fibrin(ogen) deposition (Life Technologies, Grand Island, NY, USA). Thrombus formation was modified by the infusion of cangrelor (a generous gift from The

Medicines Company) or hirudin (a gift from Dr. Sriram Krishnaswamay, Children's Hospital of Philadelphia).

7.2.2 Femoral artery and vein visualization

Mice were anesthetized with an intraperitoneal injection of either sodium pentobarbital (90 mg/kg) or ketamine/xylazine/acepromazine (100 mg/kg b.w. ketamine, 10 mg/kg b.w. xylazine 3 mg/kg b.w. acepromazine). The mouse jugular vein was then cannulated for the infusion of anti-CD41 (3 μg), anti-CD62P (5 μg), and fluorescent fibrinogen (50 μg) to visualize thrombus formation. For inhibitor studies cangrelor (10 μM final concentration) and hirudin (2 μM final concentration) were also infused directly before each treatment injury.

The femoral artery and vein were then exteriorized and connective tissue was surgically removed from on top of the vessels. A plastic ring was then adhered to the surrounding tissue to allow for the retention of constantly perfused bicarbonate buffer (37 °C, bubbled with 95%/5% N_2CO_2) to facilitate imaging with a 40X water immersion objective (Olympus, St. Louis, MO, USA) (Supplemental Figure S1A). Vessel injury was induced with a pulsed nitrogen dye laser (SRS NL100, 440nm). Two levels of injury were made with the laser: a severe injury (laser fired until blood escaped from the vessel), or a mild injury (10-12 laser pulses focused on the intimal face of the vessel) (Supplemental Figure S1B). The resulting thrombi were imaged using a BX61WI microscope (Olympus, St. Louis, MO, USA) and a CSU-X1 spinning disk confocal scanner (Yokogawa). Fluorescence imaging was performed using a diode optic tunable filter control as an

excitation source (LaserStack; Intelligent Imaging Innovations). Images were captured with an Evolve digital camera (Photometrics) (Supplemental Figure S1C).

7.2.3 Image analysis

The maximum background fluorescence signal for each channel was measured within the thrombus-free portion of the lumen within the same field of view as the thrombus. The image was then converted to a binary mask of all pixels above that maximum and either the area (μm^2) or sum fluorescence (FI 10^6 RFU) from that mask were measured for each mask.

Real time tracking of mask area and fluorescence intensity allowed for us to quantify 3 distinct metrics: initial growth rate (over 60 s for thrombus area, and 20 s for fibrinogen deposition as they were typical ranges of the linear phase of growth), peak thrombus/P-selectin area and fibrinogen FI, and final thrombus/P-selectin area and fibrinogen FI. We then performed statistical analysis on these metrics.

7.2.4 Histology

Mouse femoral artery and vein were isolated without perfusion, briefly washed with 1x PBS and fixed with 4% formalin for 4 hours. Tissue was dehydrated and processed for paraffin embedding and sectioned (5 μm). After paraffin removal and rehydration, antigen retrieval was done with citrate buffer (10 mM, pH 6) for 20 minutes, blocking of peroxidase activity with 3% H_2O_2 in 1x PBS for 20 minutes, followed by 3 washes with

deionized water of 10 minutes each. Sections were blocked with 2% normal rabbit serum (Vector Laboratories: S-5000) for 15 minutes and with Avidin/Biotin Blocking Kit (Vector Laboratories: SP-2001) as suggested by manufacturer. Primary antibody incubation was done overnight at 4^{o}C at a dilution of 1:200 for tissue factor (R&D: AF3178) and 1:150 for PECAM-1 (Santa Cruz: sc-1506). Sections were incubated with Biotinylated Rabbit Anti-Goat (Vector Laboratories: BA-5000) at a 1:1000 dilution for 45 minutes and with Vector Elite ABC kit (Vector Laboratories: PK-6200) as specified by manufacturer. Staining was developed with DAB substrate (Dako: K3467), counterstaining with hematoxylin and mounting with Cytoseal-60 (Richard-Allan Scientific: 8310-4).

7.3 Results

7.3.1 Thrombus architecture in the femoral artery

To observe thrombus formation in the mouse femoral artery we exteriorized the femoral artery and vein, removed overlaying connective tissue, and immersed the area in 37 °C physiological buffer. By rapidly firing the injury laser focused on the vessel wall blood loss could be induced from the femoral artery and vein. Blood loss was visible under the microscope but only lasted for 1-2 s post-injury, and was therefore not captured during subsequent imaging. The resulting rupture was 10-15 μm in diameter (Supplemental Figure S1D), a much smaller injury than was made in recent reports of laser injury in the mouse saphenous vein (50-100 μm diameter) [40] where blood loss was prolonged and quantifiable.

To determine if thrombi formed in the femoral artery form a core and shell architecture we monitored platelet deposition, P-selectin exposure, and fluorescent fibrinogen signal. We observed rapid platelet accumulation around the injury site forming a large amorphous mass by 60 s post-injury (Figure 1A). P-selectin exposure slowly accumulated over several minutes forming a substantial core region by 5 minutes post-injury, and a very well defined core and shell region was observable by 20 minutes post-injury (Figure 1A). During that time the platelet mass also became more aligned with the flow (Figure 1A). Concurrently, fibrin(ogen) was deposited at the injury site and spread perpendicular to flow within the vessel wall (Figure 1B and Supplemental Figure S2). The P-selectin(+) core formed largely within the vessel wall, and the P-selectin(-) shell formed in the lumen on top of the core and downstream (Figure 1B and Supplemental Figure S2). This architecture was also reproduced using a mild injury model, where the vessel endothelium is damaged, but the vessel isn't ruptured and no blood loss occurs (Supplemental Figure S3A).

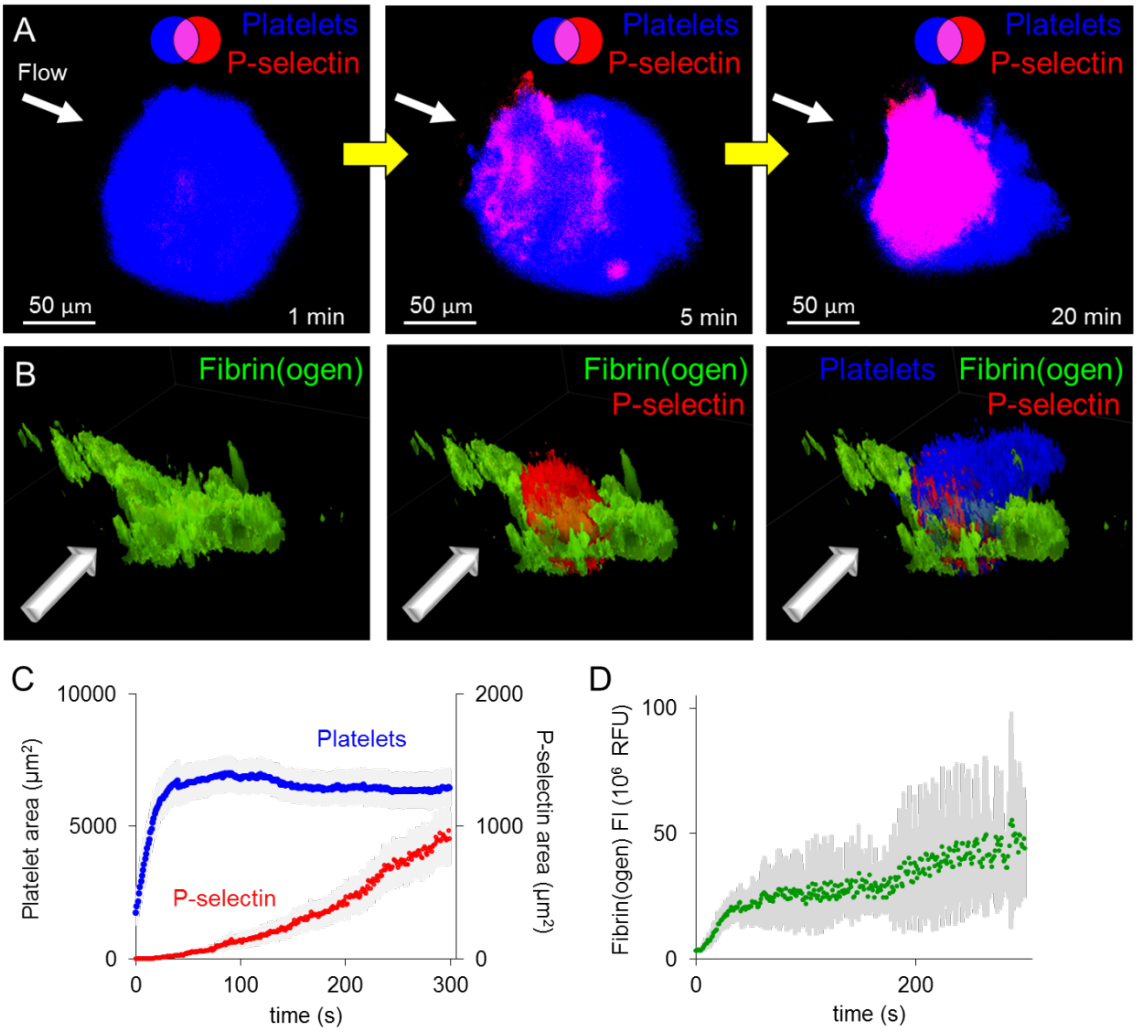

Figure 7- 1 Thrombus architecture in the femoral artery.

(A) A time course of a representative thrombus after femoral artery rupture injury, showing platelets (blue) and P-selectin (red). (B) A 3D reconstruction of a thrombus showing fibrin(ogen) (green), P-selectin (red), and platelets (blue). (C) A quantification of platelet deposition, P-selectin area, and (D) firbin(ogen) deposition from femoral artery rupture injuries (n = 20, +/- SEM).

Real time thrombus growth, core formation, and fibrin(ogen) deposition were monitored in response to both the rupture injury, and the mild injury (Figure 1C and D, Supplemental Figure S3B and C). In both types of injury platelet accumulation peaked at 30-40 s post-injury, however, the rupture injury thrombi were 50-60% larger than the mild injury thrombi. Also after reaching peak size the rupture thrombi were largely stable while the mild injury thrombi were reduced by 60-70% by 5 minutes post-injury (Figure 1C and Supplemental Figure S3B). The mild injury model formed a core region 10-fold smaller than the rupture injury, despite only a 50-60% reduction in peak thrombus size (Figure 1C and Supplemental Figure S3B). However, fibrin(ogen) deposition was greater in the mild injury compared to the rupture, suggesting that fibrin(ogen) deposition in the wall is independent of platelet accumulation and activation (Figure 1D and Supplemental Figure S3C).

7.3.2 Thrombus dynamics in the femoral artery and cremaster arterioles

In the cremaster arterioles, we injured the vessels sufficiently to induce red cell escape out of the vessel. The average peak thrombus size in the cremaster was 5.5-fold smaller than in the femoral artery, however, the thrombi appear to be quite stable with minimal reduction in thrombus area between the peak size and 5 minutes post-injury (Supplemental Figure S4). The cremaster thrombi also rapidly formed a substantial core region (Supplemental Figure S4A and B). Both of these results suggest that the femoral artery rupture injury, and not the mild injury, is a comparable injury to the cremaster injury model.

The cremaster and femoral artery thrombi peaked in area between 30-60 s post-injury, with the initial growth rate (0-20 s) of the femoral artery thrombi being 6.6-fold faster than the cremaster thrombi (Figure 1C and Supplemental Figure S4B, D and E). However, thrombus growth rates normalized by peak thrombus size showed no difference in thrombus growth dynamics (Figure 2A and B). However, normalized core formation of the femoral artery thrombi showed a significant delay in initiation (time to 10% formation) compared to the cremaster thrombi (Figure 2C and D). Taken together these results demonstrate that vessel rupture, not just damage, in both the macro- and microcirculation leads to stable thrombus formation. Also there is a consistent growth phase (0-60 s) regardless of the extent of injury, vasculature, and final thrombus size. Finally, despite forming significantly larger thrombi, there is a significant delay in platelet activation and core formation in both mild and rupture injuries in the femoral artery compared to the cremaster thrombi.

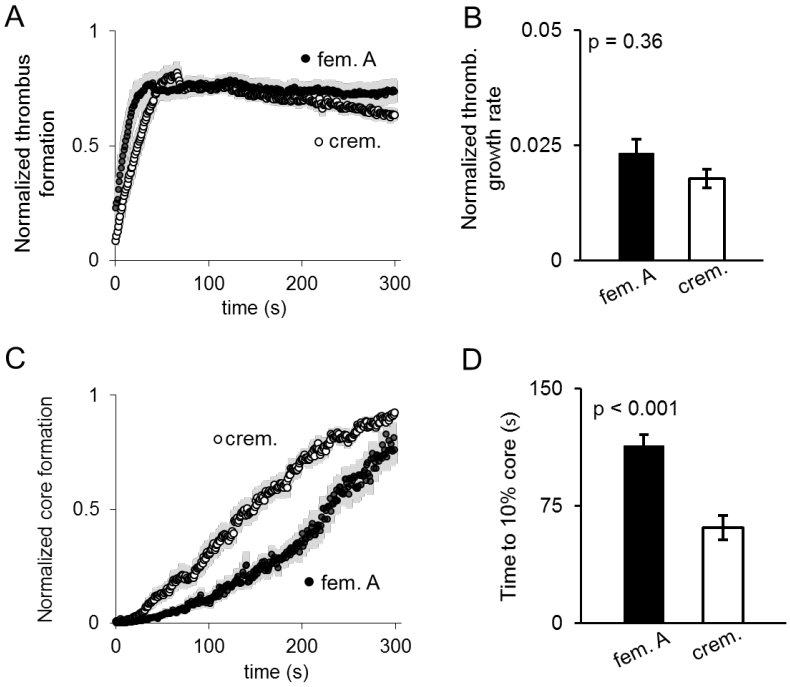

Figure 7- 2 Thrombus growth and core formation dynamics.

(A) Thrombus growth in the femoral artery (black circles) and the cremaster arterioles (open circles) were normalized to peak thrombus for each individual injury and graphed over 300 s post-injury. (B) The normalized growth rate (0-20 s post-injury) was determined for both data sets. (C) Similarly, the rate of relative core formation was calculated, and (D) the time to 10% core formation measured for each injury (femoral artery n = 20; cremaster arterioles n = 17, +/- SEM).

7.3.3 The role of ADP in femoral artery thrombus formation

ADP driven activation of platelets through P2Y12 receptors on the platelet surface has been shown to be important for stable $\alpha_{IIb}\beta_3$ integrin activation and stable thrombus formation in the cremaster and saphenous vein [12,40,138]. In the cremaster thrombi the thrombus instability leads to a loss in stable shell accumulation, but does not impact the size or activation level of the core region [12]. Infusion of cangrelor, a direct P2Y12 antagonist, showed a very similar effect in the femoral artery rupture injury model (Figure 3). Cangrelor-treated thrombi showed decreased thrombus size compared to vehicle-treated, but peak thrombus size was not significantly different between the two conditions (Figure 3A and B). The difference in final thrombus size was due to extensive embolization of the downstream region of the thrombus (Figure 3C and Supplemental movie M1). This resulted in the cangrelor-treated thrombi forming a stable structure lacking any platelets downstream from the injury site (Figure 3D). Similarly to the cremaster, the cangrelor treatment had no effect on platelet activation or core formation (Figure 3E). This phenotype was also maintained in the mild injury of the femoral artery (Supplemental Figure S5). Taken together these results show a highly-conserved role of ADP in shaping hemostatic thrombus architecture across vascular beds and injury types.

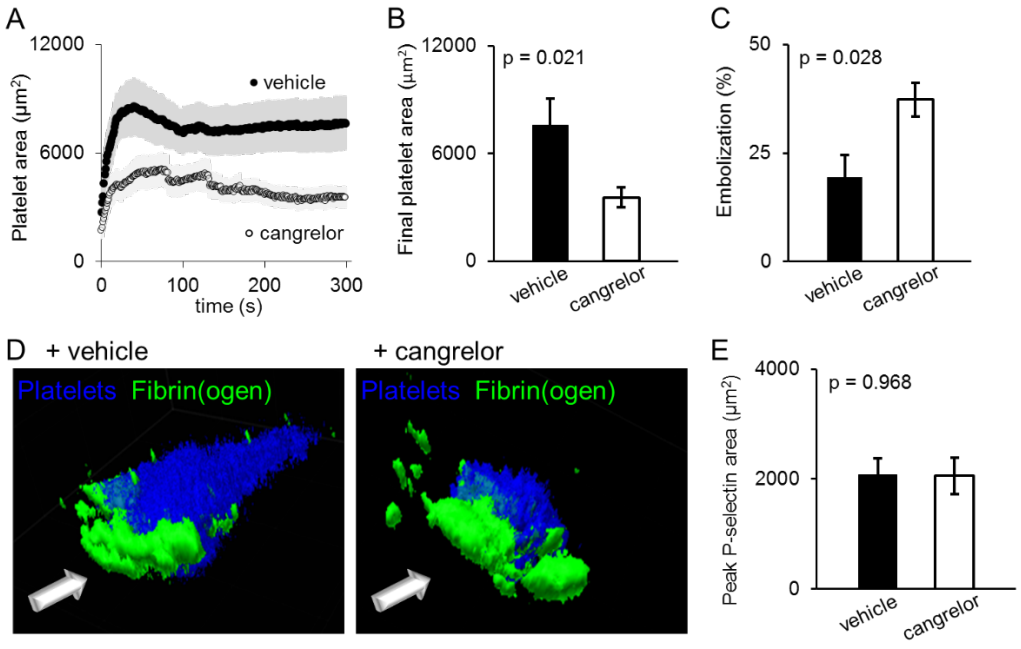

Figure 7- 3 The role of ADP signaling in thrombus architecture formation in the femoral artery.

(A) Platelet deposition for vehicle-treated (black) and cangrelor-treated (white) thrombi over 300 s post-injury. (B) The final platelet area, and (C) percent embolization for each data set. (D) Representative 3D reconstructions of thrombi formed in the presence of vehicle or cangrelor showing platelets (blue) and fibrin(ogen) (green). (E) Peak P-selectin area for vehicle (black) and cangrelor-treated (white) thrombi. (vehicle n = 8; cangrelor n = 9, +/- SEM).

7.3.4 Thrombin drives core formation but not platelet deposition in the femoral artery

Unlike ADP the role of thrombin in thrombus formation appears to be more dependent upon the nature of the vascular injury. In the cremaster arterioles inhibition of thrombin activity reduces thrombus size by 80-90% and abolishes P-selectin(+) core formation [12].

However, it has also been reported that in the mesentery arterioles thrombin activity is dependent upon injury severity [36,38,39], with more mild penetrating injuries being dependent upon thrombin and collagen induced signaling, and severe injuries shifting to more thrombin signaling dependency [36]. In the venous macrocirculation, Getz et al., showed that low tissue factor mice had no hemostatic defect in response to laser induced vessel rupture [40], suggesting a limited role for thrombin.

To investigate the role of thrombin in the arterial macrocirculation we used hirudin, a direct thrombin inhibitor in the femoral artery injury model. We observed no significant impact of thrombin inhibition on platelet deposition after a rupture injury, despite the loss of fibrin(ogen) signal (Figure 4A-C). However, thrombin inhibition did significantly deplete P-selectin exposure leading to a 60% reduction in core size by 5 minutes post-injury (Figure 4D). In response to a mild injury in the femoral artery there was also no impact on total platelet deposition (Supplemental Figure S6A and C). However, the mild injury creates much smaller and variable core regions and thrombin inhibition lead to a mild but non-significant reduction in P-selectin(+) core formation (Supplemental Figure S6B). These result demonstrate that while platelet adhesion and accumulation are not thrombin dependent in the femoral artery, fibrin formation, platelet activation, and core formation are still driven by thrombin activity, and that the role of thrombin appears to be somewhat sensitive to the extent of vascular injury.

Tissue factor has been identified as the initiator of coagulation in the cremaster laser injury model [11,133,139], so we used histology to observe the tissue factor distribution in both the cremaster microvasculature and the femoral artery (Supplemental Figure S7). Similar to previous reports [57] we found that tissue factor was localized to the vessel

adventitia in both the macro- and microcirculation. However, in the femoral artery this lead to a much greater distance between the vessel lumen and the tissue factor expressing area of the vessel wall compared to the cremaster. This distance may contribute to the delay in core formation by either delaying thrombin formation or distribution within the thrombus.

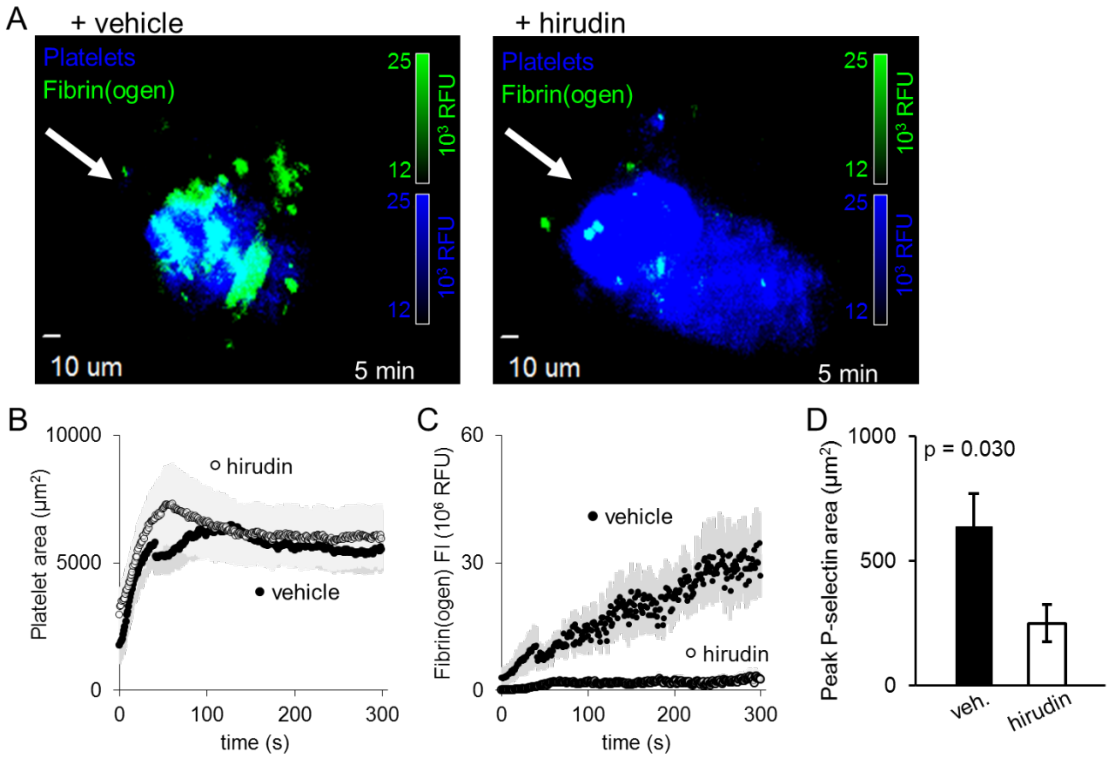

Figure 7- 4 Thrombin drives core formation but not platelet deposition in the femoral artery.

(A) A representative image of a vehicle-treated or hirudin-treated thrombus formed in the femoral artery showing platelets (blue) and fibrin(ogen) (green) 5 minutes post-injury. (B) Platelet area and (C) fibrin(ogen) deposition were monitored for 300 s post-injury. (D) P-selectin area was also monitored (vehicle n = 11; hirudin n = 14, +/- SEM).

7.3.5 Platelet GPVI signaling in response to penetrating injury of the mouse femoral artery

Similar to thrombin, the importance of GPVI signaling during thrombus formation is dependent upon the mechanism and extent of injury. Mechanisms of injury in which there is extensive endothelial cell denudation, exposing subendothelial collagen, GPVI signaling is crucial in driving thrombus formation [39,41-43]. However, in penetrating injuries increasing severity of the injury increases the importance of thrombin signaling, and lessens the impact of GPVI defects [36-39]. Consistent with these reports in the femoral artery rupture injury model there is no significant difference in platelet accumulation or activation in thrombi formed in mice treated with Jaq-1 antibody to deplete GPVI function (Supplemental Figure S8), or control mice (Figure 5). These results demonstrate that collagen exposure in this injury model is limited, and platelet deposition is driven by a collagen and thrombin independent mechanism, but core formation is still largely driven by thrombin activity.

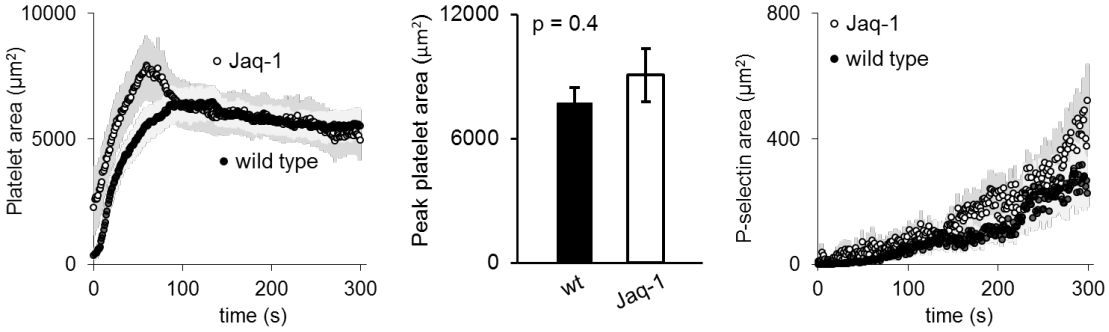

Figure 7- 5 GPVI signaling does not impact platelet accumulation or activation in the femoral artery injury model.

(A) Platelet area was monitored for wild type (black) and Jaq-1 treated mice (white). (B) Peak platelet deposition for each treatment was compared. (C) P-selectin area was also monitored over time for both wild type and Jaq-1 mice (wild type n = 9; Jaq-1 n = 12, +/- SEM).

7.3.6 Similarities and differences in thrombus formation in the femoral artery and vein

Vessel wall and hemodynamic differences between arterial and venous vessels drive differences in the hemostatic response even within the same vascular beds [33,34,140]. To investigate how thrombus architecture and signaling compares between the femoral artery and vein we monitored thrombus formation, and the effects of cangrelor and hirudin on thrombus architecture in the femoral vein (Figure 6). Thrombi in the femoral vein form a core and shell architecture similar to that seen in the femoral artery and the cremaster microvasculature (Figure 6A). Femoral vein thrombi also form with similar dynamics to femoral artery thrombi, but are ~2.5-fold smaller (Figure 6B and Supplemental Figure 98A and B). Femoral vein thrombi are also more stable than the femoral artery thrombi with less embolization after reaching peak size, which may be due to decreased shear stress in the vein (Supplemental Figure S9C). Similarly, to the femoral artery P-selectin exposure dynamics are significantly delayed compared to the cremaster (Figure 6B and Supplemental Figure S9D).

The role of ADP signaling in thrombus architecture formation was also conserved in the femoral vein, with cangrelor-treated thrombi becoming highly-unstable reducing final thrombus size, but not impacting core formation (Figure 6D-H). Thrombin inhibition also did not impact total thrombus size in the femoral vein, and did slow down core formation,

but did not significantly reduce peak core size formation by 5 minutes post-injury (Figure 6I-M). These results demonstrate that thrombus architecture and dynamics are highly conserved between the femoral artery and vein, despite vessel biology and hemodynamic differences, but the contribution of thrombin activity to core formation appears to be different within the vein.

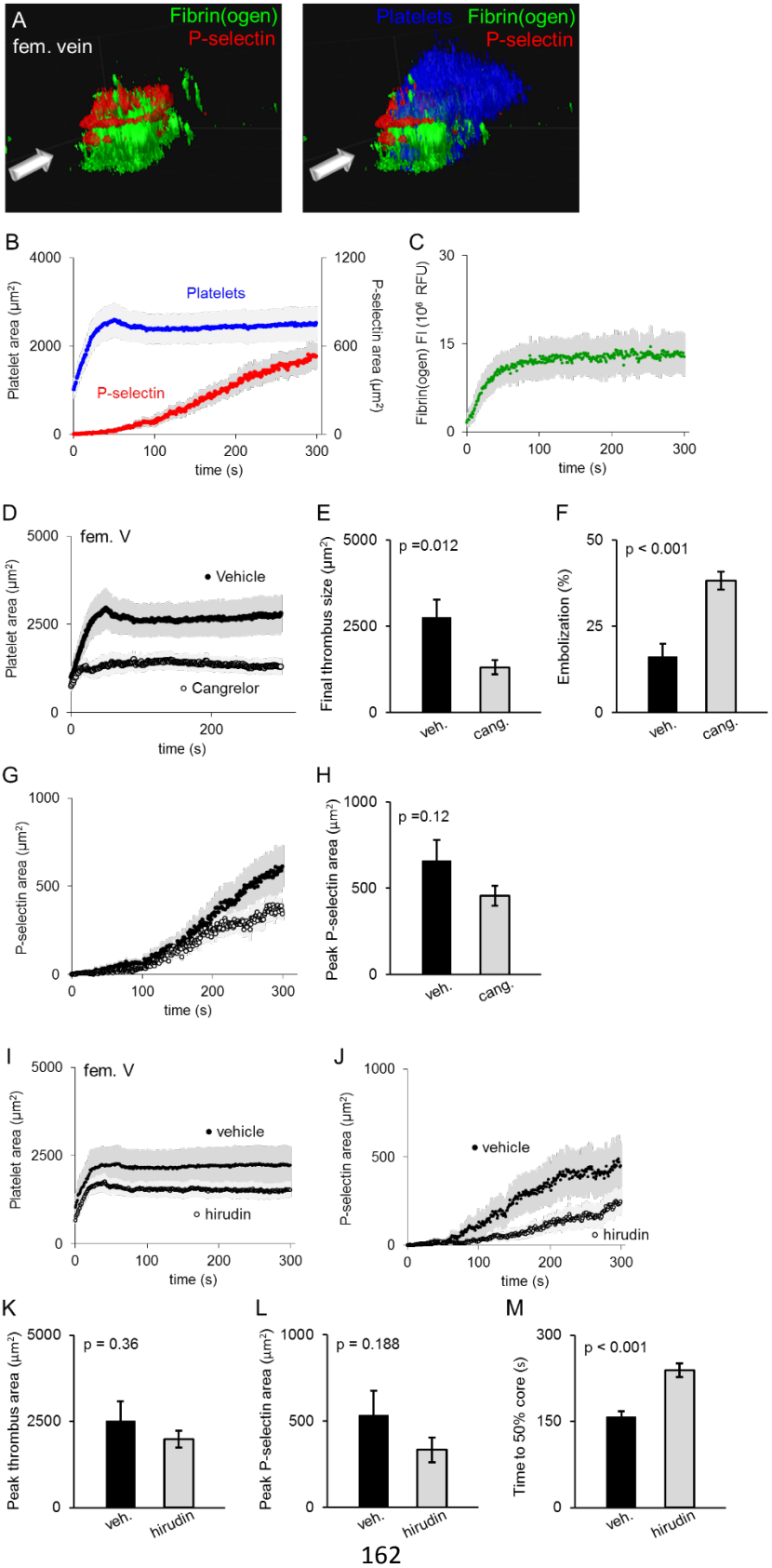
A
fem. vein
Fibrin(ogen)
P-selectin
Platelets
Fibrin(ogen)
P-selectin
B
Platelet area (µm²)
P-selectin area (µm²)
Platelets
P-selectin
time (s)
C
Fibrin(ogen) FI (10⁶ RFU)
time (s)
D
fem. V
Platelet area (µm²)
• Vehicle
◦ Cangrelor
time (s)
E
Final thrombus size (µm²)
p =0.012
veh.
cang.
F
Embolization (%)
p < 0.001
veh.
cang.
G
P-selectin area (µm²)
time (s)
H
Peak P-selectin area (µm²)
p =0.12
veh.
cang.
I
fem. V
Platelet area (µm²)
• vehicle
◦ hirudin
time (s)
J
P-selectin area (µm²)
• vehicle
◦ hirudin
time (s)
K
Peak thrombus area (µm²)
p = 0.36
veh.
hirudin
L
Peak P-selectin area (µm²)
p = 0.188
veh.
hirudin
M
Time to 50% core (s)
p < 0.001
veh.
hirudin

Figure 7- 6 Thrombus architecture and agonist contributions in the femoral vein.

(A) A representative image of the architecture of a thrombus formed in the femoral vein showing fibrin(ogen) (green), P-selectin (red), and platelets (blue). (B) Platelets, P-selectin, and (D) fibrin(ogen) deposition were monitored for 300 s post-injury (n = 22, +/- SEM). (D) Platelet area dynamcis, (E) final platelet area, and (F) percent embolization were quantified for femoral vein thrombi either in the presence of vehicle (black) or cangrelor (white). (G and H) The rate of P-selectin (+) area accumulation and peak P-selectin area for vehicle and cangrelor-treated thrombi (vehicle n = 10; cangrelor n = 12, +/- SEM). (I and J) The dynamics of platelet accumulation and P-selectin exposure in vehicle- (black) or hirudin-treated thrombi (white). (K) Quantification of peak platelet area, (L) peak P-selectin area, and (M) time to 50% core formation for vehicle- and hirudin-treated thrombi (vehicle n = 10; hirudin n = 13, +/- SEM).

7.4 Discussion

Techniques to monitor thrombus formation in vivo have been expanding, leading to numerous injury models in different vascular beds [33-35,40,133]. The contribution of various agonists varies with injury mechanism and the vascular location of injury [33,36,38,39,41,42]. Laser injury of the mouse cremaster microcirculation is perhaps the best characterized injury model. Numerous studies have shown that initial stable platelet accumulation is thrombin dependent, driven by tissue factor exposed at the injury site and propagated through factors XIII and IX [11,12,139,141,142]. Secondary thrombus growth is driven by ADP and TxA2 [12]. Continued thrombin activity restricted within the densely packed platelets proximal to the injury site drive further platelet activation resulting in α-granule release and surface P-selectin exposure [12,22,55,96]. This leads to a stable hemostatic thrombus consisting of a core and shell architecture. To determine how agonist generation and activity is altered in the macrovasculature we developed a new technique to induce a

penetrating laser injury to the mouse femoral artery and vein, and compared it to results obtained in the cremaster muscle microvasculature.

We found several key similarities between thrombus formation in the macro- and microcirculation. Namely, the core and shell architecture observed in the cremaster was conserved in the femoral artery, in response to mild and rupture injuries, and in the femoral vein. We also observed similarities in the relative rate of thrombus growth, with stable platelet recruitment being limited to 0-60 s post-injury in the femoral artery, vein, and cremaster microcirculation. Interestingly, the initial rate of thrombus growth was not affected by the extent of vessel injury, as a mild injury to the femoral artery showed similar kinetics in platelet recruitment. However, thrombus stability and final thrombus size was greatly impacted by the extent of vessel damage. We also observed similarities in the role of ADP and thrombin in impacting thrombus architecture formation. Inhibition of ADP activity with cangrelor decreased shell stability, leading to a significant decrease in lumenal and downstream thrombus growth in the femoral artery and vein, but did not affect formation of the highly activated core region in the injury site. This effect was similar to that observed in the cremaster arterioles and venules, and demonstrates why P2Y12 antagonists have been so successful in preventing occlusive thrombus formation with limited hemostatic defects. We also found a consistent role of thrombin in driving full platelet activation resulting in α-granule release and surface P-selectin exposure in the core region.

Interestingly, thrombin inhibition in the femoral artery and vein did not affect platelet accumulation, despite decreasing platelet activation and fibrin deposition. This result was in stark contrast to previous experiments in the cremaster arterioles where stable

thrombus formation was driven by thrombin activity and inhibition resulted in an 80-90% reduction in thrombus size. One key difference between the macro- and microcirculation that may contribute to this difference is the amount of the thrombus that within the vessel wall. Thrombus formation in the cremaster results in thrombi that are almost entirely in the vessel lumen, however, in the macrocirculation a significant portion of the thrombus, largely the core region, is within the vessel wall (Supplemental Figure S2). This suggests that numerous vessel wall proteins may be driving initial platelet accumulation and activation within the region that will form the core, and ADP drives shell recruitment. We were able to rule out collagen as a significant mediator of platelet recruitment or activation, and Getz et al. recently demonstrated the importance of vWF/GPIb interactions in platelet recruitment at the injury site in the saphenous vein injury model. This suggests that vWF released from injury site proximal endothelium, or polymerized during the flow of blood out of the vessel drives initial platelet recruitment at the injury site.

Also different between the thrombi formed in the femoral artery and vein and the cremaster microvasculature is the relative dynamics of core formation. Numerous studies have shown that core formation typically consists of a short lag phase, followed by a linear growth phase, and then a plateau [12,22,96]. However, in the femoral artery core formation appeared to be more exponential in growth with a prolonged lag phase (Figure 1C). However, fibrin(ogen) rapidly accumulates at the injury site with dynamics similar in the femoral artery and cremaster injury models, suggesting that thrombin generation is not delayed significantly. We hypothesize that architectural differences in the macro- and microcvasculature may delay thrombin accumulation within the thrombus. In cremaster thrombi core formation is preceded by the formation of a transition zone, defined by the

tight platelet packing and restricted solute transport that facilitates platelet activation and core formation. Therefore, we hypothesize that in the macrovasculature the expanded distance between the lumen and the adventitial tissue factor is plugged with a large transition zone that reduces protein transport within the platelet mass. Thus, thrombin has reduced access to the thrombus region on a larger scale in the macrovasculature, and is diverted within the vessel wall where much of the fibrin(ogen) is detected. This delay in thrombin activity within the thrombus would contribute to the delay in core formation, and reduce the role of thrombin in initial platelet recruitment.

Here we present a novel method for producing laser injuries in the mouse femoral artery. These injuries are comparable to the injuries produced in the cremaster microcirculation, and thus provide a method to measure the impact of changing vessel biology and hemodynamics on the hemostatic process. Thrombus architecture, however, is highly conserved throughout both the macro- and microcirculation in both the arterial and venous vasculatures, suggesting that this architecture may play an important role in establishing a hemostatic thrombus. The role of ADP was also highly conserved between both the macro- and microcirculation and the arterial and venous vasculatures. Thrombin, however, shifted from driving stable thrombus formation in the microcirculation to having no role in platelet recruitment in either the femoral artery or vein. However, thrombin was still responsible for the majority of core formation in the femoral artery, but slightly less so in the vein. Together our results demonstrate how vessel architecture can impact the hemostatic response and we propose that this technique will prove informative in understanding events in clinically-relevant vascular diseases, including atherothrombosis.

7.5 Supplemental Material

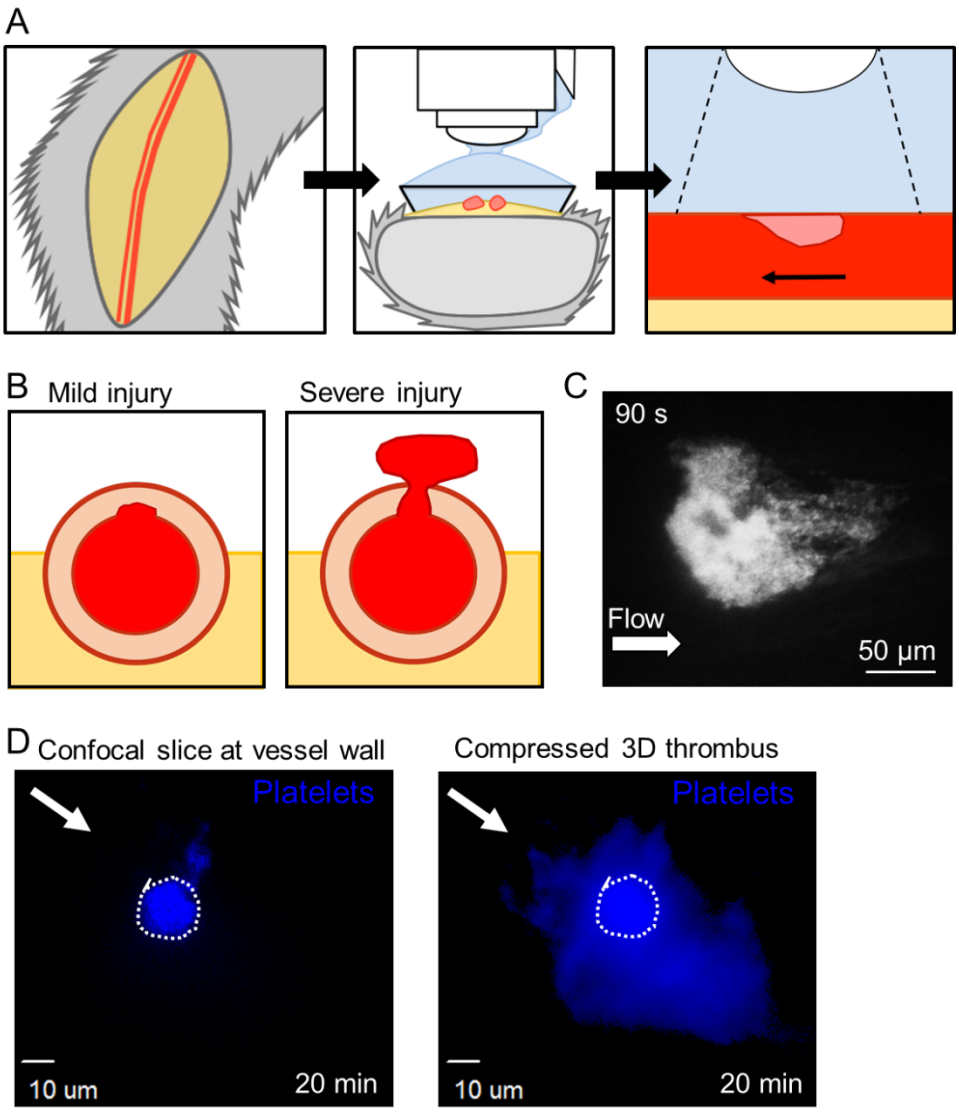

Figure 7- 7 Femoral artery laser injury model.

(A) A schematic of the mouse femoral artery and vein, the microscope immersion strategy, and orientation of thrombus formation. (B) Schematic of the mild and severe injuries created by altering the duration of laser injury to the femoral artery. (C) A representative image of thrombus formation in response to a severe injury. (D) The platelet (blue) signal right at the surface of the femoral artery wall

showing the injury site, and the compressed image of the 3D thrombus formed at the injury site showing the injury site.

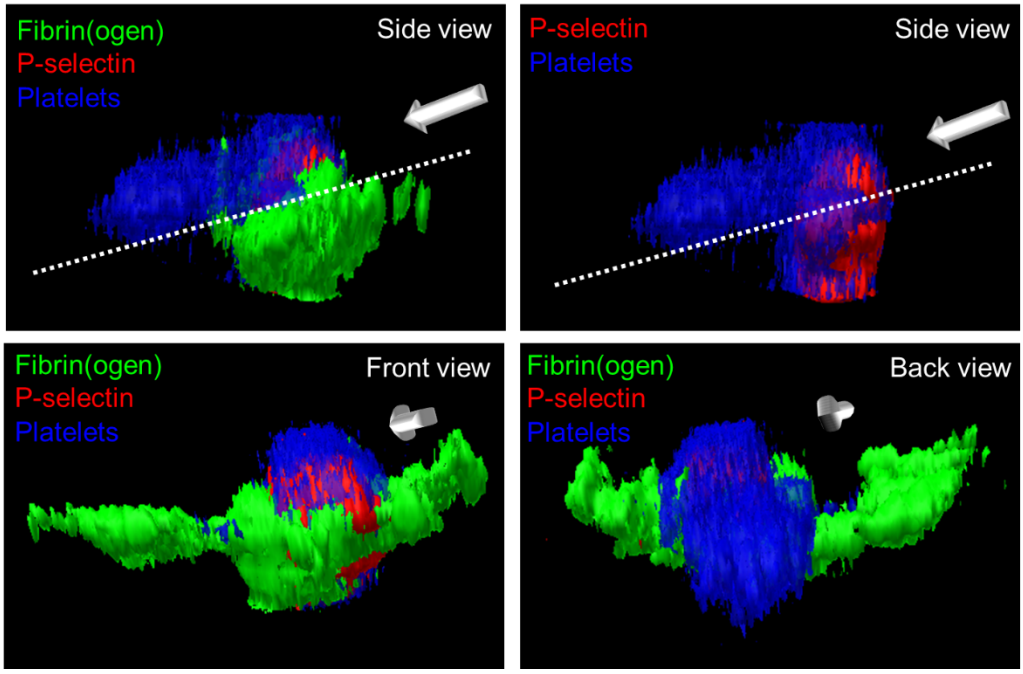

Figure 7- 8 Femoral artery thrombus architecture and orientation.

A 3D reconstruction of a thrombus formed in the femoral artery after a severe injury showing platelets (blue), P-selectin (red), and firbin(ogen) (green). The estimated vessel wall is shown with a dotted white line and the direction of flow is indicated with a white arrow.

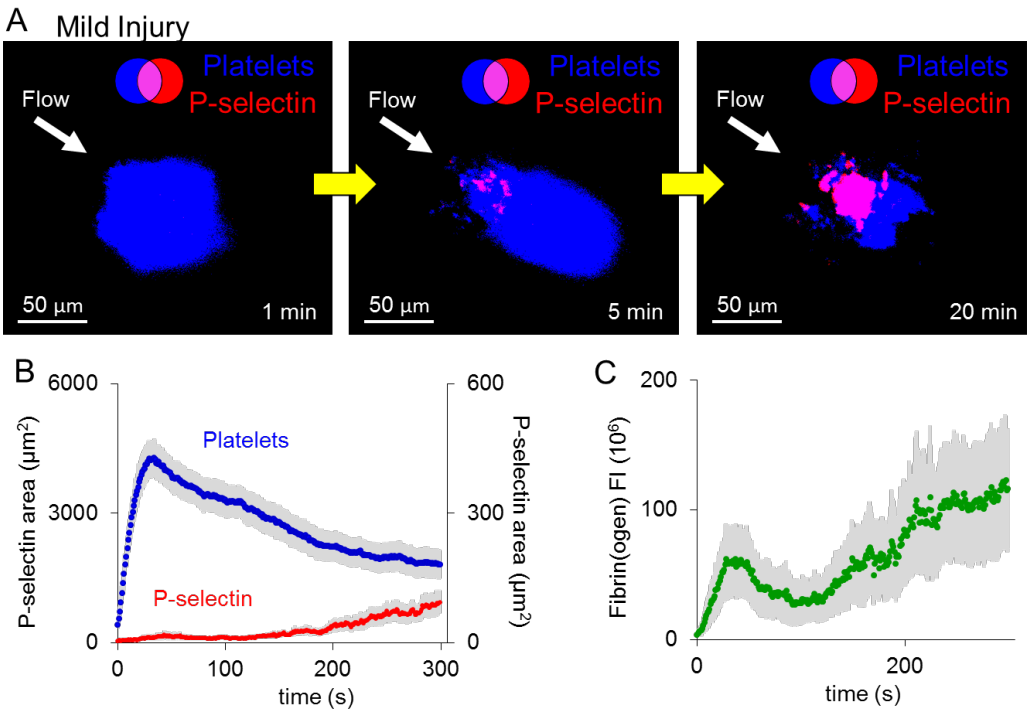

Figure 7- 9 Thrombus architecture in response to mild laser injury of the femoral artery.

(A) A representative image of a thrombus growing over time showing platelets (blue) and P-selectin (red). (B) Quantification of platelet area (blue), P-selectin area (red), and (C) fibrin(ogen) deposition at the injury site over 300 s post-injury (n = 27, +/- SEM).

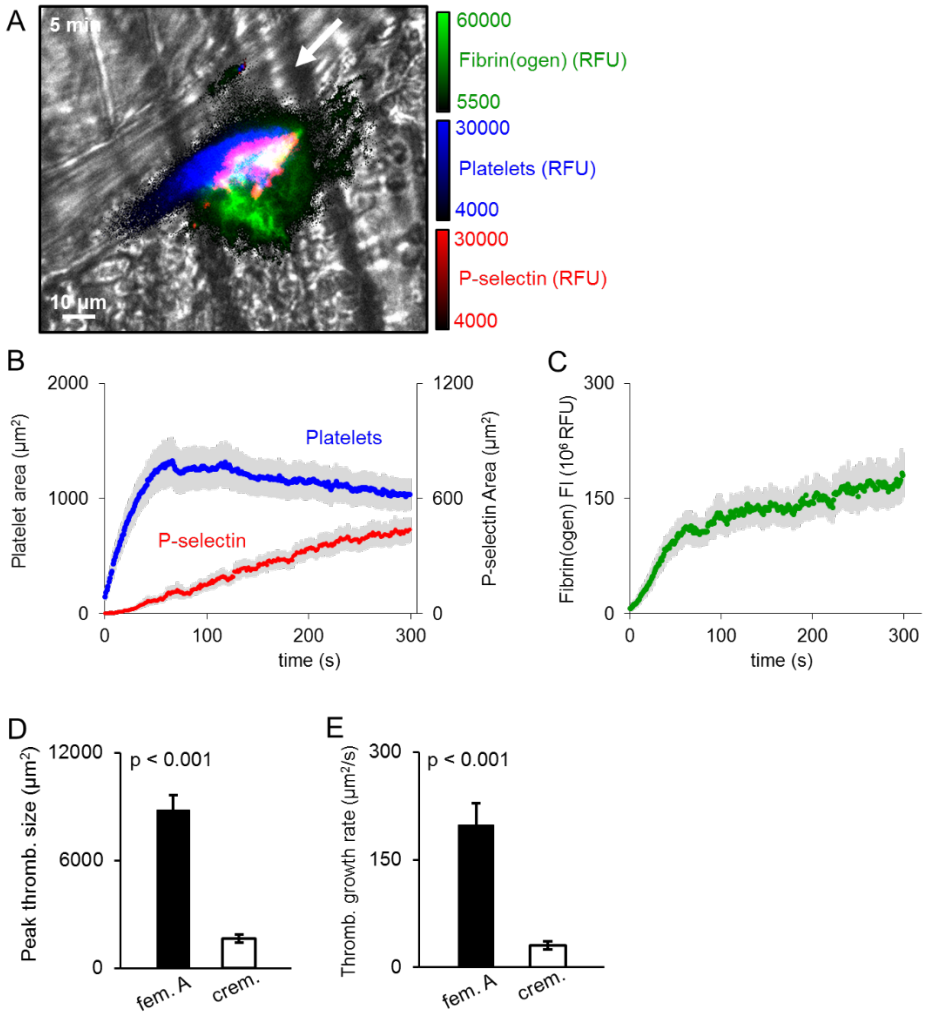

Figure 7- 10 Thrombus architecture formation in the cremaster arterioles compared to the femoral artery.

(A) A representative image of a thrombus formed after laser injury of a mouse cremaster arteriole showing platelets (blue), P-selectin (red), and fibrin(ogen) (green). (B) Quantification of platelet deposition, P-selectin area, and (C) fibrin(ogen) deposition for 300 s post-injury. (D) A comparison of average thrombus size in the femoral artery (black) and the cremaster arterioles (white), and (E) the average initial growth rate (0-20 s post-injury) for each injury model (femoral artery n = 20; cremaster n = 17, +/- SEM).

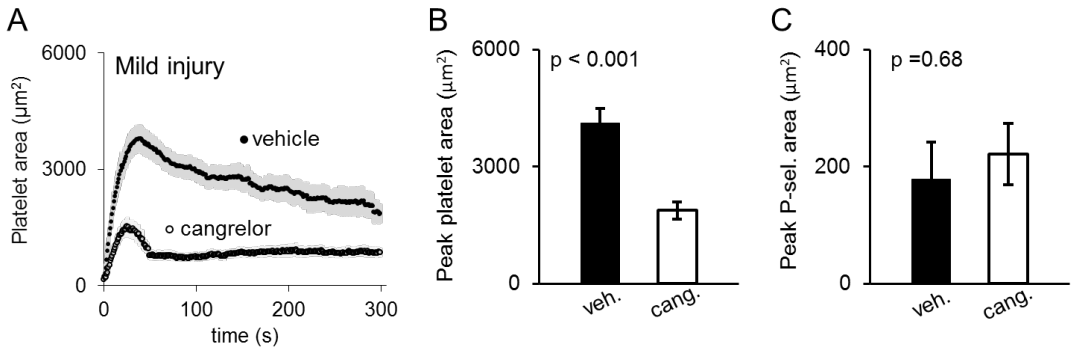

Figure 7- 11 The effect of cangrelor on thrombus formation after a mild injury in the femoral artery.

(A) Quantification of platelet area over time of either vehicle- (black) or cangrelor-treated thrombi. (B) Peak platelet area and (C) peak P-selectin area for vehicle- and cangrelor-treated thrombi (vehicle n = 14; cangrelor n = 16, +/- SEM).

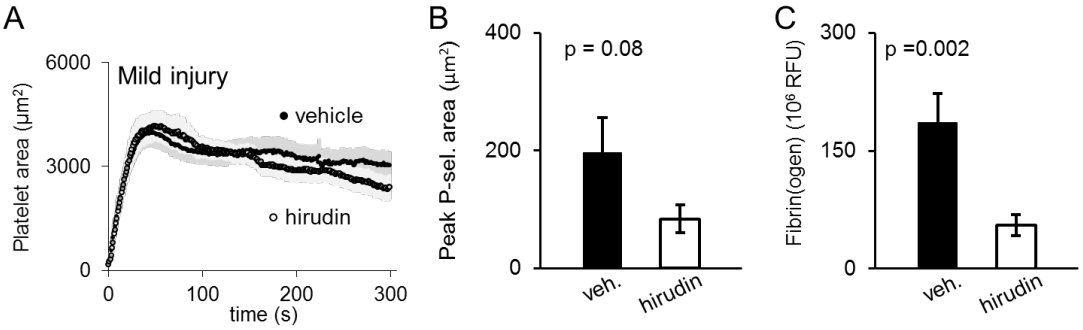

Figure 7- 12 The role of thrombin in shaping thrombus architecture after mild injury in the femoral artery.

(A) Platelet area over time of either vehicle- (black) or hirudin-treated (white) thrombi over 300 s post-injury. (B) Peak P-selectin area and (C) fibrin(ogen) deposition in vehicle- and hirudin-treated thrombi (vehicle n = 13; hirudin n = 14, +/- SEM).

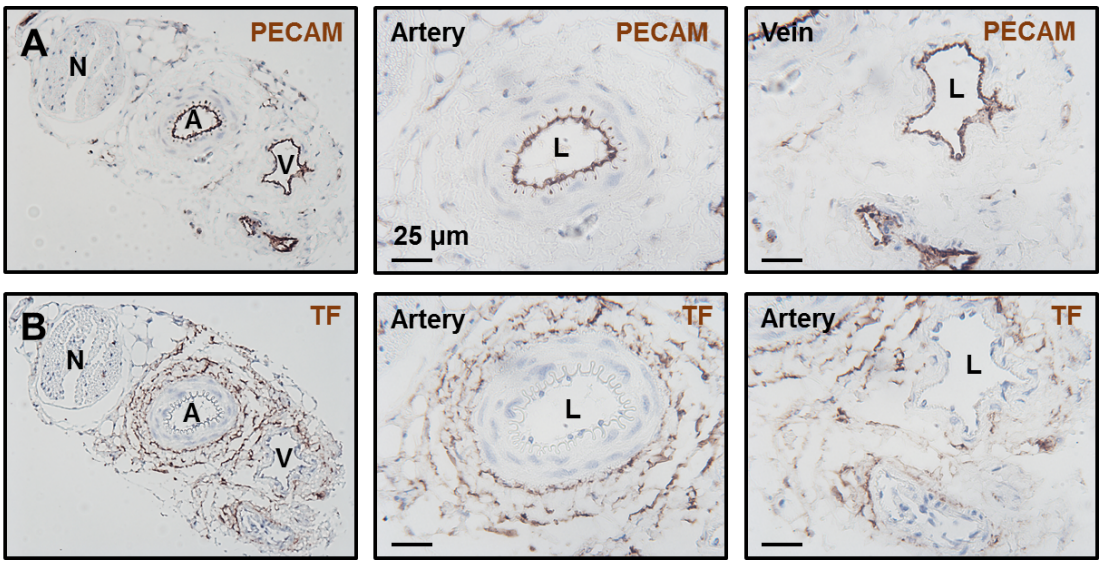

Figure 7- 13 Tissue factor distribution in the femoral artery and vein.

(A) Histological slides showing the femoral artery and vein with endothelium stained (brown). (B) The same slide as in A with tissue factor (TF) stained (brown). N = femoral nerve, A = femoral artery, V = femoral vein, and L = vessel lumen.

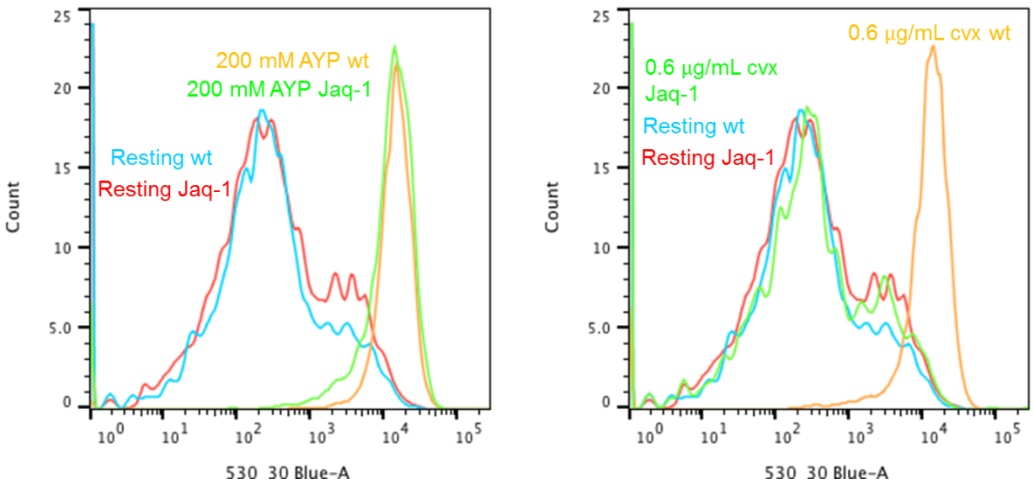

Figure 7- 14 Jaq-1 treatment depletes GPVI signaling in mouse platelets.

Platelets from mice treated injected with either saline (wt) or Jaq-1 antibody (Jaq-1) were collected and either kept resting, treated with AYP (200 mM), or treated with (0.6 μg/mL) convulxin. Platelet activation was measured with fluorescent fibrinogen binding, and wt platelets became activated with both AYP and convulxin treatment, but Jaq-1 platelets only responded to AYP stimulation.

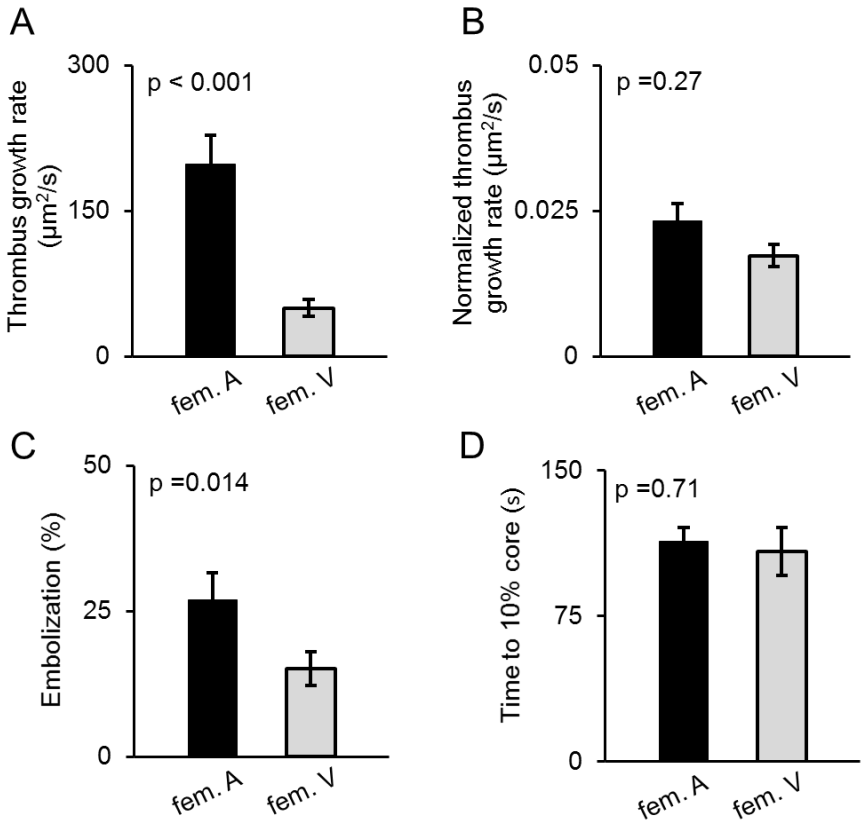

Figure 7- 15 Thrombus architecture comparison between the femoral artery and vein.

(A) Thrombus growth rate (0-20 s post-injury) for femoral artery (black) and vein (gray) thrombi, and (B) the normalized growth rate. (C) The percent embolization of the femoral artery and vein thrombi. (D) Time to 10% core formation for the femoral artery (black) and femoral vein (gray) thrombi (artery n = 20; vein n = 22, +/-SEM).

Chapter 8: Discussion

The aim of this work was to investigate the interplay between thrombus structure and the spatiotemporal distribution and transport of platelet agonists, and how this impacts thrombus formation in vivo. In vivo and ex vivo studies have shown that hemostatic thrombi form a characteristic architecture consisting of a core of highly-activated and fibrin associated platelets covered by a less-activated shell of platelets [12,22,51,55,96]. This architecture emerges during thrombus formation where platelet accumulation and consolidation [12,22,96] is happening simultaneously with various agonist species being released/formed. Platelet aggregation, shape change, and granule release are all dependent upon agonist exposure. Thus, there is a constant feedback between the spatiotemporal distribution of agonists within the thrombus, and the biochemical and biophysical nature of the intrathrombus environment.

During thrombus formation the platelet mass consolidates, particularly in the core region, which leads to dense platelet packing and contact dependent signaling between the platelets [76,88,143-147]. Apart from direct effects on signaling, this dense packing has been shown to inhibit the transport properties of soluble molecules, including coagulation factors and agonists in vitro and in situ [54,59,63,148]. To study, in vivo, how this consolidation impacts agonist distributions we developed a novel biosensor to detect the localization of thrombin activity within the platelet mass after cremaster arteriole laser injury [87]. Consistent with the observation that fibrin is restricted to the core region, we also observed that thrombin activity was isolated to the core region. The binary distribution of thrombin activity mirrored that of P-selectin exposure, which was consistent with

previous observations showing that inhibition of thrombin prevented core formation [12,22,87].

As the core had also been shown to have the highest density of platelet packing we wanted to test the hypothesis that the intrathrombus structure could restrict thrombin movements. In order to do this we designed a protein transport sensor, consisting of bovine serum albumin labeled with a photoactivatable fluorescent tag (cAlb) [22]. This allowed us, during intravital imaging in the mouse cremaster, to activate a bolus of plasma borne cAlb within the thrombus, and track its elution in real time. What we found is that protein transport was significantly restricted in the core region, and that this restrictive environment developed prior to core formation, in a region dubbed the transition zone [22].

These results were confirmed using a computational model of protein transport within a computer generated thrombus architecture, which showed that dense platelet packing inhibited the convection of proteins by the surrounding flow, and restricted the diffusion of proteins [55]. Further, we were able to perturb the formation of the densely packed transition zone, by inhibiting outside-in signaling, which lead to a significant decrease in thrombin activity within the platelet mass and thus decreased platelet activation [96]. Taken together this work creates a model of hemostatic thrombus formation in which platelets accumulate rapidly, outside-in signaling mediates retraction of the platelets proximal to the injury site driving transition zone formation, thrombin generated at the injury site is then restricted to within the transition zone driving full platelet activation, fibrin deposition, and core formation. Concurrently, ADP and TxA2 are released from the

granules of activated platelets, and being more diffusible, escape the core region and drive shell recruitment and stabilization.

This model also has implications for the regulation of plasma-borne molecular activity within different regions of the thrombus. The dense platelet packing that occurs in the transition zone likely limits the delivery of coagulation factors to tissue factor surfaces in the extravascular space [11,12,59], as well as anti-thrombotic proteins like tissue factor pathway inhibitor (TFPI) or antithrombin III, and infused pharmaceutical agents. Therefore, the thrombus forms a gradient of access based on molecular size, allowing for small molecules to move freely through the core, while larger molecules are either have restricted transport within the core or are excluded altogether [22]. Future studies will address how different coagulation factor size may impact the spatiotemporal activity of the factors. Also future studies can determine if plasma protein packing into platelet granules circumvents the thrombus structural barrier, allowing for selective delivery of bioactive molecules within the thrombus.

Future work examining this model in pathological settings will be important to determine the role of molecular transport in occlusive thrombus formation. In hemostatic thrombi we observed that platelet retraction serves to retain and promote thrombin activity in the core. However, in pathological settings where there is potent or systemic coagulation, thrombin generation may be too robust to be successfully limited by platelet packing, and dense platelet packing may instead increases thrombus stability and limit access of antithrombotic agents. Determining how these processes are shifted during pathological thrombi may inform the identification of future drug targets aimed at limiting occlusive thrombus formation without limiting hemostatic function.

To extend this model we also examined the ability of the thrombus structure to limit the extravasation of plasma proteins at the site of injury. Numerous proteins that are biologically significant to post-hemostatic processes, such as wound healing and inflammation, are present in circulating plasma and inside platelets. Upon vessel damage these plasma- and platelet-borne proteins are extravasated into the surrounding tissue. Thrombus formation forms a physical barrier to resist this transport. Therefore we hypothesized that tight platelet packing may also play a role in regulating the delivery of these bioactive proteins.

We found that, in the cremaster venules, which recapitulate the core/shell architecture, red cell loss was prevented by just a few platelets accumulating at the injury site while plasma protein extravasation continued even beyond stable thrombus formation. Also the rate of extravasation was dependent upon total platelet accumulation, up to a point, and beyond that platelet retraction, but not fibrin deposition, drove continued vessel sealing. Interestingly, ADP signaling appeared to be particularly important in forming a tightly-packed structure, independent of overall platelet activation state. Thrombin inhibition did not have the same effect, but this may be restricted to the venules where thrombus formation is less dependent on thrombin than in the arterioles. Thus, we can extend the model outlined above to include that the transition zone and core formation alter the delivery, and thus the concentration gradient, of both plasma- and platelet-borne proteins in the tissue surrounding the site of injury. Further investigation is still needed to determine how this impacts post-hemostatic processes such as wound healing and inflammation.

Formation of a tight vascular plug may also serve to shift the distribution of proteins being delivered into the tissue plane. Initial injury induces a large amount of plasma and red cell delivery into the tissue. However, thrombus-driven vessel sealing coincides with core formation and α-granule release (Figure 6-1). Proteins released from the α-granules are in close proximity to the injury site, and will easily diffuse into the extravascular tissue. This presents the possibility of two distinct phases of protein extravasation: initially plasma-derived protein phase, and then a platelet-derived protein phase begins which may each have a specific biological role.

Future studies of protein transport during pathological thrombus formation may also provide insight into the role of protein extravasation as a possible sink for thrombin. In chapter 2 we demonstrated that the pressure drop across the injury site is capable of altering thrombin localization. In vivo, vessel rupture induces a strong pressure drop across the injury site driving blood out of the vessel and into the extravascular space. This pressure drop is the difference between the pressure in the vessel lumen and the surrounding tissue. However, in common pathological thrombotic diseases - atherosclerotic plaque rupture, DVT, or aneurisms - the pressure drop is minimal potentially facilitating increased thrombin activity in the lumen of the vessel driving occlusive thrombus formation. In a high thrombin environment the ability of platelets to restrict thrombin movement may be even more important in shaping thrombus growth.

Finally, we wanted to observe how these observations made in the microcirculation extend to larger vessels that have very different biology and physics. We developed a novel technique for monitoring thrombus formation in the mouse femoral artery and vein in response to laser injury. We found that the core and shell architecture observed in the

microvasculature was conserved in the femoral artery and vein, despite the thrombi being 5-10 fold larger in the femoral artery. We also found that ADP plays a very similar role in driving shell formation in the femoral artery. Thrombin, however, appeared to play no role in platelet recruitment, but still drove core formation. We also observed a significant delay in core formation in the femoral artery and vein compared to the microvasculature. Measurements of tissue factor distribution showed that tissue factor, while plentiful in the femoral artery vessel wall, was ~10-fold further from the vessel lumen than in the cremaster arterioles. Thus, the increased core size and distance separating the tissue factor and lumen may make thrombin generation and thrombus architecture even more dependent upon platelet packing and molecular transport than our current model in the mouse microcirculation.

In conclusion, this work demonstrates the importance of molecular transport in shaping the hemostatic process, and identifies several key events in thrombus formation that are responsible to regulating intrathrombus transport. These studies outline a regulatory mechanism that shapes agonist gradients in a biochemically independent manner, and identify novel effects of outside-in, and $P2Y_{12}$ signaling in shaping the intrathrombus microenvironment and local transport properties. Future studies may also reveal how agonist transport is altered during pathological thrombus formation, and inform the design of novel therapies.

References

1. Versteeg HH, Heemskerk JW, Levi M, Reitsma PH. New fundamentals in hemostasis. *Physiol Rev*. 2013;93(1):327-358.
2. Brass LF, Newman DK, Wannemacher KM, Zhu L, Stalker TJ. Signal transduction during platelet plug formation. In: Michelson AD, ed. Platelets. New York: Elsevier; 2013:367-398.
3. Gibbins JM. Platelet adhesion signalling and the regulation of thrombus formation. *J Cell Sci*. 2004;117(Pt 16):3415-3425.
4. Munnix IC, Cosemans JM, Auger JM, Heemskerk JW. Platelet response heterogeneity in thrombus formation. *Thromb Haemost*. 2009;102(6):1149-1156.
5. Brass LF, Wannemacher KM, Ma P, Stalker TJ. Regulating thrombus growth and stability to achieve an optimal response to injury. *J Thromb Haemost*. 2011;9 Suppl 1:66-75.
6. Jackson SP, Nesbitt WS, Kulkarni S. Signaling events underlying thrombus formation. *J Thromb Haemost*. 2003;1(7):1602-1612.
7. Jorgensen L, Rowsell HC, Hovig T, Mustard JF. Resolution and organization of platelet-rich mural thrombi in carotid arteries of swine. *Am J Pathol*. 1967;51(5):681-719.
8. Stehbens WE, Biscoe TJ. The ultrastructure of early platelet aggregation in vivo. *Am J Pathol*. 1967;50(2):219-243.
9. White JG. Platelet structural physiology: the ultrastructure of adhesion, secretion, and aggregation in arterial thrombosis. *Cardiovasc Clin*. 1987;18(1):13-33.
10. Falati S, Gross PL, Merrill-Skoloff G, et al. In vivo models of platelet function and thrombosis: study of real-time thrombus formation. *Methods Mol Biol*. 2004;272:187-197.
11. Falati S, Gross P, Merrill-Skoloff G, Furie BC, Furie B. Real-time in vivo imaging of platelets, tissue factor and fibrin during arterial thrombus formation in the mouse. *NatMed*. 2002;8:1175-1180.
12. Stalker TJ, Traxler EA, Wu J, et al. Hierarchical organization in the hemostatic response and its relationship to the platelet-signaling network. *Blood*. 2013;121(10):1875-1885.
13. Muthard RW, Diamond SL. Side view thrombosis microfluidic device with controllable wall shear rate and transthrombus pressure gradient. *Lab Chip*. 2013.
14. Konecny FA. Review of cellular and molecular pathways linking thrombosis and innate immune system during sepsis. *J Res Med Sci*. 2010;15(6):348-358.
15. Zhang G, Han J, Welch EJ, et al. Lipopolysaccharide stimulates platelet secretion and potentiates platelet aggregation via TLR4/MyD88 and the cGMP-dependent protein kinase pathway. *J Immunol*. 2009;182(12):7997-8004.
16. Esmon CT, Fukudome K, Mather T, et al. Inflammation, sepsis, and coagulation. *Haematologica*. 1999;84(3):254-259.
17. Kitchens CS. Thrombocytopenia and thrombosis in disseminated intravascular coagulation (DIC). *Hematology Am Soc Hematol Educ Program*. 2009:240-246.
18. Potti A, Ramiah V, Ortel TL. Thrombophilia and thrombosis in thrombotic thrombocytopenic purpura. *Semin Thromb Hemost*. 2005;31(6):652-658.
19. Razin E, Marx G. Thrombin-induced degranulation of cultured bone marrow-derived mast cells. *JImmunol*. 1984;133:3282-3285.
20. Garcia JGN. Molecular mechanisms of thrombin-induced human and bovine endothelial cell activation. *JLabClinMed*. 1992;120:513-519.

21. Semple JW, Freedman J. Platelets and innate immunity. *Cell Mol Life Sci*. 2010;67(4):499-511.
22. Welsh JD, Stalker TJ, Voronov R, et al. A systems approach to hemostasis: 1. The interdependence of thrombus architecture and agonist movements in the gaps between platelets. *Blood*. 2014;124(11):1808-1815.
23. Fuchs TA, Brill A, Wagner DD. Neutrophil extracellular trap (NET) impact on deep vein thrombosis. *Arterioscler Thromb Vasc Biol*. 2012;32(8):1777-1783.
24. Wakefield TW, Myers DD, Henke PK. Mechanisms of venous thrombosis and resolution. *Arterioscler Thromb Vasc Biol*. 2008;28(3):387-391.
25. Mackman N. New insights into the mechanisms of venous thrombosis. *J Clin Invest*. 2012;122(7):2331-2336.
26. Goel MS, Diamond SL. Adhesion of normal erythrocytes at depressed venous shear rates to activated neutrophils, activated platelets, and fibrin polymerized from plasma. *Blood*. 2002;100:3797-3803.
27. Andrews DA, Low PS. Role of red blood cells in thrombosis. *Curr Opin Hematol*. 1999;6(2):76-82.
28. Silvain J, Collet JP, Nagaswami C, et al. Composition of coronary thrombus in acute myocardial infarction. *J Am Coll Cardiol*. 2011;57(12):1359-1367.
29. Lee R, Adlam D, Clelland CA, Channon KM. Lines of Zahn in coronary artery thrombus. *Eur Heart J*. 2012;33(9):1039.
30. Friedman M, Van den Bovenkamp GJ. The pathogenesis of a coronary thrombus. *Am J Pathol*. 1966;48(1):19-44.
31. Cines DB, Lebedeva T, Nagaswami C, et al. Clot contraction: compression of erythrocytes into tightly packed polyhedra and redistribution of platelets and fibrin. *Blood*. 2014;123(10):1596-1603.
32. Wolberg AS. Thrombin generation and fibrin clot structure. *Blood Rev*. 2007;21(3):131-142.
33. Denis CV, Wagner DD. Platelet adhesion receptors and their ligands in mouse models of thrombosis. *Arterioscler Thromb Vasc Biol*. 2007;27(4):728-739.
34. Rumbaut RE, Slaff DW, Burns AR. Microvascular thrombosis models in venules and arterioles in vivo. *Microcirculation*. 2005;12(3):259-274.
35. Cooley BC. Murine arterial thrombus induction mechanism influences subsequent thrombodynamics. *Thromb Res*. 2015;135(5):939-943.
36. Hechler B, Nonne C, Eckly A, et al. Arterial thrombosis: relevance of a model with two levels of severity assessed by histologic, ultrastructural and functional characterization. *J Thromb Haemost*. 2010;8(1):173-184.
37. Mangin P, Yap CL, Nonne C, et al. Thrombin overcomes the thrombosis defect associated with platelet GPVI/FcRgamma deficiency. *Blood*. 2006;107(11):4346-4353.
38. Kalia N, Auger JM, Atkinson B, Watson SP. Critical role of FcR gamma-chain, LAT, PLCgamma2 and thrombin in arteriolar thrombus formation upon mild, laser-induced endothelial injury in vivo. *Microcirculation*. 2008;15(4):325-335.
39. Dubois C, Panicot-Dubois L, Merrill-Skoloff G, Furie B, Furie BC. Glycoprotein VI-dependent and -independent pathways of thrombus formation in vivo. *Blood*. 2006;107(10):3902-3906.
40. Getz TM, Piatt R, Petrich BG, Monroe D, Mackman N, Bergmeier W. Novel mouse hemostasis model for real-time determination of bleeding time and hemostatic plug composition. *J Thromb Haemost*. 2015;13(3):417-425.
41. Massberg S, Gawaz M, Gruner S, et al. A crucial role of glycoprotein VI for platelet recruitment to the injured arterial wall in vivo. *J Exp Med*. 2003;197(1):41-49.

42. Massberg S, Konrad I, Bultmann A, et al. Soluble glycoprotein VI dimer inhibits platelet adhesion and aggregation to the injured vessel wall in vivo. *Faseb J*. 2004;18(2):397-399.
43. Munnix IC, Strehl A, Kuijpers MJ, et al. The glycoprotein VI-phospholipase Cgamma2 signaling pathway controls thrombus formation induced by collagen and tissue factor in vitro and in vivo. *Arterioscler Thromb Vasc Biol*. 2005;25(12):2673-2678.
44. Bender M, Hagedorn I, Nieswandt B. Genetic and antibody-induced glycoprotein VI deficiency equally protects mice from mechanically and FeCl(3) -induced thrombosis. *J Thromb Haemost*. 2011;9(7):1423-1426.
45. Chien S, Lipowsky HH. Correlation of hemodynamics in macrocirculation and microcirculation. *Int J Microcirc Clin Exp*. 1982;1(4):351-365.
46. Khan AI, Kerfoot SM, Heit B, et al. Role of CD44 and hyaluronan in neutrophil recruitment. *J Immunol*. 2004;173(12):7594-7601.
47. Dietzel S, Pircher J, Nekolla AK, et al. Label-free determination of hemodynamic parameters in the microcirculaton with third harmonic generation microscopy. *PLoS One*. 2014;9(6):e99615.
48. Feihl F, Liaudet L, Waeber B. The macrocirculation and microcirculation of hypertension. *Curr Hypertens Rep*. 2009;11(3):182-189.
49. Schafer SC, Pellegrin M, Wyss C, et al. Intravital microscopy reveals endothelial dysfunction in resistance arterioles in Angiotensin II-induced hypertension. *Hypertens Res*. 2012;35(8):855-861.
50. Isakson BE, Best AK, Duling BR. Incidence of protein on actin bridges between endothelium and smooth muscle in arterioles demonstrates heterogeneous connexin expression and phosphorylation. *Am J Physiol Heart Circ Physiol*. 2008;294(6):H2898-2904.
51. Muthard RW, Diamond SL. Blood clots are rapidly assembled hemodynamic sensors: flow arrest triggers intraluminal thrombus contraction. *Arterioscler Thromb Vasc Biol*. 2012;32(12):2938-2945.
52. Voronov RS, Stalker TJ, Brass LF, Diamond SL. Simulation of intrathrombus fluid and solute transport using in vivo clot structures with single platelet resolution. *Ann Biomed Eng*. 2013;41(6):1297-1307.
53. Kim OV, Xu Z, Rosen ED, Alber MS. Fibrin networks regulate protein transport during thrombus development. *PLoS Comput Biol*. 2013;9(6):e1003095.
54. Leiderman K, Fogelson AL. Grow with the flow: a spatial-temporal model of platelet deposition and blood coagulation under flow. *Math Med Biol*. 2011;28(1):47-84.
55. Tomaiuolo M, Stalker TJ, Welsh JD, Diamond SL, Sinno T, Brass LF. A systems approach to hemostasis: 2. Computational analysis of molecular transport in the thrombus microenvironment. *Blood*. 2014;124(11):1816-1823.
56. Leiderman K, Fogelson AL. The influence of hindered transport on the development of platelet thrombi under flow. *Bull Math Biol*. 2013;75(8):1255-1283.
57. Drake TA, Morrissey JH, Edgington TS. Selective cellular expression of tissue factor in human tissues. Implications for disorders of hemostasis and thrombosis. *Am J Pathol*. 1989;134(5):1087-1097.
58. Fogelson AL, Tania N. Coagulation under flow: the influence of flow-mediated transport on the initiation and inhibition of coagulation. *Pathophysiol Haemost Thromb*. 2005;34(2-3):91-108.
59. Hathcock JJ, Nemerson Y. Platelet deposition inhibits tissue factor activity: in vitro clots are impermeable to factor Xa. *Blood*. 2004;104(1):123-127.

60. Neeves KB, Illing DA, Diamond SL. Thrombin flux and wall shear rate regulate fibrin fiber deposition state during polymerization under flow. *Biophys J*. 2010;98(7):1344-1352.
61. Diamond SL. Engineering design of optimal strategies for blood clot dissolution. *Annu Rev Biomed Eng*. 1999;1:427-462.
62. Okorie UM, Denney WS, Chatterjee MS, Neeves KB, Diamond SL. Determination of surface tissue factor thresholds that trigger coagulation at venous and arterial shear rates: amplification of 100 fM circulating tissue factor requires flow. *Blood*. 2008;111(7):3507-3513.
63. Kuharsky AL, Fogelson AL. Surface-mediated control of blood coagulation: the role of binding site densities and platelet deposition. *Biophys J*. 2001;80(3):1050-1074.
64. Dörmann D, Clemetson KJ, Kehrel BE. The GPIb thrombin-binding site is essential for thrombin-induced platelet procoagulant activity. *Blood*. 2000;96:2469-2478.
65. Celikel R, McClintock RA, Roberts JR, et al. Modulation of alpha-thrombin function by distinct interactions with platelet glycoprotein Ibalpha. *Science*. 2003;301(5630):218-221.
66. Colace TV, Muthard RW, Diamond SL. Thrombus growth and embolism on tissue factor-bearing collagen surfaces under flow: role of thrombin with and without fibrin. *Arterioscler Thromb Vasc Biol*. 2012;32(6):1466-1476.
67. Gailani D, Broze GJ, Jr. Factor XI activation in a revised model of blood coagulation. *Science*. 1991;253(5022):909-912.
68. Ito Y, Liu LS, Matsuo R, Imanishi Y. Synthesis and nonthrombogenicity of polymer membrane with surface-graft polymers carrying thrombin inhibitor. *J Biomed Mater Res*. 1992;26(8):1065-1080.
69. Cho H, Baker BR, Wachsmann-Hogiu S, et al. Aptamer-based SERRS sensor for thrombin detection. *Nano Lett*. 2008;8(12):4386-4390.
70. Chatterjee MS, Denney WS, Jing H, Diamond SL. Systems biology of coagulation initiation: kinetics of thrombin generation in resting and activated human blood. *PLoS Comput Biol*. 2010;6(9).
71. Hemker HC, Giesen P, Al Dieri R, et al. Calibrated automated thrombin generation measurement in clotting plasma. *Pathophysiol Haemost Thromb*. 2003;33(1):4-15.
72. Guy RD, Fogelson AL, Keener JP. Fibrin gel formation in a shear flow. *Math Med Biol*. 2007;24(1):111-130.
73. Smith SA, Morrissey JH. Rapid and efficient incorporation of tissue factor into liposomes. *J Thromb Haemost*. 2004;2(7):1155-1162.
74. Sudo R, Chung S, Zervantonakis IK, et al. Transport-mediated angiogenesis in 3D epithelial coculture. *Faseb j*. 2009;23(7):2155-2164.
75. Polacheck WJ, Charest JL, Kamm RD. Interstitial flow influences direction of tumor cell migration through competing mechanisms. *Proc Natl Acad Sci U S A*. 2011;108(27):11115-11120.
76. Stalker TJ, Wu J, Morgans A, et al. Endothelial cell specific adhesion molecule (ESAM) localizes to platelet-platelet contacts and regulates thrombus formation in vivo. *J Thromb Haemost*. 2009;7(11):1886-1896.
77. Neeves KB, Maloney SF, Fong KP, et al. Microfluidic focal thrombosis model for measuring murine platelet deposition and stability: PAR4 signaling enhances shear-resistance of platelet aggregates. *J Thromb Haemost*. 2008;6(12):2193-2201.

78. Higgins DL, Lewis SD, Shafer JA. Steady state kinetic parameters for the thrombin-catalyzed conversion of human fibrinogen to fibrin. *J Biol Chem*. 1983;258(15):9276-9282.
79. Parazynski SE, Hargens AR, Tucker B, Aratow M, Styf J, Crenshaw A. Transcapillary fluid shifts in tissues of the head and neck during and after simulated microgravity. *J Appl Physiol (1985)*. 1991;71(6):2469-2475.
80. van Gestel MA, Heemskerk JW, Slaaf DW, et al. Real-time detection of activation patterns in individual platelets during thromboembolism in vivo: differences between thrombus growth and embolus formation. *J Vasc Res*. 2002;39(6):534-543.
81. Hayashi T, Mogami H, Murakami Y, et al. Real-time analysis of platelet aggregation and procoagulant activity during thrombus formation in vivo. *Pflugers Arch*. 2008;456(6):1239-1251.
82. Xu Z, Chen N, Shadden S, et al. Study of blood flow effects on growth of thrombi using a multiscale model. *Soft Matter*. 2009;5:769-779.
83. Savage B, Saldivar E, Ruggeri ZM. Initiation of platelet adhesion by arrest onto fibrinogen or translocation on von Willebrand factor. *Cell*. 1996;84(2):289-297.
84. Nesbitt WS, Westein E, Tovar-Lopez FJ, et al. A shear gradient-dependent platelet aggregation mechanism drives thrombus formation. *Nat Med*. 2009;15(6):665-673.
85. Kuijpers MJ, Munnix IC, Cosemans JM, et al. Key role of platelet procoagulant activity in tissue factor-and collagen-dependent thrombus formation in arterioles and venules in vivo differential sensitivity to thrombin inhibition. *Microcirculation*. 2008;15(4):269-282.
86. Neeves KB, Diamond SL. A membrane-based microfluidic device for controlling the flux of platelet agonists into flowing blood. *Lab Chip*. 2008;8(5):701-709.
87. Welsh JD, Colace TV, Muthard RW, Stalker TJ, Brass LF, Diamond SL. Platelet-targeting sensor reveals thrombin gradients within blood clots forming in microfluidic assays and in mouse. *J Thromb Haemost*. 2012;10:2344-2353.
88. Wannemacher KM, Zhu L, Jiang H, et al. Diminished contact-dependent reinforcement of Syk activation underlies impaired thrombus growth in mice lacking Semaphorin 4D. *Blood*. 2010;116(25):5707-5715.
89. Zhu L, Bergmeier W, Wu J, et al. Regulated surface expression and shedding support a dual role for semaphorin 4D in platelet responses to vascular injury. *Proc Natl Acad Sci U S A*. 2007;104(5):1621-1626.
90. Wang W, King MR. Multiscale modeling of platelet adhesion and thrombus growth. *Ann Biomed Eng*. 2012;40(11):2345-2354.
91. Xu Z, Lioi J, Mu J, et al. A multiscale model of venous thrombus formation with surface-mediated control of blood coagulation cascade. *Biophys J*. 2010;98(9):1723-1732.
92. Raj T, Flygare WH. Diffusion studies of bovine serum albumin by quasielastic light scattering. *Biochemistry*. 1974;13(16):3336-3340.
93. Harmison CR, Landaburu RH, Seegers WH. Some physicochemical properties of bovine thrombin. *J Biol Chem*. 1961;236:1693-1696.
94. de Graaf RA, van Kranenburg A, Nicolay K. In vivo (31)P-NMR diffusion spectroscopy of ATP and phosphocreatine in rat skeletal muscle. *Biophys J*. 2000;78(4):1657-1664.
95. Law DA, DeGuzman FR, Heiser P, Ministri-Madrid K, Killeen N, Phillips DR. Integrin cytoplasmic tyrosine motif is required for outside-in alphaIIbbeta3 signalling and platelet function. *Nature*. 1999;401:808-811.

96. Stalker TJ, Welsh JD, Tomaiuolo M, et al. A systems approach to hemostasis: 3. Thrombus consolidation regulates intrathrombus solute transport and local thrombin activity. *Blood*. 2014;124(11):1824-1831.
97. Aleman MM, Walton BL, Byrnes JR, et al. Elevated prothrombin promotes venous, but not arterial, thrombosis in mice. *Arterioscler Thromb Vasc Biol*. 2013;33(8):1829-1836.
98. Brass LF, Zhu L, Stalker TJ. Minding the gaps to promote thrombus growth and stability. *J Clin Invest*. 2005;115(12):3385-3392.
99. Skaer RJ, Emmines JP, Skaer HB. The fine structure of cell contacts in platelet aggregation. *J Ultrastruct Res*. 1979;69(1):28-42.
100. Humbert M, Nurden P, Bihour C, et al. Ultrastructural studies of platelet aggregates from human subjects receiving clopidogrel and from a patient with an inherited defect of an ADP-dependent pathway of platelet activation. *Arterioscler Thromb Vasc Biol*. 1996;16(12):1532-1543.
101. Kollman JM, Pandi L, Sawaya MR, Riley M, Doolittle RF. Crystal structure of human fibrinogen. *Biochemistry*. 2009;48(18):3877-3886.
102. Colace TV, Diamond SL. Direct observation of von Willebrand factor elongation and fiber formation on collagen during acute whole blood exposure to pathological flow. *Arterioscler Thromb Vasc Biol*. 2013;33(1):105-113.
103. Schenk O, Gartner K, Fichtner W, Stricker A. PARDISO: a high-performance serial and parallel sparse linear solver in semiconductor device simulation. *Future Gener Comp Sy* 2001;18:69-78.
104. de Graaf RA, van Kranenburh A, Nicolay K. In vivo (31)P-NMR diffusion spectroscopy of ATP and phosphocreatine in rat skeletal muscle. *Biophys J*. 2000;78:1657-1664.
105. Amestoy PR, Duff IS, l'Excellent JY. Multifrontal parallel distributed symmetric and unsymmetric solvers. *Comput Method Appl M* 2000;184:501-520.
106. Rosenson RS, McCormick A, Uretz EF. Distribution of blood viscosity values and biochemical correlates in healthy adults. *Clin Chem*. 1996;42(8 Pt 1):1189-1195.
107. Bellido-Martin L, Chen V, Jasuja R, Furie B, Furie BC. Imaging fibrin formation and platelet and endothelial cell activation in vivo. *Thromb Haemost*. 2011;105(5):776-782.
108. Dubois C, Panicot-Dubois L, Gainor JF, Furie BC, Furie B. Thrombin-initiated platelet activation in vivo is vWF independent during thrombus formation in a laser injury model. *J Clin Invest*. 2007;117(4):953-960.
109. Gross PL, Furie BC, Merrill-Skoloff G, Chou J, Furie B. Leukocyte-versus microparticle-mediated tissue factor transfer during arteriolar thrombus development. *J Leukoc Biol*. 2005;78(6):1318-1326.
110. Welsh JD, Stalker TJ, Voronov R, et al. A systems approach to hemostasis: 1. The interdependence of thrombus architecture and agonist movements in the gaps between platelets. *Blood*. 2014;In press.
111. Tomaiuolo M, Stalker TJ, Welsh JD, Diamond SL, Sinno T, Brass LF. A systems approach to hemostasis: 2. Computational analysis of molecular transport in the thrombus microenvironment. *Blood*. 2014;In press.
112. Ono A, Westein E, Hsiao S, et al. Identification of a fibrin-independent platelet contractile mechanism regulating primary hemostasis and thrombus growth. *Blood*. 2008;112(1):90-99.
113. Calaminus SD, Auger JM, McCarty OJ, Wakelam MJ, Machesky LM, Watson SP. MyosinIIa contractility is required for maintenance of platelet structure during spreading

on collagen and contributes to thrombus stability. *J Thromb Haemost*. 2007;5(10):2136-2145.
114. Law DA, DeGuzman FR, Heiser P, Ministri-Madrid K, Killeen N, Phillips DR. Integrin cytoplasmic tyrosine motif is required for outside-in alphaIIbbeta3 signalling and platelet function. *Nature*. 1999;401(6755):808-811.
115. Mahabeleshwar GH, Feng W, Phillips DR, Byzova TV. Integrin signaling is critical for pathological angiogenesis. *J Exp Med*. 2006;203(11):2495-2507.
116. Falati S, Gross P, Merrill-Skoloff G, Furie BC, Furie B. Real-time in vivo imaging of platelets, tissue factor and fibrin during arterial thrombus formation in the mouse. *Nat Med*. 2002;8(10):1175-1181.
117. Brinkman HC. A calculation of the viscous force exerted by a flowing fluid on a dense swarm of particles. *Appl Sci Res*. 1947;A1:27-34.
118. Vandendries ER, Hamilton JR, Coughlin SR, Furie B, Furie BC. PAR4 is required for platelet thrombus propagation but not fibrin generation in a mouse model of thrombosis. *Proc Natl Acad Sci U S A*. 2007;104(1):288-292.
119. Spero RC, Sircar RK, Schubert R, Taylor RM, 2nd, Wolberg AS, Superfine R. Nanoparticle diffusion measures bulk clot permeability. *Biophys J*. 2011;101(4):943-950.
120. Wufsus AR, Macera NE, Neeves KB. The hydraulic permeability of blood clots as a function of fibrin and platelet density. *Biophys J*. 2013;104(8):1812-1823.
121. Bellido-Martin L, Chen V, Jasuja R, Furie B, Furie BC. Imaging fibrin formation and platelet and endothelial cell activation in vivo. *Thrombosis and haemostasis*. 2011;105(5):776-782.
122. Betterle C, Fabris F, de Marco L, Del Prete GF, Girolami A. Clotting factors and platelets. Immunofluorescence evidence that fibrinogen and factor VIII are present in human washed platelets, whereas prothrombin complex factors and factor XIII are lacking. *Haemostasis*. 1977;6(3):171-179.
123. Bergstrom K, Egberg N. Determination of vitamin K sensitive coagulation factors in plasma: studies on three methods using synthetic chromogenic substrates. *Thromb Res*. 1978;12(3):531-547.
124. Grazul-Bilska AT, Johnson ML, Bilski JJ, et al. Wound healing: the role of growth factors. *Drugs Today (Barc)*. 2003;39(10):787-800.
125. Golebiewska EM, Poole AW. Platelet secretion: From haemostasis to wound healing and beyond. *Blood Rev*. 2015;29(3):153-162.
126. Dvorak HF, Brown LF, Detmar M, Dvorak AM. Vascular permeability factor/vascular endothelial growth factor, microvascular hyperpermeability, and angiogenesis. *Am J Pathol*. 1995;146(5):1029-1039.
127. Nurden AT, Nurden P, Sanchez M, Andia I, Anitua E. Platelets and wound healing. *Front Biosci*. 2008;13:3532-3548.
128. Gear AR, Camerini D. Platelet chemokines and chemokine receptors: linking hemostasis, inflammation, and host defense. *Microcirculation*. 2003;10(3-4):335-350.
129. Wagner DD, Burger PC. Platelets in inflammation and thrombosis. *Arterioscler Thromb Vasc Biol*. 2003;23(12):2131-2137.
130. Signarvic RS, Cierniewska A, Stalker TJ, et al. RGS/Gi2alpha interactions modulate platelet accumulation and thrombus formation at sites of vascular injury. *Blood*. 2010;116(26):6092-6100.
131. Atkinson BT, Jasuja R, Chen VM, Nandivada P, Furie B, Furie BC. Laser-induced endothelial cell activation supports fibrin formation. *Blood*. 2010;116(22):4675-4683.

132. Dvorak HF, Detmar M, Claffey KP, Nagy JA, van de Water L, Senger DR. Vascular permeability factor/vascular endothelial growth factor: an important mediator of angiogenesis in malignancy and inflammation. *Int Arch Allergy Immunol*. 1995;107(1-3):233-235.
133. Kretz CA, Vaezzadeh N, Gross PL. Tissue factor and thrombosis models. *Arterioscler Thromb Vasc Biol*. 2010;30(5):900-908.
134. Figueroa XF, Chen CC, Campbell KP, et al. Are voltage-dependent ion channels involved in the endothelial cell control of vasomotor tone? *Am J Physiol Heart Circ Physiol*. 2007;293(3):H1371-1383.
135. Mui KL, Bae YH, Gao L, et al. N-Cadherin Induction by ECM Stiffness and FAK Overrides the Spreading Requirement for Proliferation of Vascular Smooth Muscle Cells. *Cell Rep*. 2015.
136. Saito T, Hasegawa Y, Ishigaki Y, et al. Importance of endothelial NF-kappaB signalling in vascular remodelling and aortic aneurysm formation. *Cardiovasc Res*. 2013;97(1):106-114.
137. Wang CH, Chen KT, Mei HF, Lee JF, Cherng WJ, Lin SJ. Assessment of mouse hind limb endothelial function by measuring femoral artery blood flow responses. *J Vasc Surg*. 2011;53(5):1350-1358.
138. Stolla M, Stefanini L, Roden RC, et al. The kinetics of {alpha}IIb{beta}3 activation determines the size and stability of thrombi in mice: implications for antiplatelet therapy. *Blood*. 2011;117(3):1005-1013.
139. Falati S, Liu Q, Gross P, et al. Accumulation of tissue factor into developing thrombi in vivo is dependent upon microparticle P-selectin glycoprotein ligand 1 and platelet P-selectin. *J Exp Med*. 2003;197(11):1585-1598.
140. Neyman M, Gewirtz J, Poncz M. Analysis of the spatial and temporal characteristics of platelet-delivered factor VIII-based clots. *Blood*. 2008;112(4):1101-1108.
141. Milanov P, Ivanciu L, Abriss D, et al. Engineered factor IX variants bypass FVIII and correct hemophilia A phenotype in mice. *Blood*. 2012;119(2):602-611.
142. Ivanciu L, Toso R, Margaritis P, et al. A zymogen-like factor Xa variant corrects the coagulation defect in hemophilia. *Nat Biotechnol*. 2011;29(11):1028-1033.
143. Stalker TJ, Wu J, Hall RA, Brass LF. The tight junction protein ESAM is recruited to platelet-platelet contacts and forms stable signaling complexes that affect thrombus growth and stability. *J Thromb Haemost*. 2007.
144. Naik MU, Stalker TJ, Brass LF, Naik UP. JAM-A protects from thrombosis by suppressing integrin alphaIIbbeta3-dependent outside-in signaling in platelets. *Blood*. 2012;119(14):3352-3360.
145. Zhu L, Stalker TJ, Jiang H, Wang T, Gruber P, Brass L. Loss of sema4D signaling between platelets detabilizes arterial thrombi and reduces myocardial infarct size. *J Thromb Haemost*. 2007.
146. Zhu L, Stalker TJ, Fong KP, et al. Disruption of SEMA4D ameliorates platelet hypersensitivity in dyslipidemia and confers protection against the development of atherosclerosis. *Arterioscler Thromb Vasc Biol*. 2009;29(7):1039-1045.
147. Brass LF, Stalker TJ. Minding the Gaps--and the Junctions, Too. *Circulation*. 2012;125(20):2414-2416.
148. Stalker TJ, Welsh JD, Brass LF. Shaping the platelet response to vascular injury. *Curr Opin Hematol*. 2014;21(5):410-417.